RESEARCH MEMORANDUM

THE EFFECT OF CONICAL CAMBER ON THE STATIC LONGITUDINAL, LATERAL, AND DIRECTIONAL CHARACTERISTICS OF A 45° SWEPTBACK WING AT MACH NUMBERS UP TO 0.96

By Robert I. Sammonds and Robert M. Reynolds

Ames Aeronautical Laboratory
Moffett Field, Calif.

NATIONAL ADVISORY COMMITTEE
FOR AERONAUTICS

WASHINGTON
July 3, 1956

W

NATIONAL ADVISORY COMMITTEE FOR AERONAUTICS

RESEARCH MEMORANDUM

THE EFFECT OF CONICAL CAMBER ON THE STATIC LONGITUDINAL, LATERAL, AND DIRECTIONAL CHARACTERISTICS OF A 45° SWEPTBACK WING AT MACH NUMBERS UP TO 0.96

By Robert I. Sammonds and Robert M. Reynolds

SUMMARY

An investigation has been conducted to determine the effect of conical camber on the drag due to lift and on the static longitudinal, lateral, and directional stability characteristics of an aspect-ratio-3, 45° sweptback wing in combination with a streamline body. Tests were made at Mach numbers up to 0.96 at a Reynolds number of 1.5 million and at Reynolds numbers up to 8 million at a Mach number of 0.22, both with and without roughness strips near the leading edge of both the upper and lower surfaces of the wing.

The addition of conical camber to the basic wing reduced the drag due to lift at moderate and large lift coefficients and increased the maximum lift-drag ratios. The detrimental effects of compressibility became more pronounced as the camber was increased. At lift coefficients near zero, conical camber increased the drag of the basic wing-body combination.

In general, at low angles of attack the effect of camber on the lift and pitching-moment curve slopes and on the side force and yawing moment was small. However, the maximum effective dihedral of the wing was increased, for most test conditions, by cambering the wing.

INTRODUCTION

The tactical requirement of high subsonic cruising speeds at high altitude has placed increasing importance on the attainment of high lift-drag ratios at the highest possible Mach numbers without seriously penalizing the supersonic dash capabilities of the airplane. As a significant portion of the total drag of an airplane can be associated with the production of lift, methods for reducing the drag due to lift are being investigated.

[redacted]

[redacted]

Research has been conducted to determine the effectiveness of a conical type of camber in reducing the drag due to lift of several low-aspect-ratio triangular and sweptback wings at subsonic and supersonic speeds (refs. 1 and 2). As a part of this research, the effects of conical camber on the aerodynamic characteristics of an aspect-ratio-3, 45° sweptback wing in combination with a streamline body have been investigated. A portion of the results of this investigation has been reported in reference 2. The present report presents the results for an extended range of subsonic Mach numbers, including the effects of conical camber on the static lateral and directional characteristics of the wing-body combination.

These tests were conducted in the Ames 12-foot pressure wind tunnel at Mach numbers up to 0.96 at a Reynolds number of 1.5 million, and at Reynolds numbers up to 8 million at a Mach number of 0.22, both with and without roughness strips near the leading edge of both the upper and lower surfaces of the wing.

NOTATION

A aspect ratio, $\frac{b^2}{S}$

b span

c chord

$\bar{c}$ mean aerodynamic chord, $\frac{\int_0^{b/2} c^2 dy}{\int_0^{b/2} c\, dy}$

C_D drag coefficient, $\frac{\text{drag}}{qS}$

C_{D_o} drag coefficient at zero lift of the plane wing

C_L lift coefficient, $\frac{\text{lift}}{qS}$

C_{L_d} equivalent design lift coefficient at design Mach number of 1.0 (See ref. 2.)

C_l rolling-moment coefficient, $\frac{\text{rolling moment}}{qSb}$

C_m pitching-moment coefficient, $\frac{\text{pitching moment}}{qS\bar{c}}$, referred to the quarter point of the mean aerodynamic chord

C_n yawing-moment coefficient, $\frac{\text{yawing moment}}{qSb}$

C_y side-force coefficient, $\frac{\text{side force}}{qS}$

$\frac{L}{D}$ lift-drag ratio

$\left(\frac{L}{D}\right)_{max}$ maximum lift-drag ratio

l over-all length of basic body

M free-stream Mach number

q free-stream dynamic pressure

R Reynolds number based on wing mean aerodynamic chord

r local radius of body

r_o maximum radius of body

S wing area

s spanwise distance from wing plane of symmetry to edge of circumscribed triangular wing

x,y,z Cartesian coordinates in streamwise, spanwise, and vertical directions, respectively

C_{l_β} $\left(\frac{\Delta C_l}{\Delta \beta}\right)_\alpha$ = constant

C_{n_β} $\left(\frac{\Delta C_n}{\Delta \beta}\right)_\alpha$ = constant

C_{y_β} $\left(\frac{\Delta C_y}{\Delta \beta}\right)_\alpha$ = constant

$\frac{dC_L}{d\alpha}$ rate of change of lift coefficient with angle of attack, $C_L = 0$

$\frac{dC_{l_\beta}}{d\alpha}$ rate of change of dihedral effect with angle of attack, $C_L \approx 0$

$\frac{dC_m}{dC_L}$ rate of change of pitching-moment coefficient with lift coefficient, $C_L = 0$

α angle of attack corrected for tunnel-wall interference

α_u geometric angle of attack

β angle of sideslip

MODELS

The models tested in the Ames 12-foot pressure wind tunnel consisted of one uncambered and two conically cambered wings, each mounted in the midwing position on a streamline body of revolution. The wings had an aspect ratio of 3.0, 45° sweepback of the leading edge, a taper ratio of 0.40, and a maximum thickness of approximately 5 percent in streamwise planes. A sketch of the projected model plan form showing the basic model dimensions is presented in figure 1. The body was designed to have a minimum wave drag for a given volume (Sears-Haack body). Figure 1 gives the equation of the body coordinates and shows the cutoff at the rear of the body to accommodate the sting and the four-component strain-gage balance used to measure the forces and moments. These models were previously used for the investigation reported in reference 2.

The plane (uncambered) wing consisted of NACA 64A006 sections perpendicular to the quarter-chord line of the swept airfoil sections with a leading-edge modification consisting of an increase in the nose radii as shown in figure 2. Coordinates for the plane wing are given in table I.

The two cambered wings had the same thickness distribution as the plane wing, and the camber surfaces were designed, in accordance with the theoretical methods reported in reference 2, to have equivalent design lift coefficients of 0.22 and 0.29, at a Mach number of 1.0. The coordinates for these two wings are given in tables II and III. The mean-surface shape of the sweptback wing, cambered for a design lift coefficient of 0.29, is shown in figure 3. Since this surface shape was obtained by calculating the camber shape of a triangular wing (with a specified design lift coefficient) which circumscribes the sweptback wing, the surface shapes of the two wings will be identical over the common area. Furthermore, since the mean surface of the wings is conical with respect to the wing apex, the surface trace will be similar for all locations of the cutting plane (A-A, fig. 3) along the x axis. However, it should be noted that, as presented in figure 3, the s term is defined as the distance from the wing plane of symmetry to the edge of the circumscribed triangular wing and that at the tips of the sweptback wing, the y/s term will be less than 1.

TESTS AND PROCEDURES

Measurements were made of the lift, drag, and pitching moments of the three wing-body combinations for a range of angles of attack for Reynolds numbers of 3, 6, and 8 million at a Mach number of 0.22; for Reynolds numbers of 1.5 and 2.86 million at a Mach number of 0.60; and for Mach numbers from 0.80 to 0.96 at a Reynolds number of 1.5 million.

Measurements of the lift, drag, and pitching moments were also made for the wing-body combinations with roughness strips placed along conical rays near the leading edge of both the upper and lower surfaces of the wing (see fig. 1). These roughness strips consisted of number 60 carborundum grit imbedded in Vulcalock. The same range of angles of attack, Reynolds numbers, and Mach numbers were used for the wings both with and without roughness.

Additional measurements were made of the side force, yawing moment, and rolling moment of the three wing-body combinations (with roughness) at a sideslip angle of -6° for the same range of Reynolds numbers and Mach numbers previously stated.

CORRECTIONS TO DATA

The data are presented as standard NACA coefficients about the stability system of axes. The drag coefficient and angle of attack have been corrected by the method of reference 3 for the induced effects of the tunnel walls resulting from lift on the model. The following corrections were added to the measured values:

$$\Delta\alpha = 0.16\ C_L, \text{ deg}$$

$$\Delta C_D = 0.00279\ C_L^2$$

The induced effects of the tunnel walls on the pitching moment, side force, yawing moment, and rolling moment were calculated and found to be negligible.

Corrections were also applied to the data to account for the constriction (blockage) effects of the tunnel walls (ref. 4) and the air-stream inclination. At a Mach number of 0.90, the blockage correction amounted to an increase of less than 1 percent in the measured values of Mach number and dynamic pressure. The correction for air-stream inclination was 0.1°.

The drag data were adjusted to correspond to the drag which would exist if the base pressure were equal to free-stream static pressure.

RESULTS

The lift, drag, and pitching-moment data for the wing-body combinations with the plane wing and with the two cambered wings are presented in figures 4 to 9. In these figures, the drag data have been presented in the form $C_D - (C_L^2/\pi A)$ for plotting convenience. It should be noted that when presented in this form $(C_D - (C_L^2/\pi A))$ the estimated drag values for the theoretical condition of full leading-edge suction[1] would be constant for all lift coefficients at a value equal to C_{D_o}. The total drag coefficients, C_D, are presented in figures 10 and 11 as a function of Reynolds number and Mach number, respectively, for constant values of lift coefficient. Figures 12 to 14 show the lift-drag ratios for the three wings both with and without roughness. The maximum lift-drag ratios and the lift coefficients for maximum lift-drag ratio are presented in figures 15 and 16 along with estimated values of the maximum lift-drag ratio for the theoretical conditions of full leading-edge suction and no leading-edge suction.[1] Figures 17 and 18 present the slope of the lift and pitching-moment curves, near zero lift, as a function of Reynolds number and Mach number, respectively.

The basic rolling-moment, side-force, and yawing-moment coefficients for the three models are presented in figures 19 to 21 for a sideslip angle (β) of -6° and with leading-edge roughness. The static stability derivatives (C_{l_β}, C_{n_β}, and C_{y_β}), obtained by dividing the static coefficients (C_l, C_n, and C_y) by the sideslip angle, -6°, are presented in figures 22 and 23 as a function of Reynolds number and Mach number, respectively, for an angle of attack of 0°. Also presented in figures 22 and 23, for angles of attack near 0°, are the changes in dihedral effect for a unit change in angle of attack.

DISCUSSION

Since the Reynolds numbers of these tests were low compared to probable full-scale conditions, the boundary layer of the models would likely be different from that for full scale. It was felt that the boundary layer for the models (low Reynolds number) would be largely laminar at zero lift with a forward chordwise shift of the transition from laminar to turbulent flow with increasing lift and Reynolds number, and that the full-scale boundary layer would be largely turbulent, with transition occurring well forward on the wing for all lift conditions. This movement of transition on the models would result in a sizable change in skin friction with

[1]The formulae used to estimate the drag coefficients for the theoretical conditions of full leading-edge suction and no leading-edge suction are $C_D = C_{D_o} + (C_L^2/\pi A)$ and $C_D = C_{D_o} + C_L^2/57.3(dC_L/d\alpha)$, respectively, where C_{D_o} is the drag at zero lift of the plane (uncambered) wing.

changing lift and Reynolds number, and the aerodynamic characteristics of the models would not be representative of that for the full-scale condition. In order to reduce the changes in skin friction on the model, an effort was made to fix the location of boundary-layer transition on the model irrespective of lift coefficient and Reynolds number by placing roughness strips along conical rays near the leading edge of both the upper and lower surfaces of the wing.

It should be noted that this addition of roughness near the wing leading edge would be expected to result in an increase in the drag of the wing-body combination due not only to the increase in skin friction resulting from the forward movement of transition but due also to the drag of the roughness strips themselves. However, since these roughness strips were the same for each of the three wings, it is felt that this contribution to the total drag of the wing-body combinations would be nearly the same for each of the three models and could be ignored in comparing the data for the three wings.

Although no measurements were made to determine whether or not the roughness strips actually fixed transition near the leading edge of the wing, it is felt that the data with roughness are more applicable to full-scale conditions. As such, the following discussion will be concerned primarily with the data for the wings with roughness.

Drag Characteristics

Examination of the basic data presented in figures 7 to 9 shows that cambering the wing generally decreased the drag at high lift coefficients and increased the drag at lift coefficients near zero. However, it should be pointed out that for the more highly cambered wing ($C_{L_d} = 0.29$) the increase in drag due to camber at a lift coefficient of zero amounted to as much as 0.003 for the wing with roughness, although without roughness (figs. 4 to 6), this increase in drag amounted to as much as 0.007. This difference in the drag increment due to camber at zero lift with and without roughness is in accord with the results presented in reference 2. Evidence presented in the above reference indicates that, without roughness, the boundary layer of the plane wing at zero lift may have been largely laminar, with a change in the skin-friction drag resulting from a forward movement of transition when the roughness strips were added. For the cambered wing, however, these data of reference 2 indicated that the camber may have induced transition naturally near the wing leading edge, with no appreciable movement of transition resulting from the addition of roughness. It can also be seen from figures 7 and 10 that increasing Reynolds number for a constant Mach number (0.22) delayed to higher lift coefficients the substantial benefits of drag reduction due to camber. Also, at these higher lift coefficients for Mach numbers less than 0.80, the wing with the most camber had the least drag. For Mach numbers from

about 0.90 to 0.96 for a Reynolds number of 1.5 million and lift coefficient above 0.2, the drag reductions due to camber were less than those obtained at the lower Mach numbers (figs. 9 and 11). Furthermore, for Mach numbers greater than 0.80 at these same lift coefficients, the moderately cambered wing had as low if not lower drag than the more highly cambered wing. It thus appears that the benefits of camber are reduced as the drag divergence Mach number is exceeded and that the adverse effects of compressibility on the drag become more pronounced as the camber is increased. This effect of compressibility is in agreement with the data reported in reference 2.

Lift-Drag Ratio

The data presented in figures 12 through 16, for the wing with roughness, show that throughout the range of these tests, cambering the wing resulted in increased maximum lift-drag ratios as compared to those for the plane wing. However, it should be pointed out that since, for a Mach number of 0.22 and Reynolds numbers between 3 and 8 million, the plane wing was developing nearly full leading-edge suction, the benefits due to camber were necessarily small (figs. 12 and 15). It is interesting to note at the high Mach numbers (Reynolds number of 1.5 million), the adverse effects of compressibility resulted in a rapid decrease in maximum lift-drag ratio for all three wings, with the benefits of camber on the maximum lift-drag ratio completely disappearing at Mach numbers of 0.93 and above. It should be mentioned that no attempt has been made in this investigation to alleviate the compressibility drag losses by contouring the body, and, hence, that the decrease in maximum lift-drag ratio for both the plane and cambered wing could probably have been delayed to higher Mach numbers if either an area-rule or Kuchemann type modification had been employed in the design of the wing-body combination (ref. 5).

The data presented in figures 15 and 16 show that with roughness, the maximum lift-drag ratios of the cambered wings were almost coincident with the estimated lift-drag ratios for the condition of full leading-edge suction except at the high Mach numbers. At Mach numbers above about 0.86, the effects of compressibility resulted in a rapid divergence of these theoretical and experimental curves, with the experimental data approaching that for the theoretical condition of no leading-edge suction. It is interesting to note that, without roughness, there was a substantial difference in the maximum lift-drag ratios obtained for the cambered wings and full leading-edge suction for the entire Mach number range. However, this may be attributed to the aforementioned differences in the boundary-layer conditions for the plane and cambered wings, without roughness.

Lift and Pitching Moment

In general, the effect of camber and Reynolds number on the lift and pitching-moment curve slopes was small for the range of Mach and Reynolds numbers investigated (figs. 17 and 18). However, the use of conical camber, in most cases, did delay to higher lift coefficients the abrupt change in slope of both the lift and pitching-moment curves (figs. 7 to 9). Increasing the Mach number generally resulted in the expected increase in the slope of the lift and pitching-moment curves for all three wings.

Static Lateral and Directional Stability

It can be seen from figures 19 to 23 that the variation with angle of attack of the rolling moment, yawing moment, and side force was nearly linear at the low angles of attack. No appreciable effect of either camber, Reynolds number, or Mach number is indicated except for the effect of Mach number on the variation of effective dihedral with angle of attack. For all three wings, increasing the Mach number from 0.60 to 0.90 for a Reynolds number of 1.5 million resulted in an increase in the variation of effective dihedral with angle of attack; at Mach numbers above 0.90 this trend was reversed.

It is of interest to note that the lowest angle of attack at which the lateral or directional characteristics experienced an abrupt change in slope (figs. 19 to 21) coincided with the angle of attack at which there was a rapid increase in drag (figs. 7 to 9). In addition, it can be seen that increasing either Reynolds number or camber delayed these changes in slope to higher angles of attack.

It is apparent from figures 19 to 21 that increasing either Reynolds number, Mach number, or camber generally increased the maximum effective dihedral of the wing except at Mach numbers above 0.92. At this Mach number and above, there was practically no effect of camber on the maximum effective dihedral.

CONCLUSIONS

Data have been presented showing the effect of conical camber, Mach number, and Reynolds number on the drag due to lift and the static longitudinal, lateral, and directional stability characteristics of an aspect-ratio-3, 45° sweptback wing in combination with a streamline body. The results of this investigation showed:

1. The use of conical camber reduced the drag due to lift at moderate and large lift coefficients and increased the maximum lift-drag ratios although the detrimental effects of compressibility became more pronounced as the camber was increased. At lift coefficients near zero the use of conical camber generally increased the drag of the basic wing-body combination.

2. In general, the effect of camber on the lift and pitching-moment curve slopes and on the side force and yawing moment was small at low angles of attack. However, except at the highest Mach numbers, cambering the wing resulted in a large increase in the maximum effective dihedral of the wing.

Ames Aeronautical Laboratory
National Advisory Committee for Aeronautics
Moffett Field, Calif., Apr. 2, 1956

REFERENCES

1. Hall, Charles F.: Lift, Drag, and Pitching Moment of Low-Aspect-Ratio Wings at Subsonic and Supersonic Speeds. NACA RM A53A30, 1953.

2. Boyd, John W., Migotsky, Eugene, and Wetzel, Benton E.: A Study of Conical Camber for Triangular and Sweptback Wings. NACA RM A55G19, 1955.

3. Glauert, H.: The Elements of Aerofoil and Airscrew Theory. The Macmillan Co., N. Y., 1943, p. 191.

4. Herriot, John G.: Blockage Corrections for Three-Dimensional-Flow Closed-Throat Wind Tunnels, with Consideration of the Effect of Compressibility. NACA Rep. 995, 1950. (Formerly NACA RM A7B28.)

5. McDevitt, John B.: An Experimental Investigation of Two Methods for Reducing Transonic Drag of Swept-Wing and Body Combinations. NACA RM A55B21, 1955.

TABLE I.- COORDINATES OF AIRFOIL SECTIONS FOR PLANE WING
[Coordinates are presented for sections parallel to the plane of symmetry]

2y/b	x percent c	z percent c	x percent c	z percent c	2y/b	x percent c	z percent c	x percent c	z percent c
0[a]	0	0	47.325	2.522	0.67[d]	0	0	47.325	2.522
	.672	.464	52.440	2.438		.672	.745	52.440	2.438
	1.008	.559	57.404	2.304		1.008	.842	57.404	2.304
	1.678	.704	62.223	2.132		1.678	.972	62.223	2.132
	3.340	.964	66.903	1.931		3.340	1.242	66.903	1.931
	6.623	1.317	71.452	1.709		6.623	1.609	71.452	1.709
	9.850	1.571	75.872	1.468		9.850	1.847	75.872	1.468
	13.023	1.776	80.170	1.217		13.023	2.030	80.170	1.217
	19.213	2.077	84.352	.963		19.213	2.236	84.352	.963
	25.200	2.289	88.421	.715		25.200	2.354	88.421	.715
	30.997	2.429	92.384	.473		30.997	2.429	92.384	.473
	36.610	2.511	96.212	.238		36.610	2.511	96.212	.238
	42.050	2.541	100.000	.009		42.050	2.541	100.000	.009
0.25[b]	0	0	47.325	2.522	0.83[e]	0	0	47.325	2.522
	.672	.572	52.440	2.438		.672	.817	52.440	2.438
	1.008	.663	57.404	2.304		1.008	.920	57.404	2.304
	1.678	.808	62.223	2.132		1.678	1.050	62.223	2.132
	3.340	1.067	66.903	1.931		3.340	1.322	66.903	1.931
	6.623	1.426	71.452	1.709		6.623	1.685	71.452	1.709
	9.850	1.677	75.872	1.468		9.850	1.931	75.872	1.468
	13.023	1.868	80.170	1.217		13.023	2.100	80.170	1.217
	19.213	2.135	84.352	.963		19.213	2.281	84.352	.963
	25.200	2.310	88.421	.715		25.200	2.372	88.421	.715
	30.997	2.429	92.384	.473		30.997	2.429	92.384	.473
	36.610	2.511	96.212	.238		36.610	2.511	96.212	.238
	42.050	2.541	100.000	.009		42.050	2.541	100.000	.009
0.50[c]	0	0	47.325	2.522	1.00[f]	0	0	47.325	2.522
	.672	.676	52.440	2.438		.672	.891	52.440	2.438
	1.008	.768	57.404	2.304		1.008	.988	57.404	2.304
	1.678	.907	62.223	2.132		1.678	1.118	62.223	2.132
	3.340	1.176	66.903	1.931		3.340	1.393	66.903	1.931
	6.623	1.528	71.452	1.709		6.623	1.750	71.452	1.709
	9.850	1.778	75.872	1.468		9.850	1.993	75.872	1.468
	13.023	1.963	80.170	1.217		13.023	2.155	80.170	1.217
	19.213	2.194	84.352	.963		19.213	2.317	84.352	.963
	25.200	2.333	88.421	.715		25.200	2.382	88.421	.715
	30.997	2.429	92.384	.473		30.997	2.429	92.384	.473
	36.610	2.511	96.212	.238		36.610	2.511	96.212	.238
	42.050	2.541	100.000	.009		42.050	2.541	100.000	.009

[a]Leading-edge radius: 0.190 percent chord
[b]Leading-edge radius: 0.236 percent chord
[c]Leading-edge radius: 0.370 percent chord
[d]Leading-edge radius: 0.520 percent chord
[e]Leading-edge radius: 0.713 percent chord
[f]Leading-edge radius: 0.924 percent chord

TABLE II.- COORDINATES OF AIRFOIL SECTIONS FOR WING CAMBERED FOR $C_{L_d} = 0.22$ at M = 1.0

[Coordinates are presented for sections parallel to the plane of symmetry]

2y/b	x percent c	z percent c	x percent c	z percent c	x percent c	z percent c
0[a]	0	0	25.000	2.289	71.452	1.709
	.672	.464	30.997	2.429	75.872	1.468
	1.008	.559	36.610	2.511	80.170	1.217
	1.678	.704	42.050	2.541	84.352	.963
	3.340	.964	47.325	2.522	88.421	.715
	6.623	1.317	52.440	2.438	92.384	.473
	9.850	1.571	57.404	2.304	96.212	.238
	13.023	1.776	62.223	2.132	100.000	.009
	19.213	2.077	66.903	1.931		

2y/b	x percent c	z, percent c Upper surface	z, percent c Lower surface	2y/b	x percent c	z, percent c Upper surface	z, percent c Lower surface
0.25[b]	0	-0.435	-0.435	0.67	47.325	2.522	-2.522
	.672	.206	-.740		52.440	2.438	-2.438
	1.008	.335	-.793		57.404	2.304	-2.304
	1.678	.541	-.869		62.223	2.132	-2.132
	3.340	.892	-1.037		66.903	1.931	-1.931
	6.623	1.317	-1.317		71.452	1.709	-1.709
	9.850	1.571	-1.571		75.872	1.468	-1.468
	13.023	1.776	-1.776		80.170	1.217	-1.217
	19.213	2.077	-2.077		84.352	.963	-.963
	25.200	2.289	-2.289		88.421	.715	-.715
	30.997	2.429	-2.429		92.384	.473	-.473
	36.610	2.511	-2.511		96.212	.238	-.238
	42.050	2.541	-2.541		100.000	.009	-.009
	47.325	2.522	-2.522				
	52.440	2.438	-2.438	0.83[e]	0	-2.450	-2.450
	57.404	2.304	-2.304		.672	-1.478	-2.955
	62.223	2.132	-2.132		1.008	-1.348	-2.929
	66.903	1.931	-1.931		1.678	-1.115	-2.877
	71.452	1.709	-1.709		3.340	-.622	-2.774
	75.872	1.468	-1.468		6.623	.104	-2.605
	80.170	1.217	-1.217		9.850	.635	-2.528
	84.352	.963	-.963		13.023	1.063	-2.502
	88.421	.715	-.715		19.213	1.685	-2.476
	92.384	.473	-.473		25.200	2.100	-2.489
	96.212	.238	-.238		30.997	2.346	-2.515
	100.000	.009	-.009		36.610	2.490	-2.541
					42.050	2.541	-2.541
0.50[c]	0	-1.046	-1.046		47.325	2.522	-2.522
	.672	-.361	-1.333		52.440	2.438	-2.438
	1.008	-.213	-1.352		57.404	2.304	-2.304
	1.678	.028	-1.380		62.223	2.132	-2.132
	3.340	.491	-1.444		66.903	1.931	-1.931
	6.623	1.074	-1.555		71.452	1.709	-1.709
	9.850	1.463	-1.685		75.872	1.468	-1.468
	13.023	1.741	-1.815		80.170	1.217	-1.217
	19.213	2.077	-2.077		84.352	.963	-.963
	25.200	2.289	-2.289		88.421	.715	-.715
	30.997	2.429	-2.429		92.384	.473	-.473
	36.610	2.511	-2.511		96.212	.238	-.238
	42.050	2.541	-2.541		100.000	.009	-.009
	47.325	2.522	-2.522				
	52.440	2.438	-2.438	1.00[f]	0	-3.678	-3.678
	57.404	2.304	-2.304		.672	-2.495	-4.294
	62.223	2.132	-2.132		1.008	-2.382	-4.310
	66.903	1.931	-1.931		1.678	-2.171	-4.245
	71.452	1.709	-1.709		3.340	-1.701	-4.067
	75.872	1.468	-1.468		6.623	-.907	-3.775
	80.170	1.217	-1.217		9.850	-.308	-3.548
	84.352	.963	-.963		13.023	.178	-3.370
	88.421	.715	-.715		19.213	.988	-3.176
	92.384	.473	-.473		25.200	1.523	-3.046
	96.212	.238	-.238		30.997	1.912	-2.950
	100.000	.009	-.009		36.610	2.171	-2.852
					42.050	2.349	-2.738
0.67[d]	0	-1.631	-1.631		47.325	2.414	-2.641
	.672	-.821	-2.009		52.440	2.382	-2.479
	1.008	-.680	-2.020		57.404	2.285	-2.317
	1.678	-.443	-2.030		62.223	2.132	-2.132
	3.340	.054	-1.998		66.903	1.931	-1.931
	6.623	.702	-1.944		71.452	1.709	-1.709
	9.850	1.166	-1.976		75.872	1.468	-1.468
	13.023	1.534	-2.030		80.170	1.217	-1.217
	19.213	1.998	-2.160		84.352	.963	-.963
	25.200	2.279	-2.300		88.421	.715	-.715
	30.997	2.429	-2.429		92.384	.473	-.473
	36.610	2.511	-2.511		96.212	.238	-.238
	42.050	2.541	-2.541		100.000	.009	-.009

[a] Leading-edge radius: 0.190 percent chord
[b] Leading-edge radius: 0.236 percent chord
[c] Leading-edge radius: 0.370 percent chord
[d] Leading-edge radius: 0.520 percent chord
[e] Leading-edge radius: 0.713 percent chord
[f] Leading-edge radius: 0.924 percent chord

TABLE III.- COORDINATES OF AIRFOIL SECTIONS FOR WING CAMBERED FOR $C_{L_d} = 0.29$ at M = 1.0

[Coordinates are presented for sections parallel to the plane of symmetry]

2y/b	x percent c	z percent c	x percent c	z percent c	x percent c	z percent c
0[a]	0	0	25.200	2.889	71.452	1.709
	.672	.464	30.997	2.429	75.872	1.468
	1.008	.559	36.610	2.511	80.170	1.217
	1.678	.704	42.050	2.541	84.352	.963
	3.340	.964	47.325	2.522	88.421	.715
	6.623	1.317	52.440	2.438	92.384	.473
	9.850	1.571	57.404	2.304	96.212	.238
	13.023	1.776	62.223	2.132	100.000	.009
	19.213	2.077	66.903	1.931		

2y/b	x percent c	z, percent c Upper surface	z, percent c Lower surface	2y/b	x percent c	z, percent c Upper surface	z, percent c Lower surface
0.25[b]	0	-.579	-.579	0.67	47.325	2.522	-2.522
	.672	.175	-.945		52.440	2.438	-2.438
	1.008	.343	-.984		57.404	2.304	-2.304
	1.678	.572	-1.052		62.223	2.132	-2.132
	3.340	.968	-1.159		66.903	1.931	-1.931
	6.623	1.418	-1.418		71.452	1.709	-1.709
	9.850	1.677	-1.677		75.872	1.468	-1.468
	13.023	1.868	-1.868		80.170	1.217	-1.217
	19.213	2.135	-2.135		84.352	.963	-.963
	25.200	2.310	-2.310		88.421	.715	-.715
	30.997	2.429	-2.429		92.384	.473	-.473
	36.610	2.511	-2.511		96.212	.238	-.238
	42.050	2.541	-2.541		100.000	.009	-.009
	47.325	2.522	-2.522				
	52.440	2.438	-2.438	0.83[e]	0	-3.292	-3.292
	57.404	2.304	-2.304		.672	-2.139	-3.811
	62.223	2.132	-2.132		1.008	-1.997	-3.849
	66.903	1.931	-1.931		1.678	-1.646	-3.823
	71.452	1.709	-1.709		3.340	-.985	-3.681
	75.872	1.468	-1.468		6.623	-.013	-3.422
	80.170	1.217	-1.217		9.850	.583	-3.266
	84.352	.963	-.963		13.023	1.063	-3.098
	88.421	.715	-.715		19.213	1.672	-2.851
	92.384	.473	-.473		25.200	2.035	-2.683
	96.212	.238	-.238		30.997	2.281	-2.592
	100.000	.009	-.009		36.610	2.463	-2.553
					42.050	2.541	-2.541
0.50[c]	0	-1.407	-1.407		47.325	2.522	-2.522
	.672	-.472	-1.833		52.440	2.438	-2.438
	1.008	-.278	-1.852		57.404	2.304	-2.304
	1.678	0	-1.852		62.223	2.132	-2.132
	3.340	.509	-1.852		66.903	1.931	-1.931
	6.623	1.176	-1.870		71.452	1.709	-1.709
	9.850	1.592	-1.935		75.872	1.468	-1.468
	13.023	1.889	-2.018		80.170	1.217	-1.217
	19.213	2.176	-2.176		84.352	.963	-.963
	25.200	2.333	-2.333		88.421	.715	-.715
	30.997	2.429	-2.429		92.384	.473	-.473
	36.610	2.511	-2.511		96.212	.238	-.238
	42.050	2.541	-2.541		100.000	.009	-.009
	47.325	2.522	-2.522				
	52.440	2.438	-2.438	1.00[f]	0	-4.942	-4.942
	57.404	2.304	-2.304		.672	-3.678	-5.541
	62.223	2.132	-2.132		1.008	-3.516	-5.557
	66.903	1.931	-1.931		1.678	-3.159	-5.509
	71.452	1.709	-1.709		3.340	-2.447	-5.298
	75.872	1.468	-1.468		6.623	-1.442	-4.974
	80.170	1.217	-1.217		9.850	-.648	-4.666
	84.352	.963	-.963		13.023	-.065	-4.391
	88.421	.715	-.715		19.213	.681	-3.905
	92.384	.473	-.473		25.200	1.215	-3.500
	96.212	.238	-.238		30.997	1.620	-3.240
	100.000	.009	-.009		36.610	1.944	-3.046
					42.050	2.139	-2.900
0.67[d]	0	-2.192	-2.192		47.325	2.268	-2.738
	.672	-1.134	-2.668		52.440	2.285	-2.544
	1.008	-.961	-2.700		57.404	2.251	-2.333
	1.678	-.670	-2.689		62.223	2.132	-2.132
	3.340	-.108	-2.603		66.903	1.931	-1.931
	6.623	.724	-2.495		71.452	1.709	-1.709
	9.850	1.296	-2.441		75.872	1.468	-1.468
	13.023	1.631	-2.408		80.170	1.217	-1.217
	19.213	2.084	-2.376		84.352	.963	-.963
	25.200	2.322	-2.398		88.421	.715	-.715
	30.997	2.429	-2.441		92.384	.473	-.473
	36.610	2.511	-2.511		96.212	.238	-.238
	42.050	2.541	-2.541		100.000	.009	-.009

[a] Leading-edge radius: 0.190 percent chord
[b] Leading-edge radius: 0.236 percent chord
[c] Leading-edge radius: 0.370 percent chord
[d] Leading-edge radius: 0.520 percent chord
[e] Leading-edge radius: 0.713 percent chord
[f] Leading-edge radius: 0.924 percent chord

[redacted]

Equation of body coordinates

$$\frac{r}{r_0} = \left[1 - \left(1 - \frac{2x}{l}\right)^2\right]^{\frac{3}{4}}$$

Note: 1. All dimensions in inches unless otherwise noted
2. All wing dimensions for a projected plan form

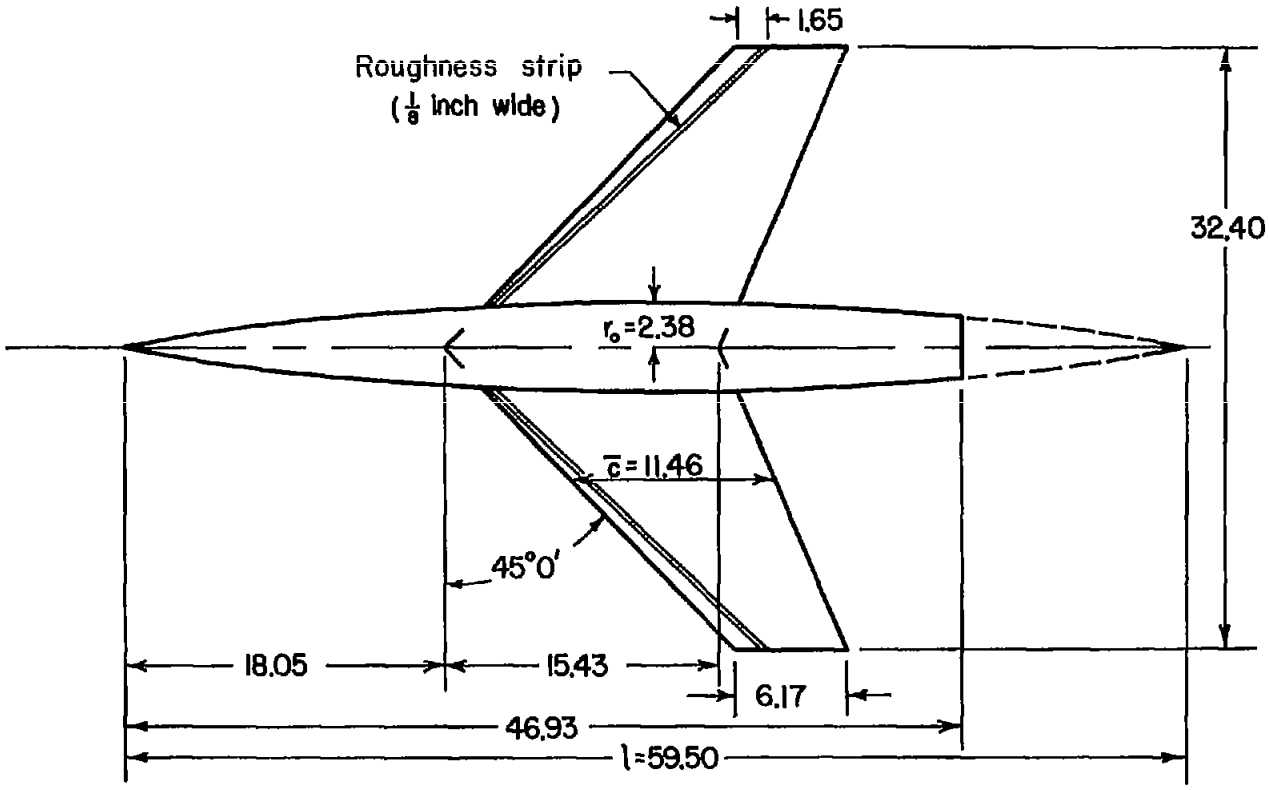

Figure 1.- Model arrangement.

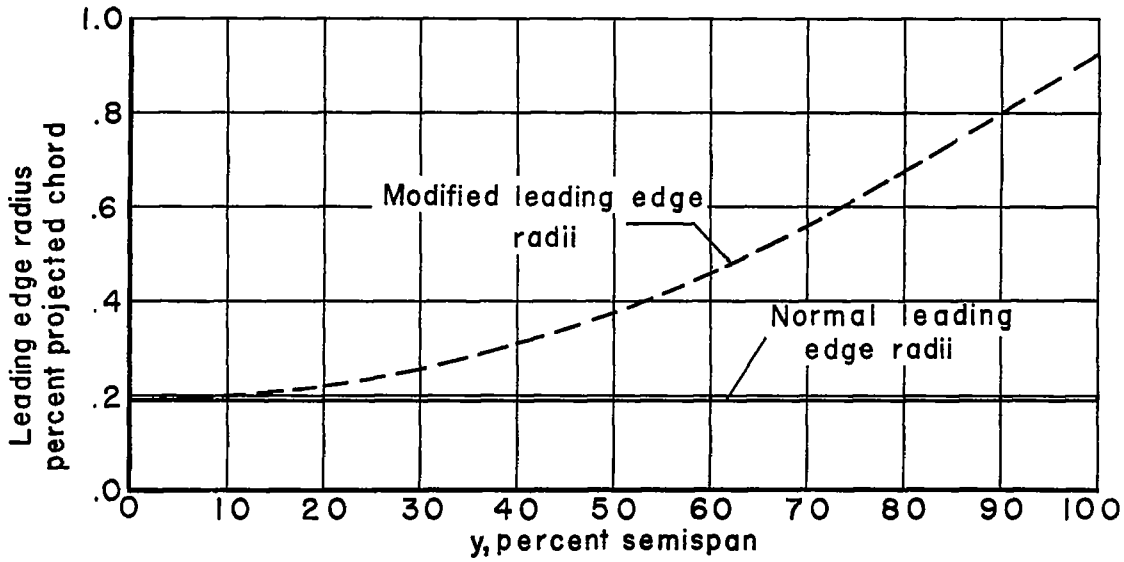

Figure 2.- Comparison of normal and modified leading-edge radii for swept-back wings.

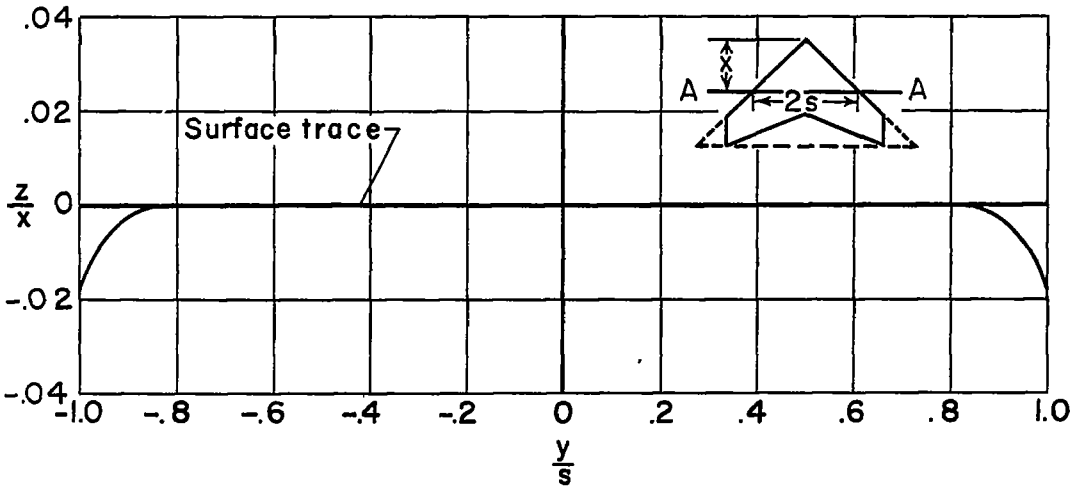

Figure 3.- The mean-surface shape of the conically cambered sweptback wing, $C_{L_d} = 0.29$.

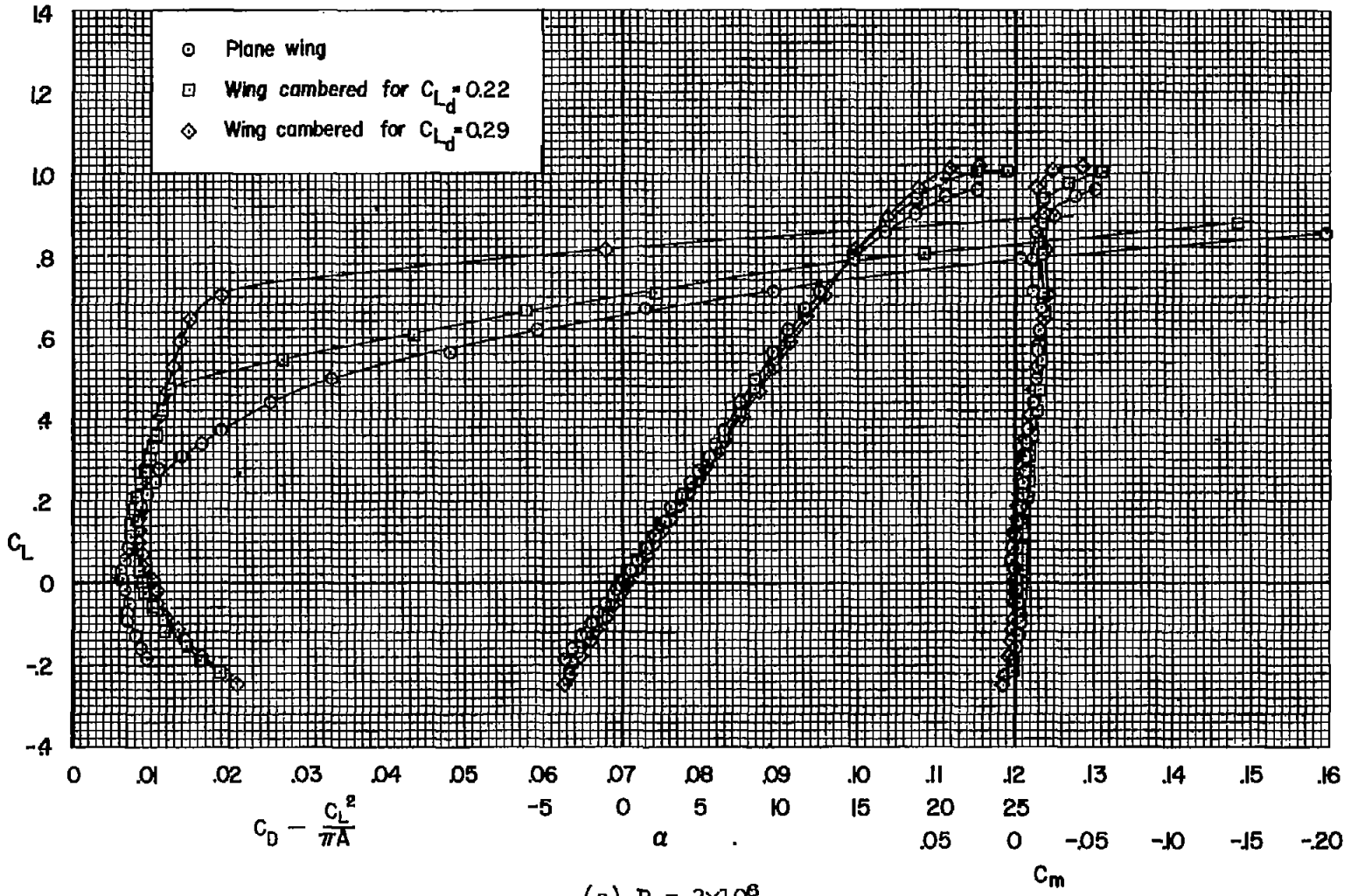

(a) R = 3×10^6

Figure 4.- Effect of conical camber on the drag, lift, and pitching moment; without roughness, M = 0.22.

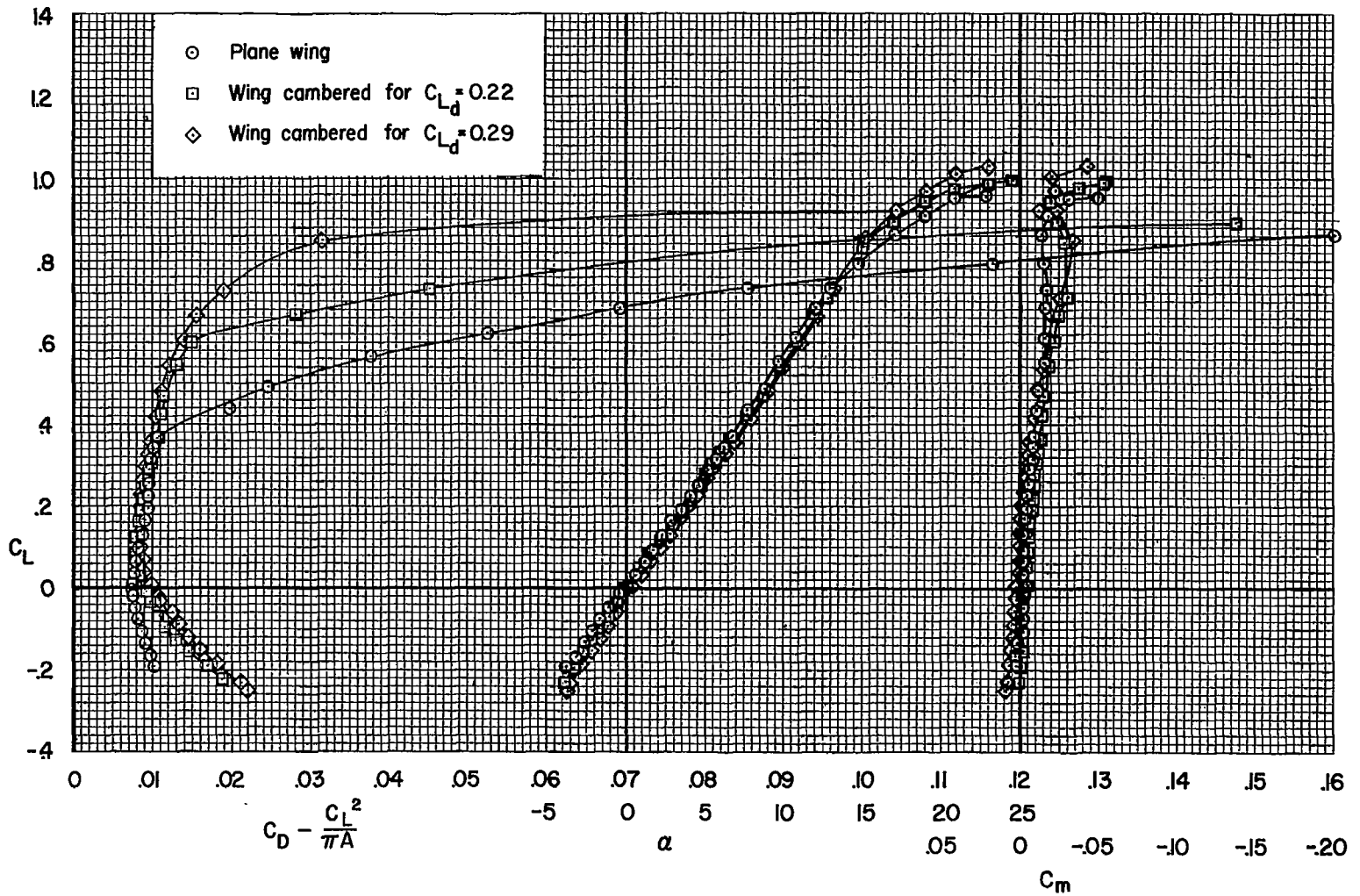

(b) R = 6×10^6

Figure 4.- Continued.

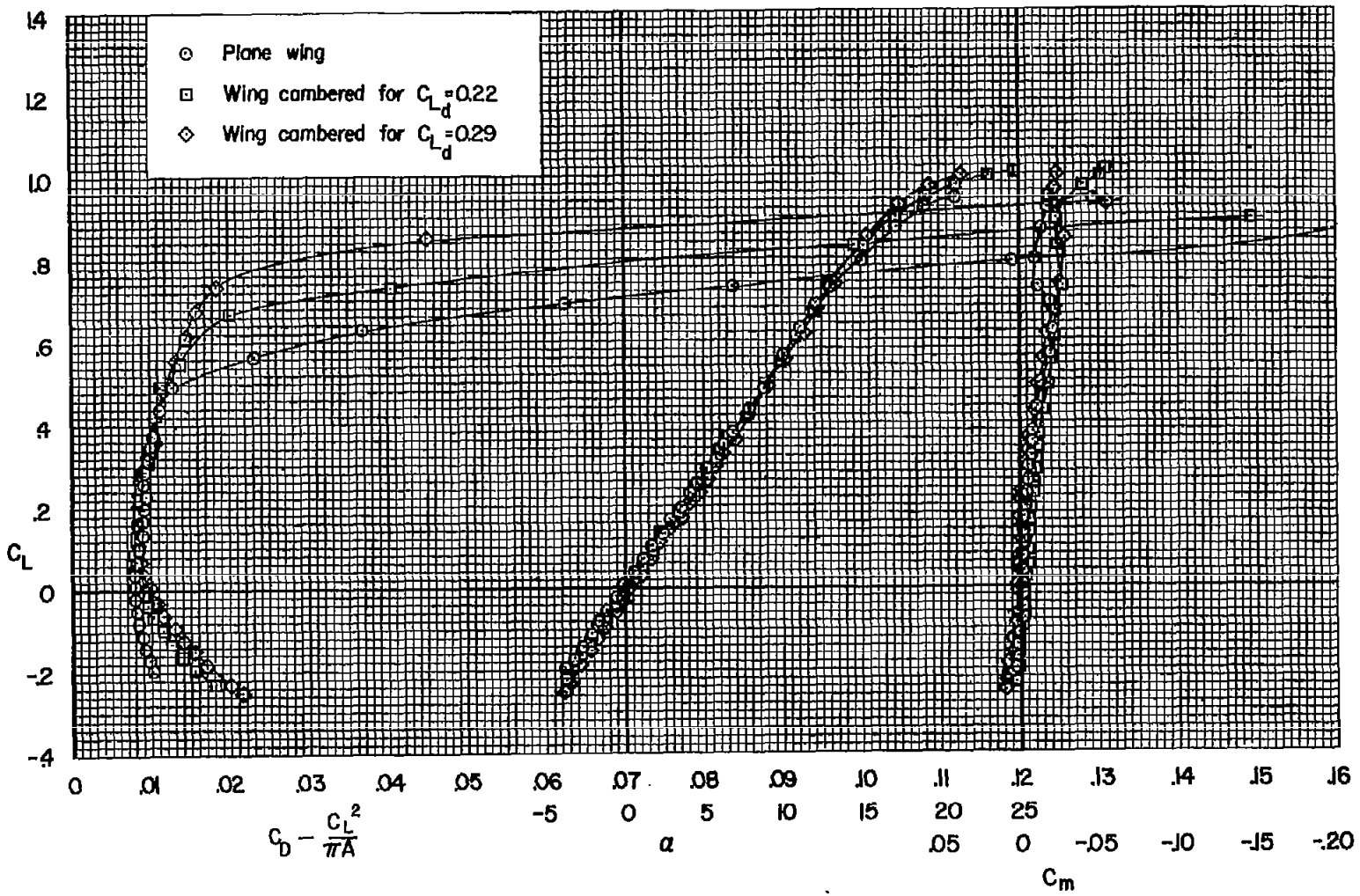

(c) R = 8×10^6

Figure 4.- Concluded.

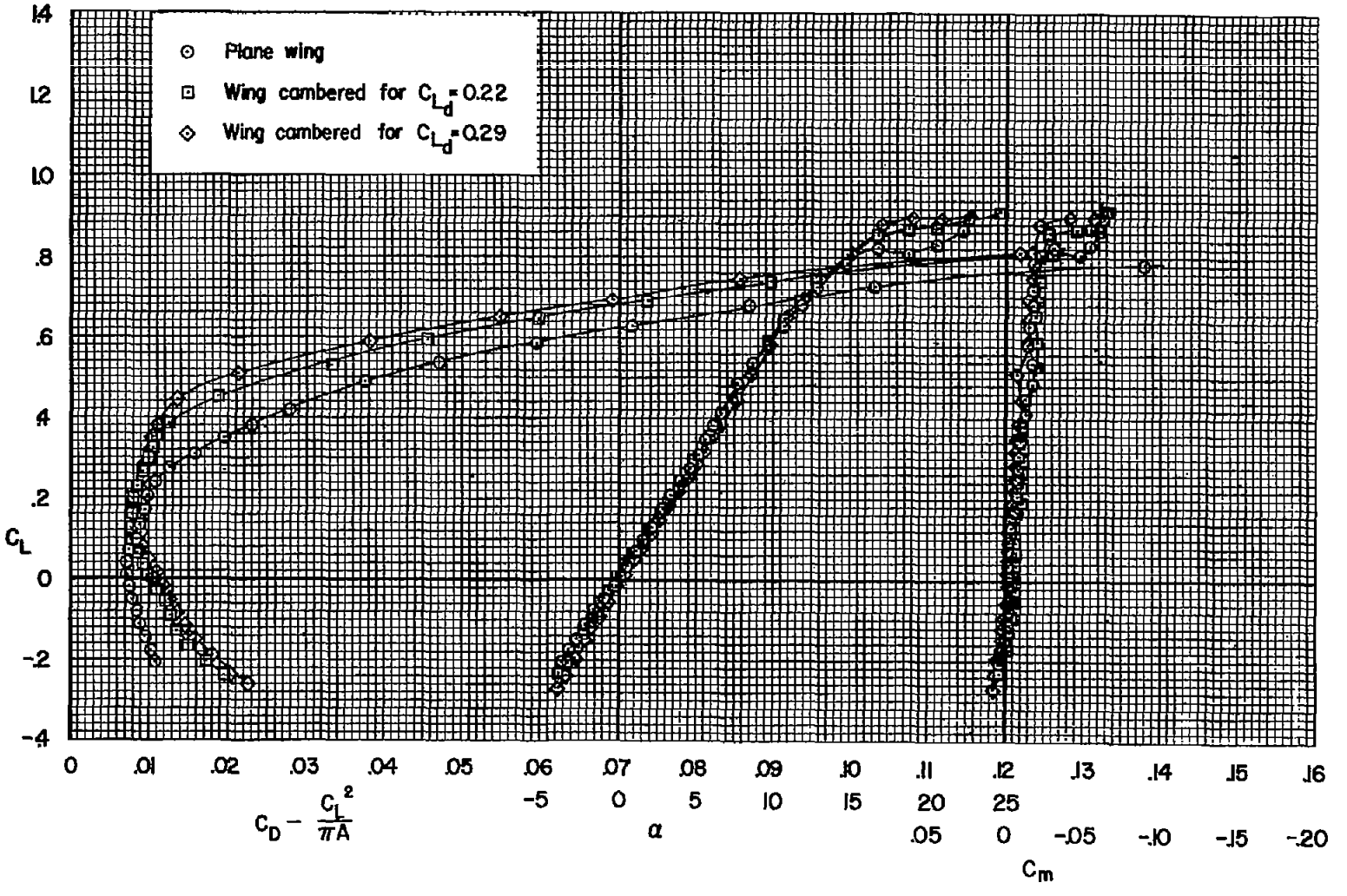

(a) R = 1.5×10^6

Figure 5.- Effect of conical camber on the drag, lift, and pitching moment; without roughness, M = 0.60.

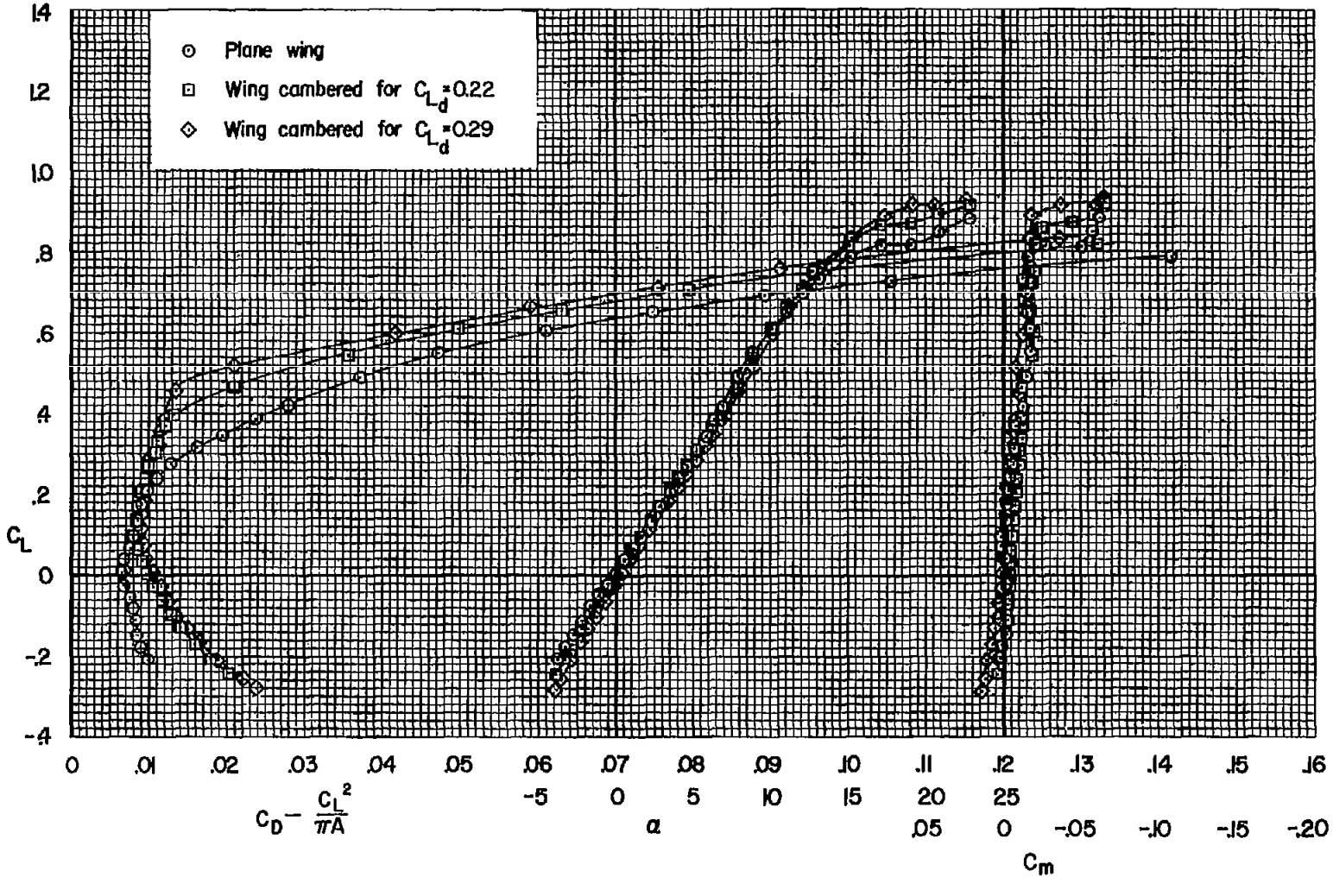

(b) R = 2.86×10⁶

Figure 5.- Concluded.

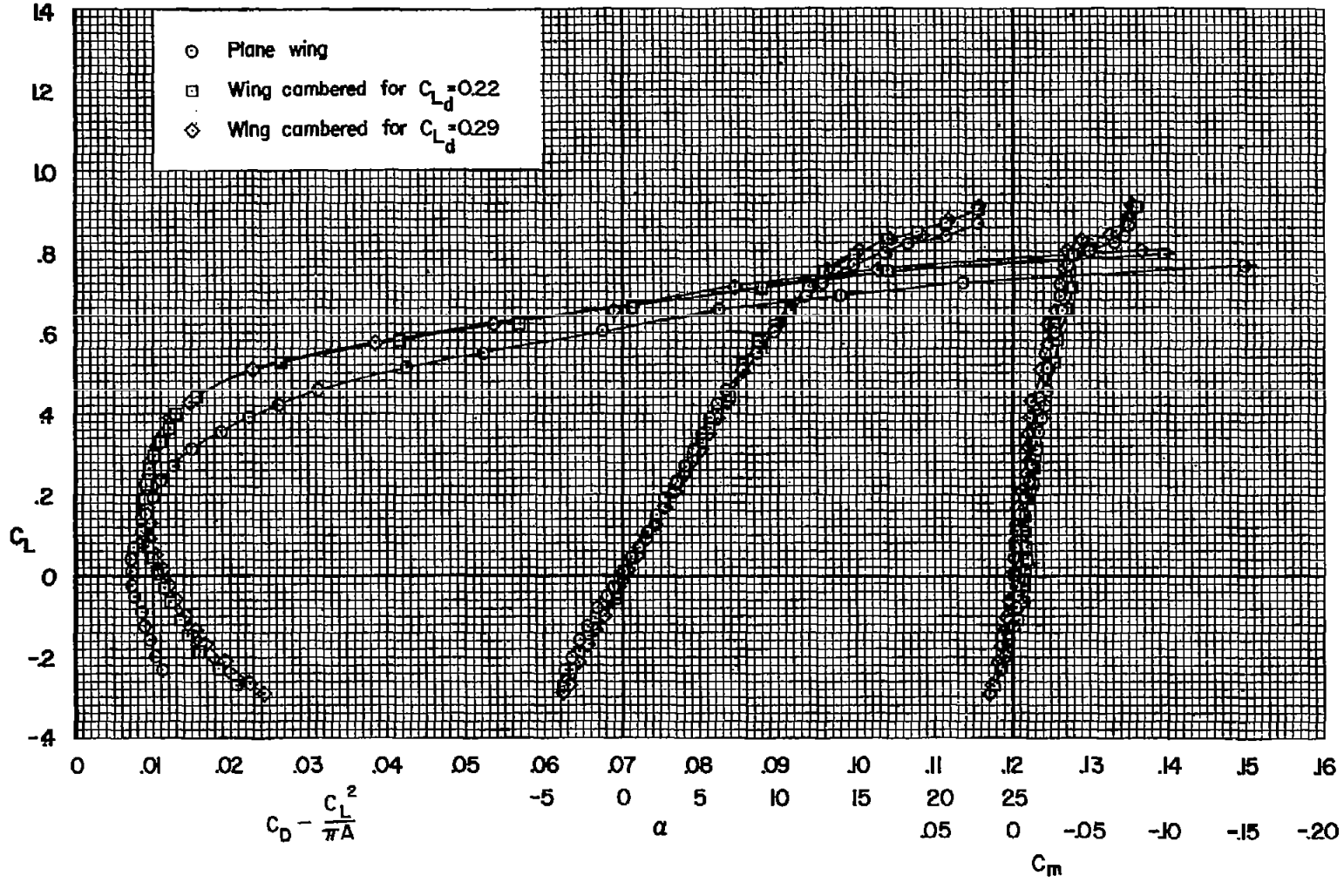

(a) M = 0.80

Figure 6.- Effect of conical camber on the drag, lift, and pitching moment; without roughness, $R = 1.5 \times 10^6$.

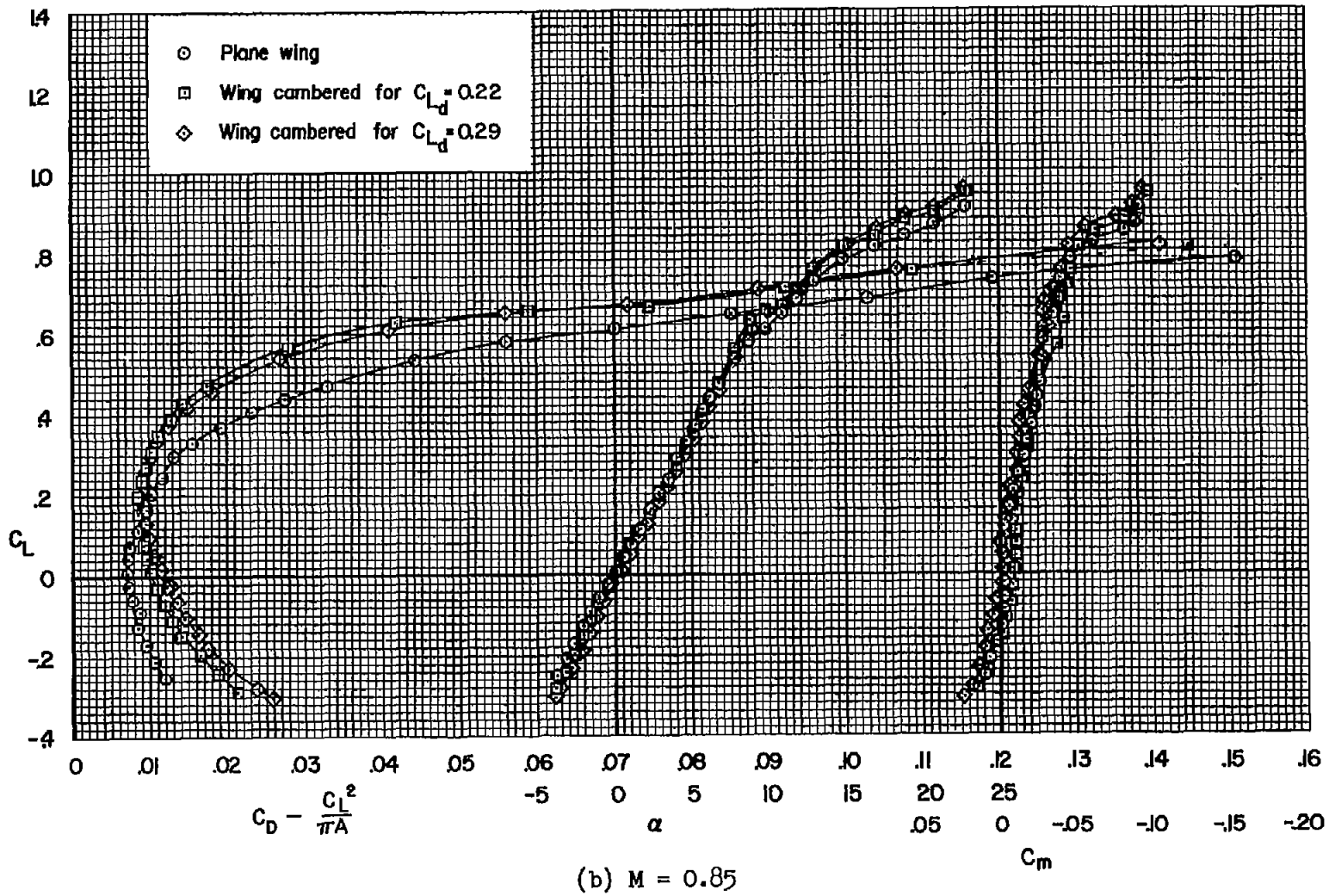

(b) M = 0.85

Figure 6.- Continued.

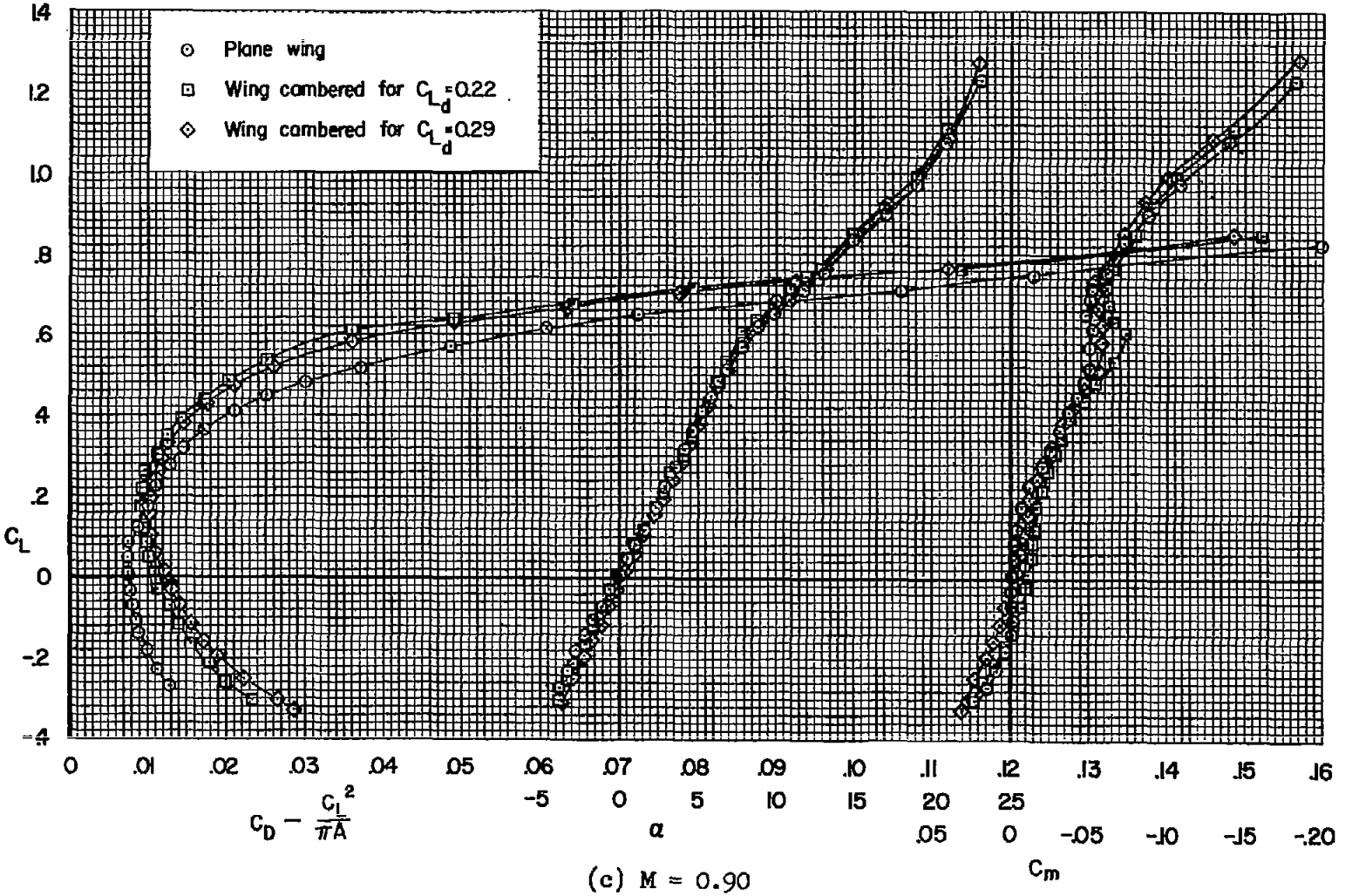

(c) M = 0.90

Figure 6.- Continued.

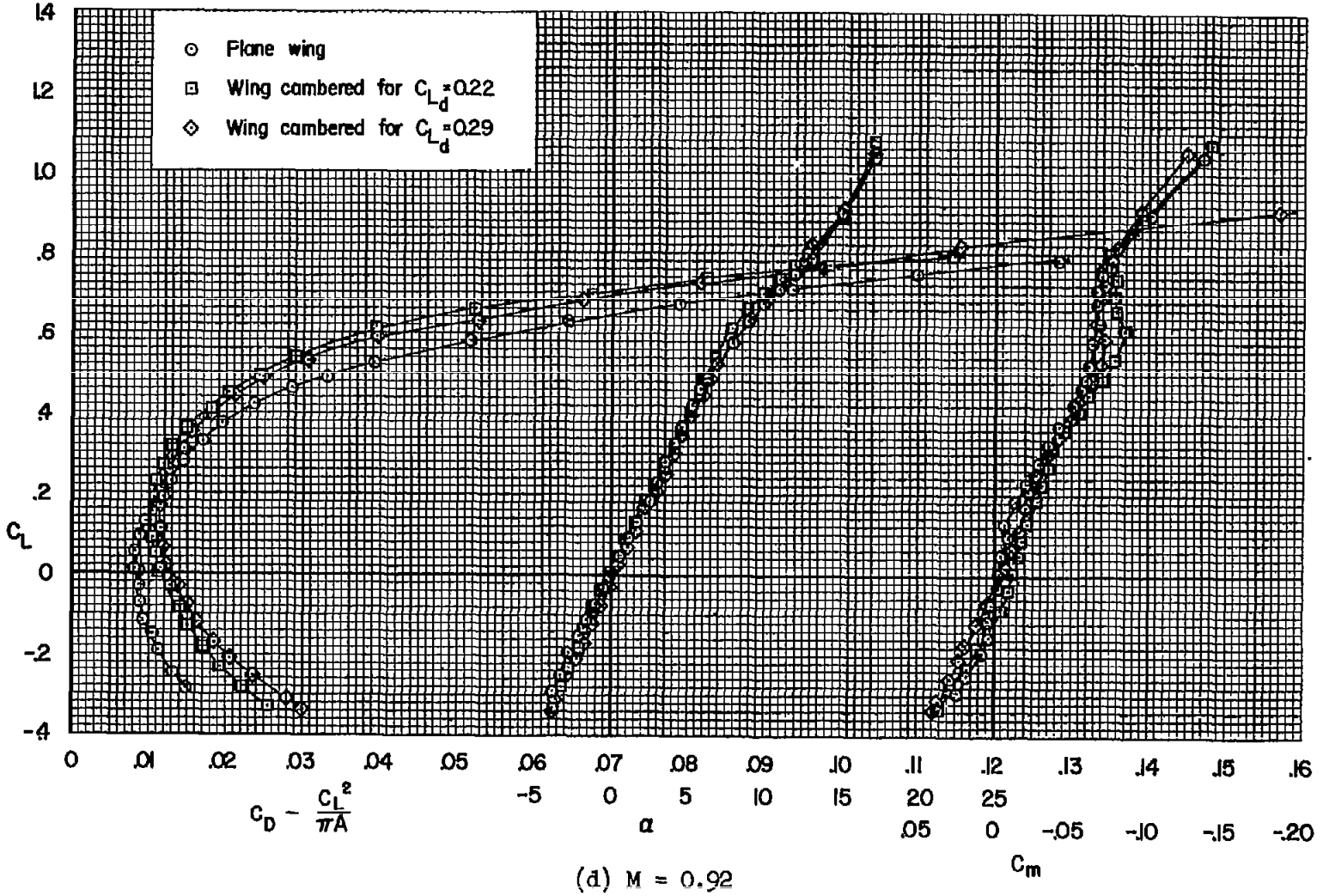

(d) M = 0.92

Figure 6.- Continued.

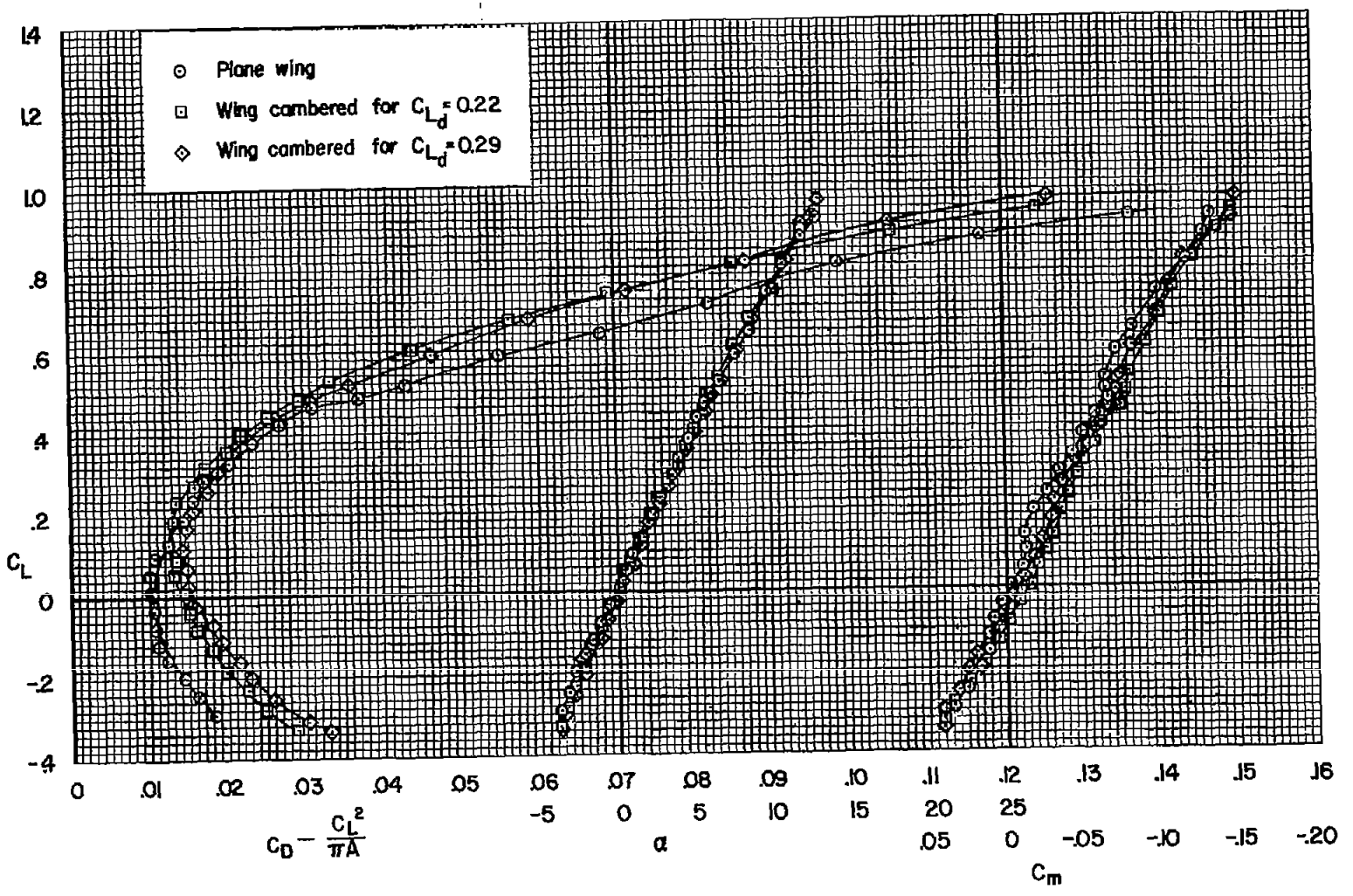

(e) M = 0.94

Figure 6.- Continued.

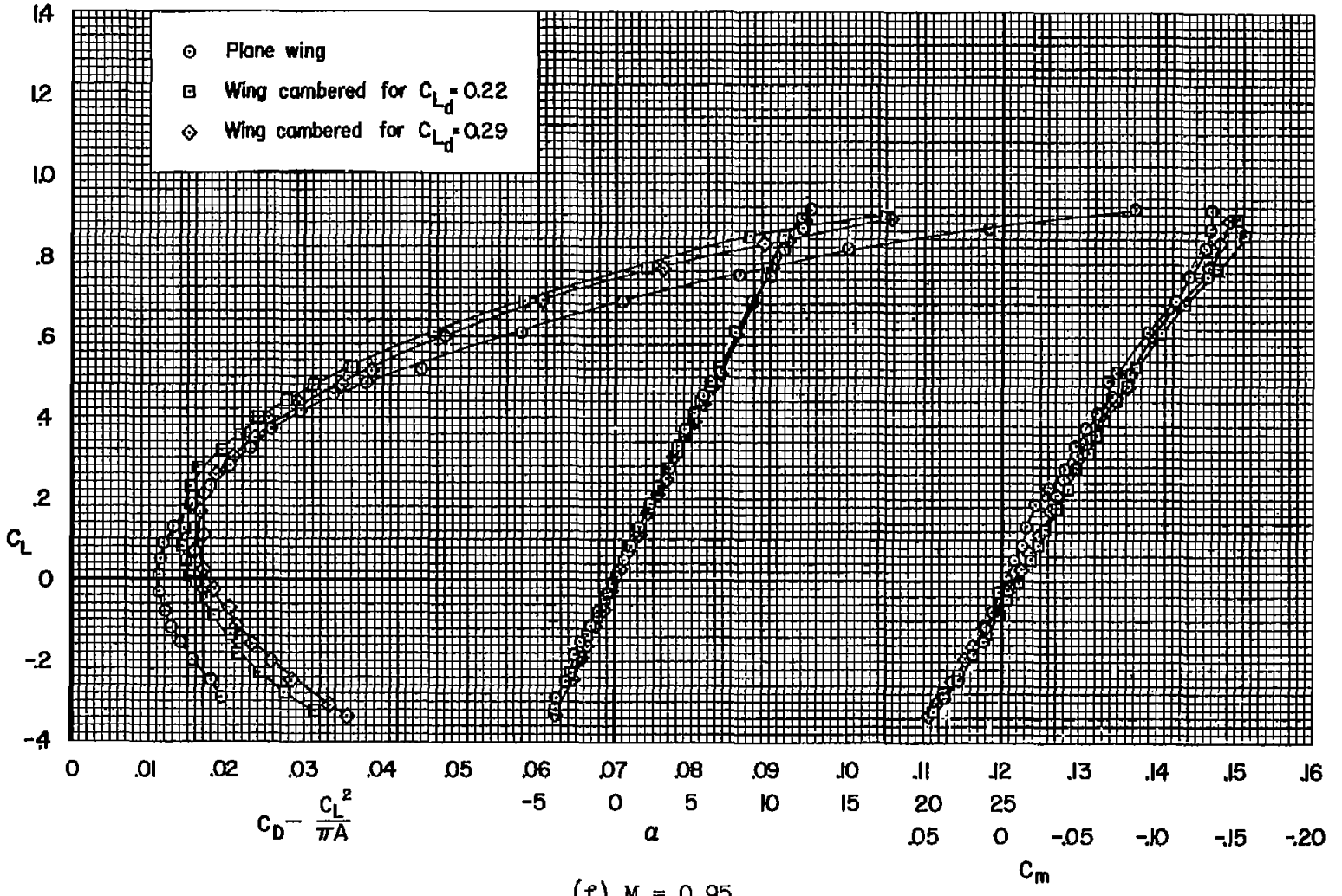

(f) M = 0.95

Figure 6.- Continued.

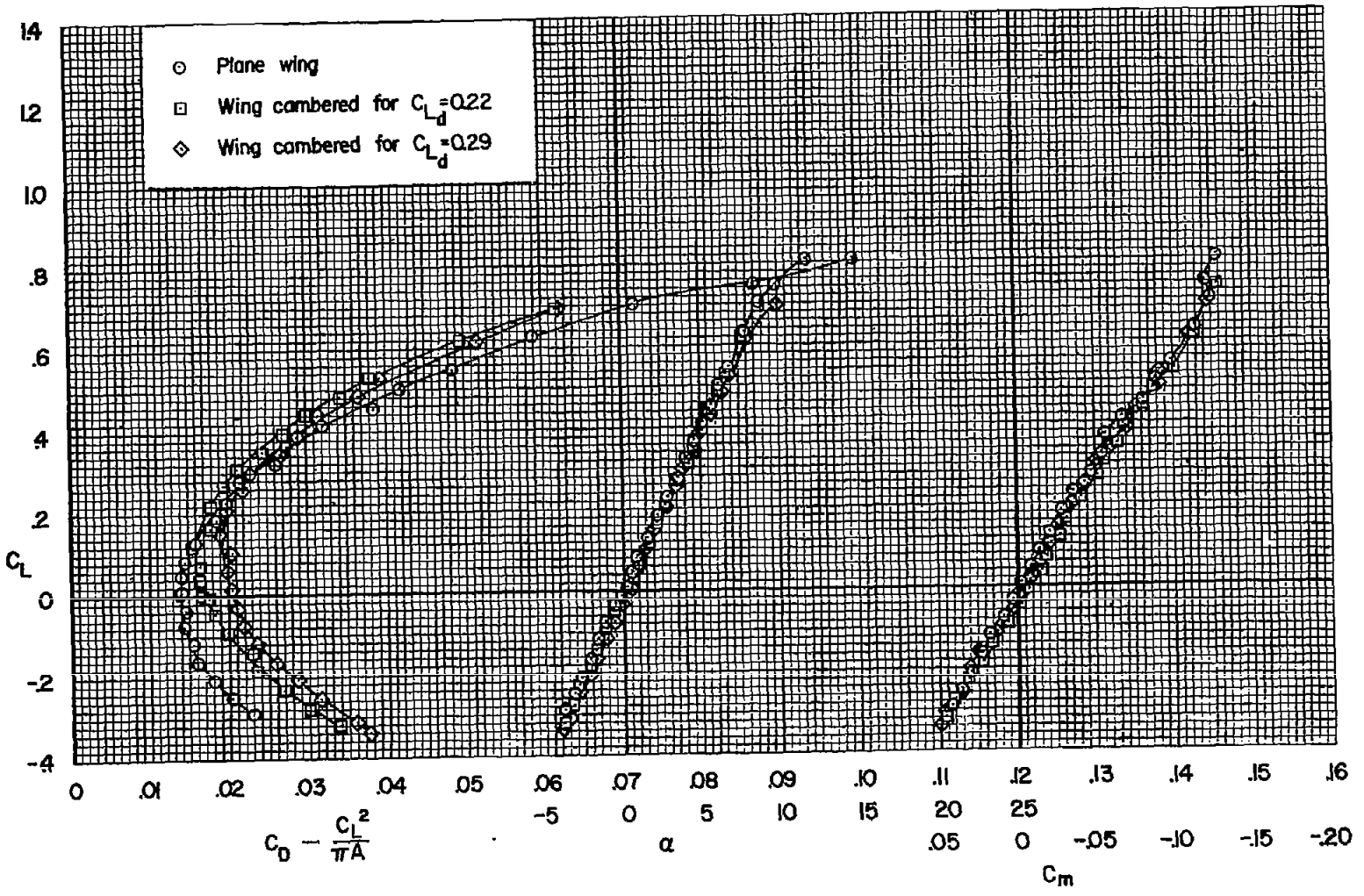

(g) M = 0.96

Figure 6.- Concluded.

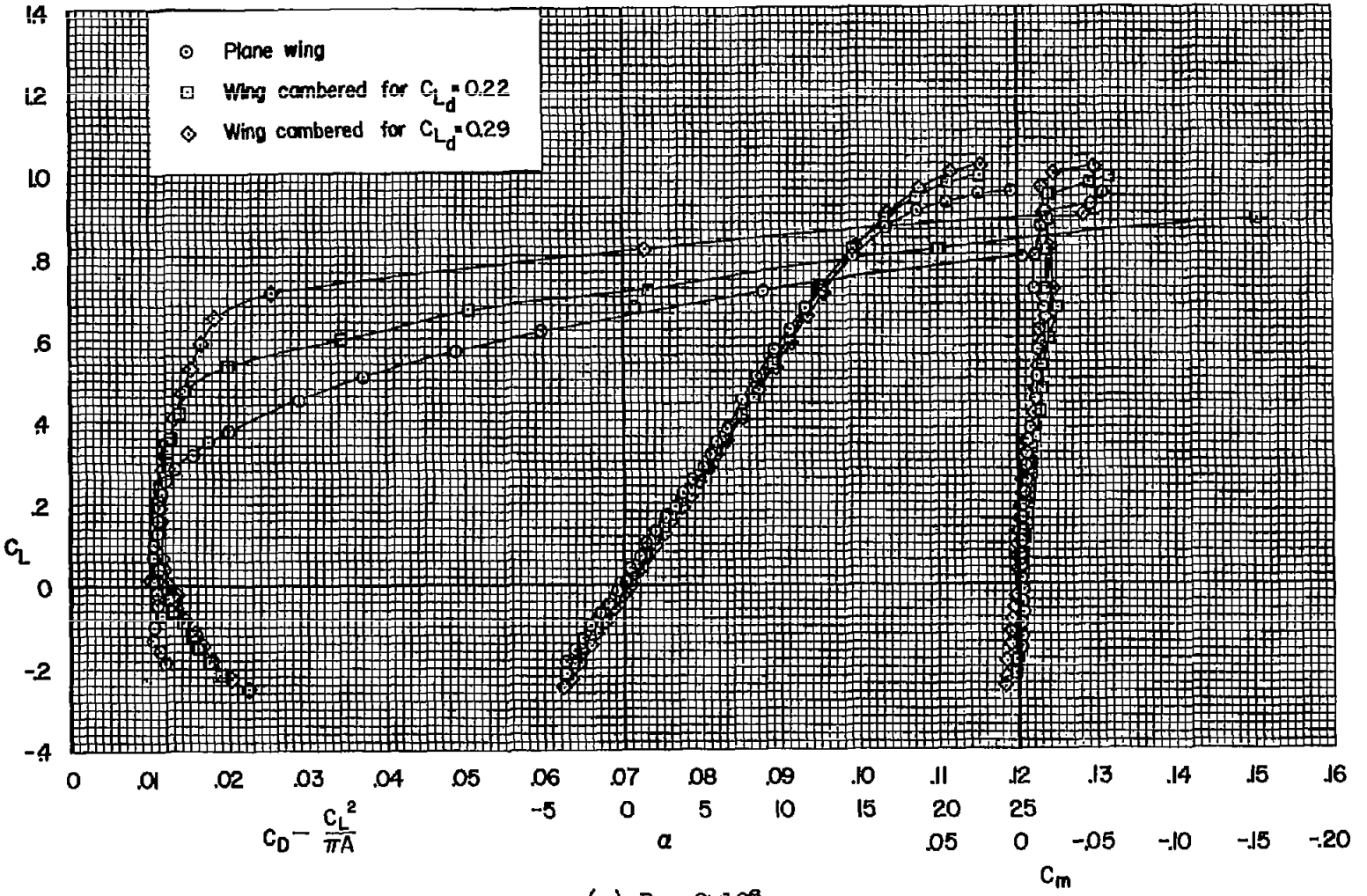

(a) R = 3×10^6

Figure 7.- Effect of conical camber on the drag, lift, and pitching moment; with roughness, M = 0.22.

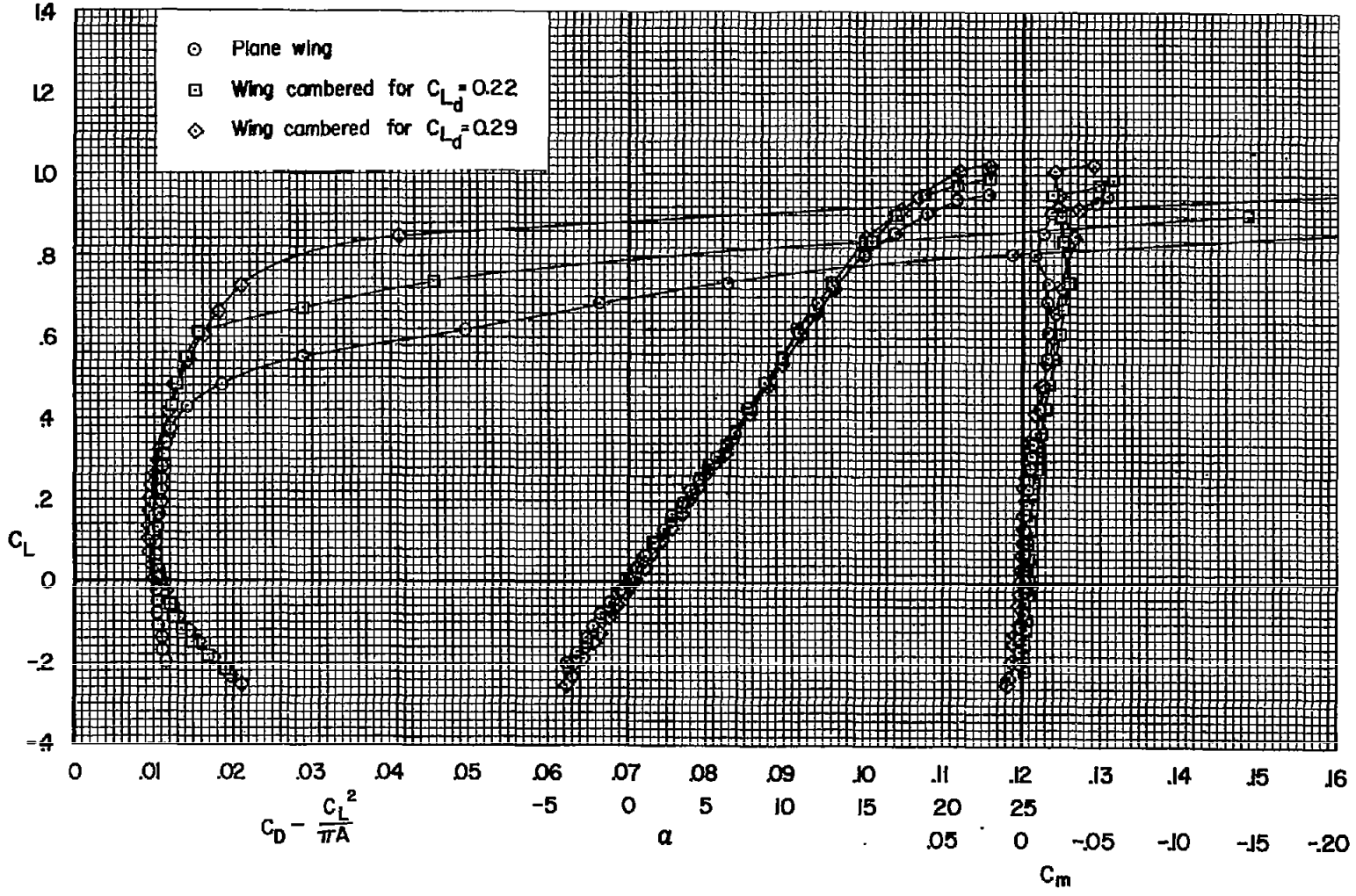

(b) R = 6×10^6

Figure 7.- Continued.

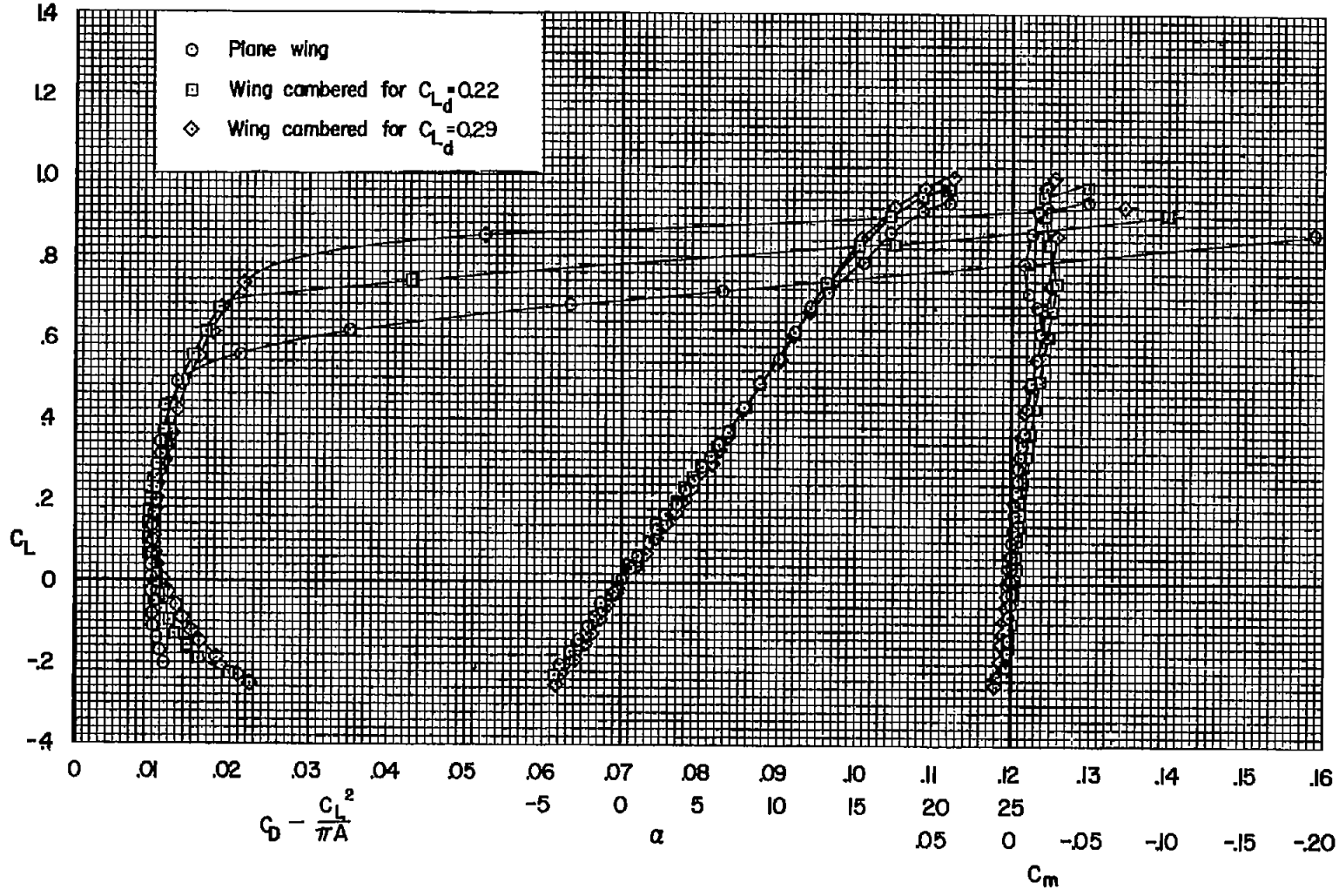

(c) R = 8x10^6

Figure 7.- Concluded.

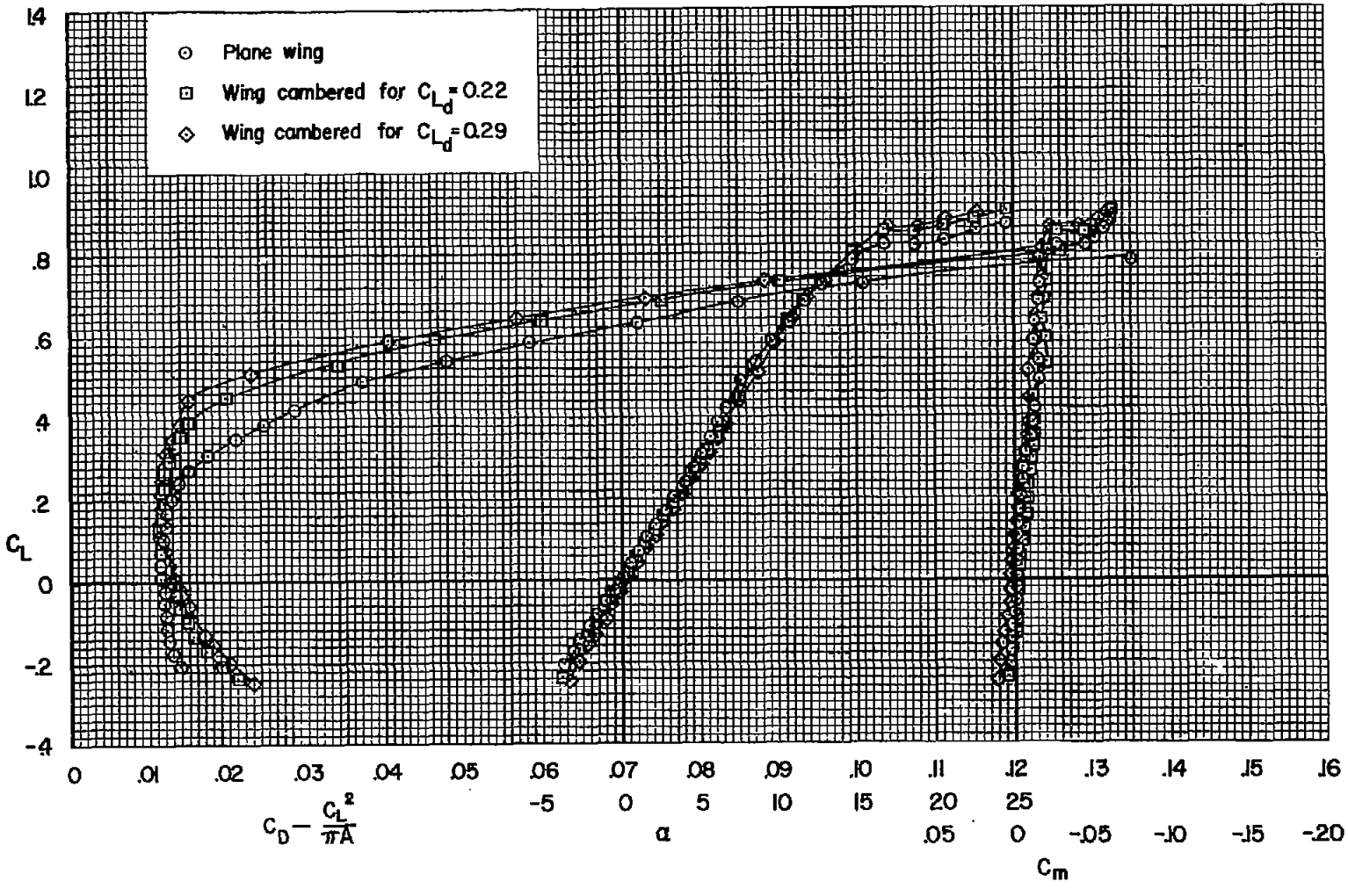

(a) R = 1.5×10^6

Figure 8.- Effect of conical camber on the drag, lift, and pitching moment; with roughness, M = 0.60.

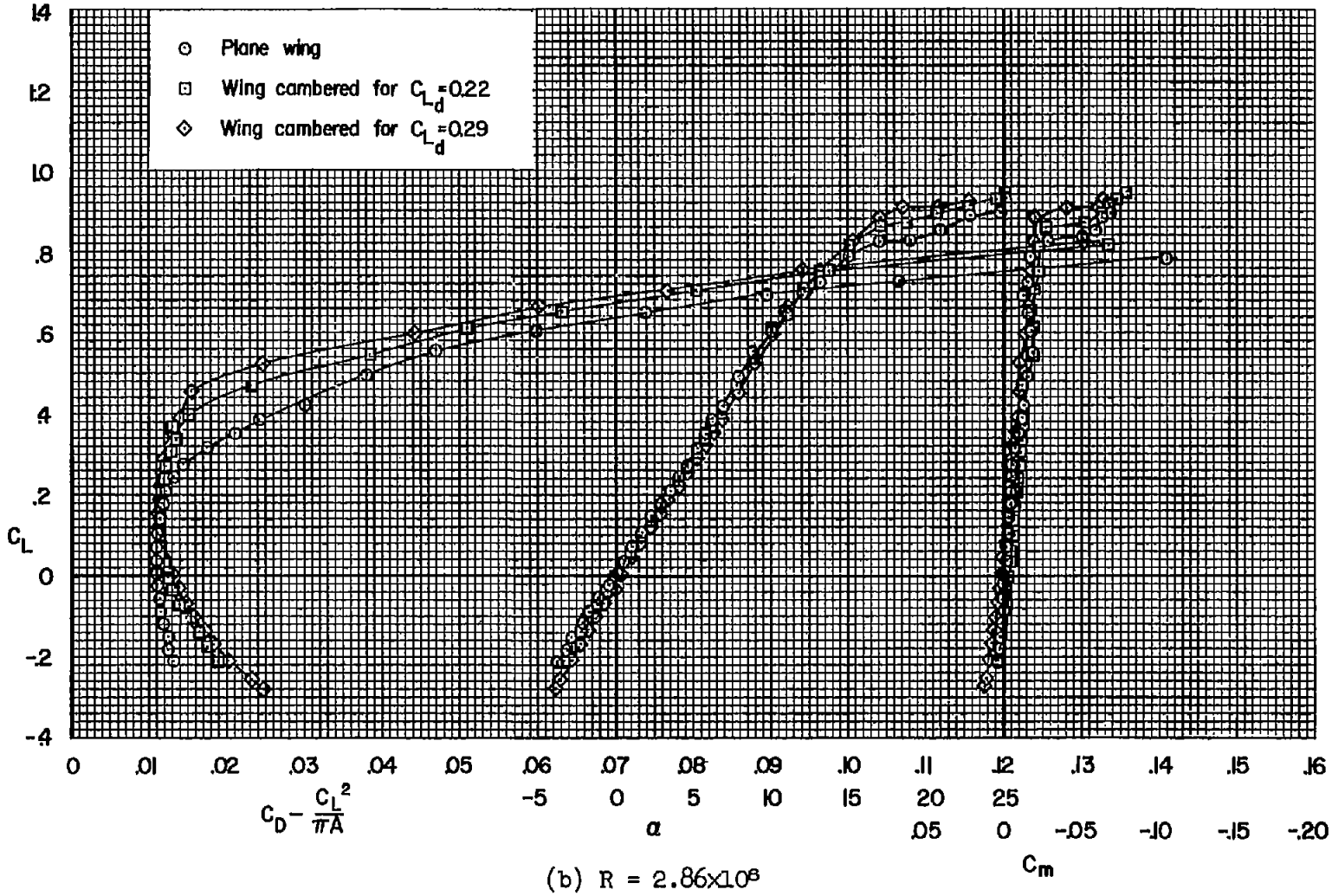

(b) R = 2.86×10^6

Figure 8.- Concluded.

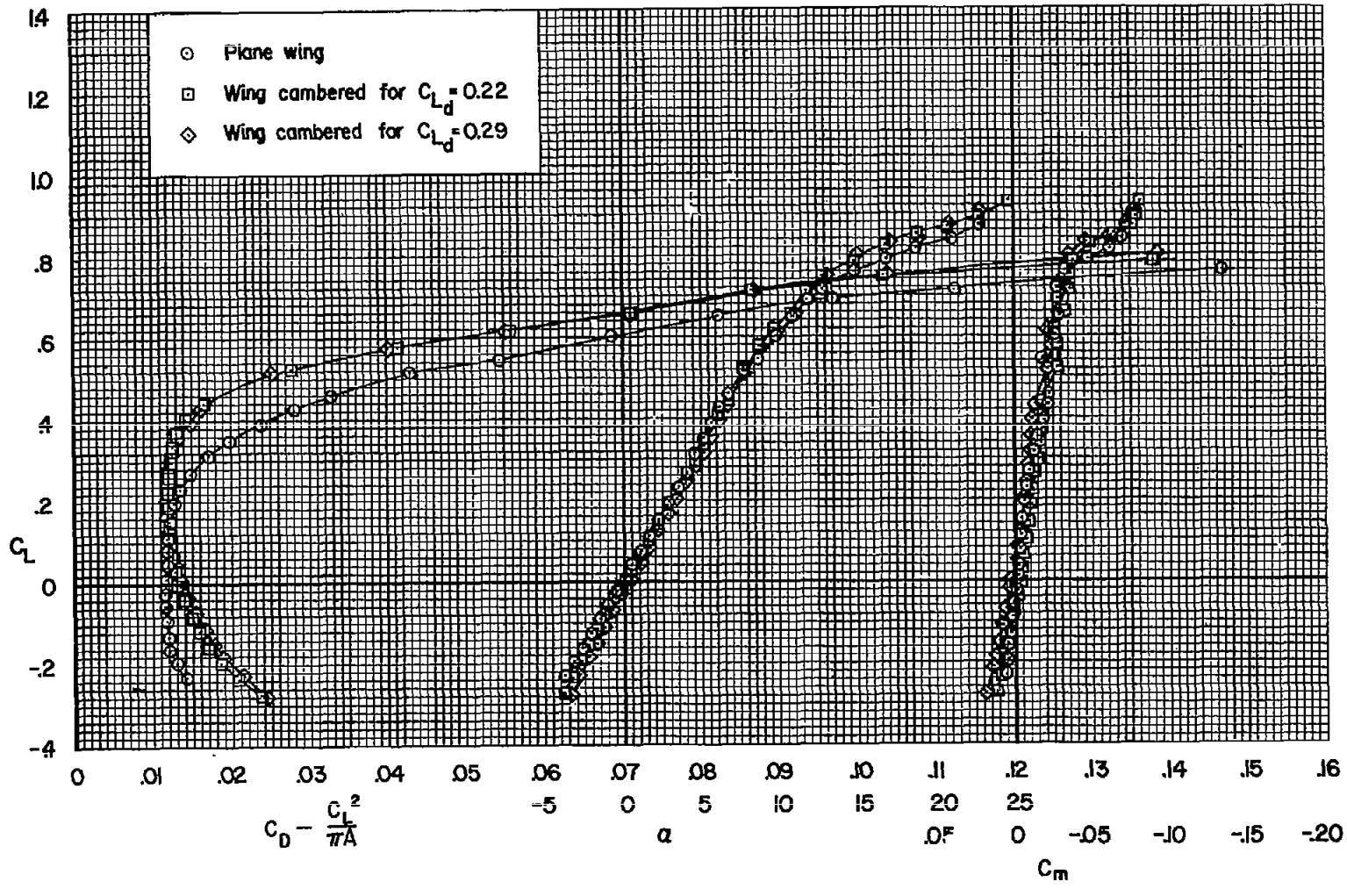

(a) M = 0.80

Figure 9.- Effect of conical camber on the drag, lift, and pitching moment; with roughness, $R = 1.5 \times 10^6$.

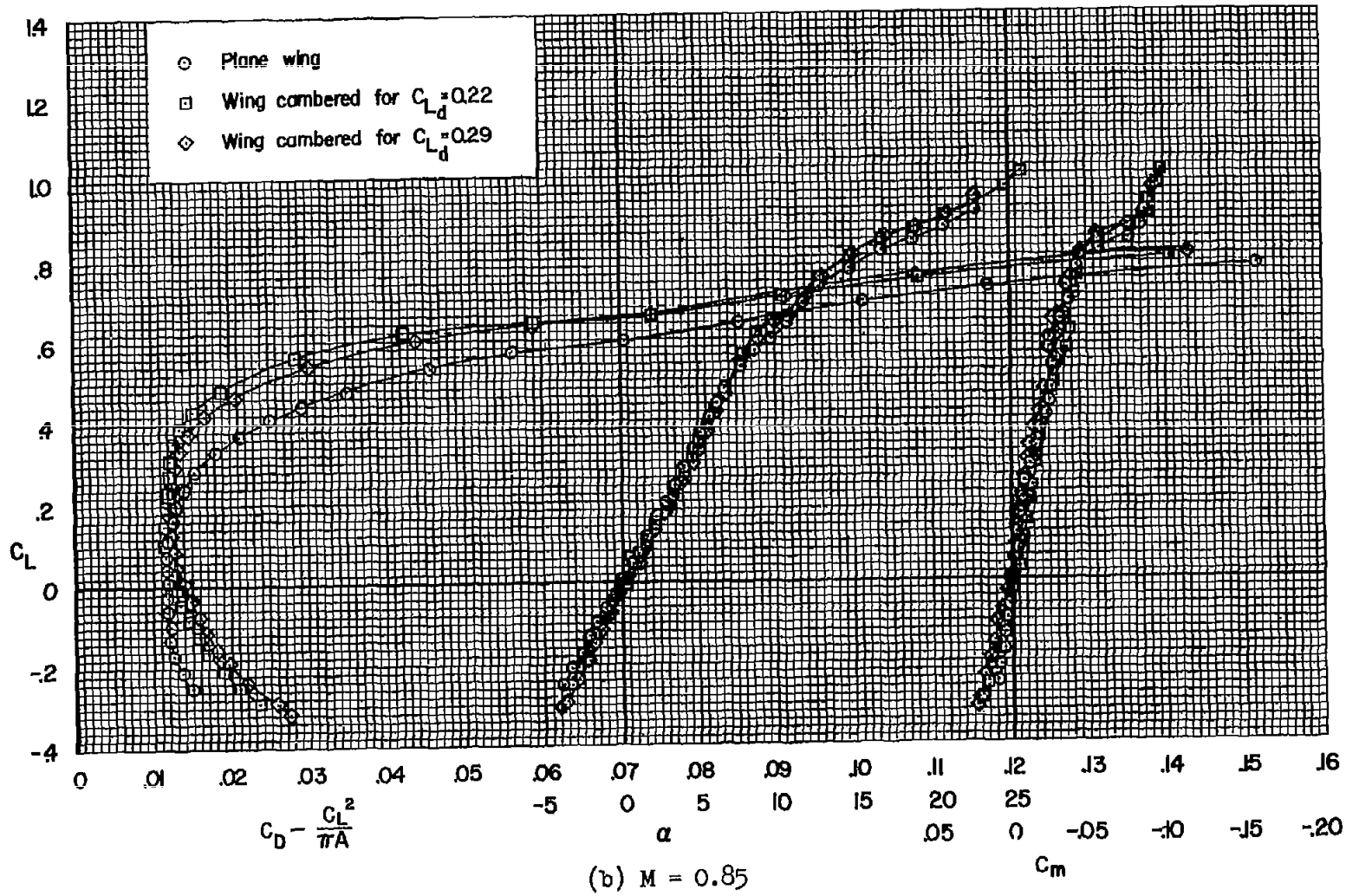

(b) M = 0.85

Figure 9.- Continued.

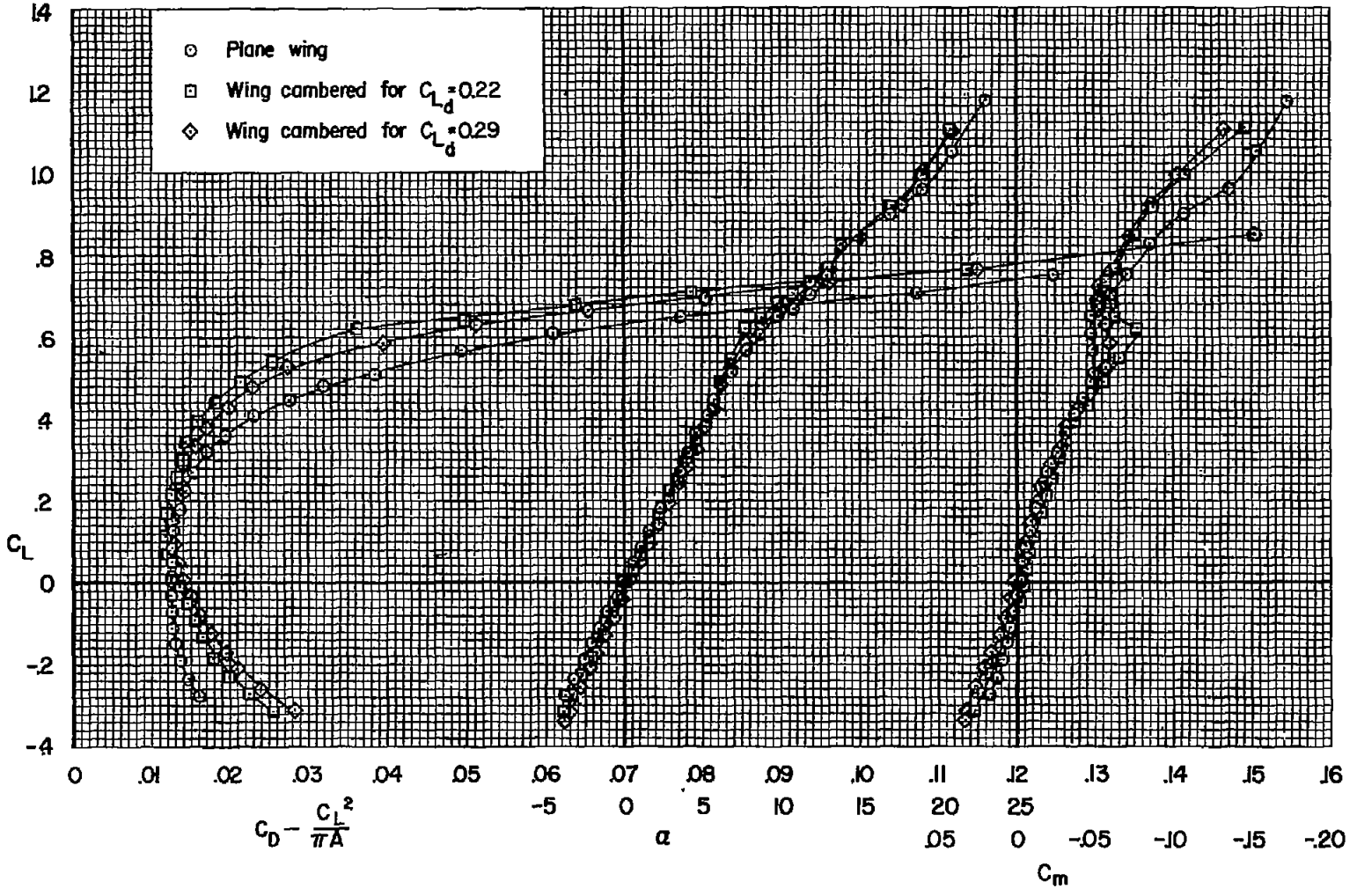

(c) M = 0.90

Figure 9.- Continued.

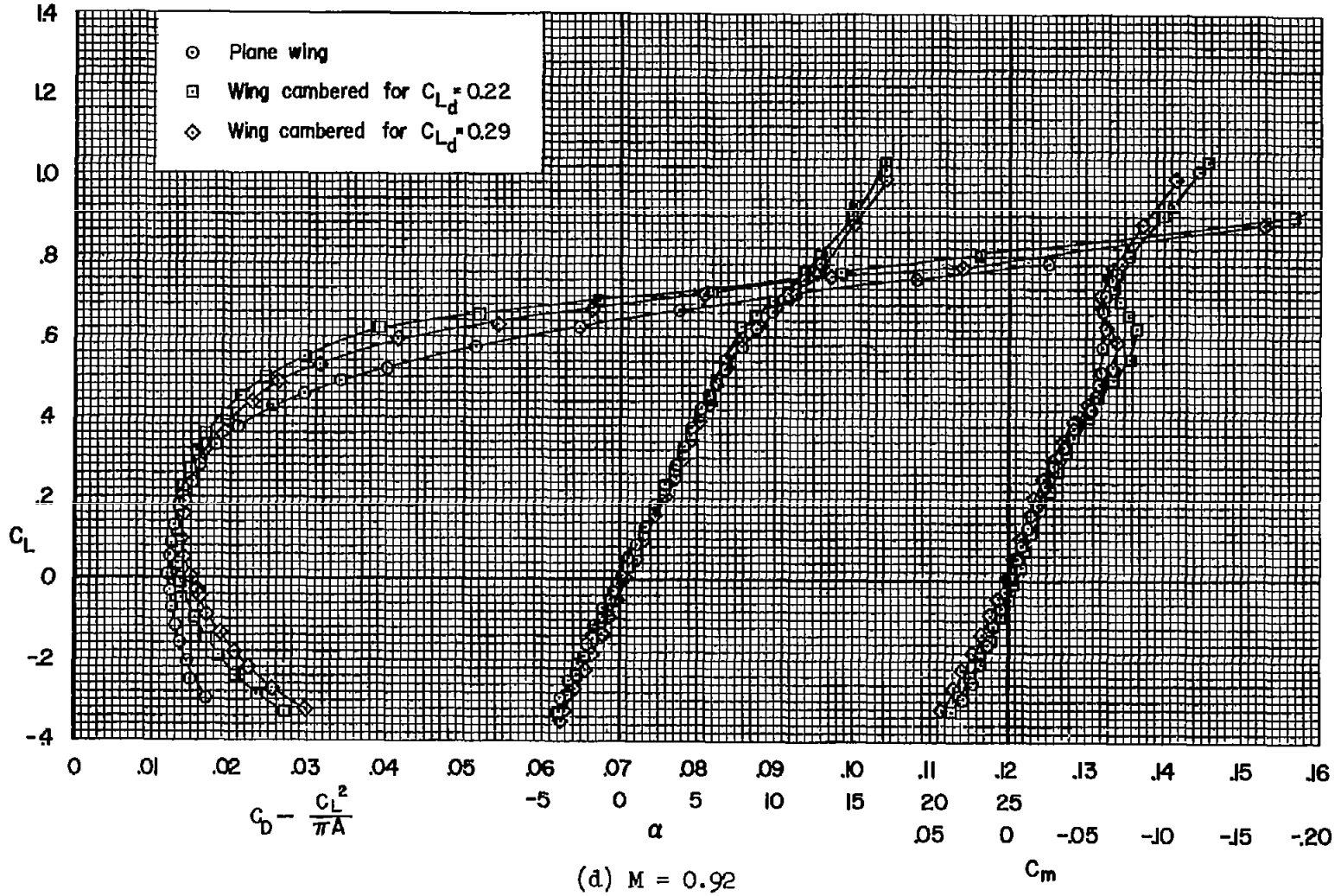

(d) M = 0.92

Figure 9.- Continued.

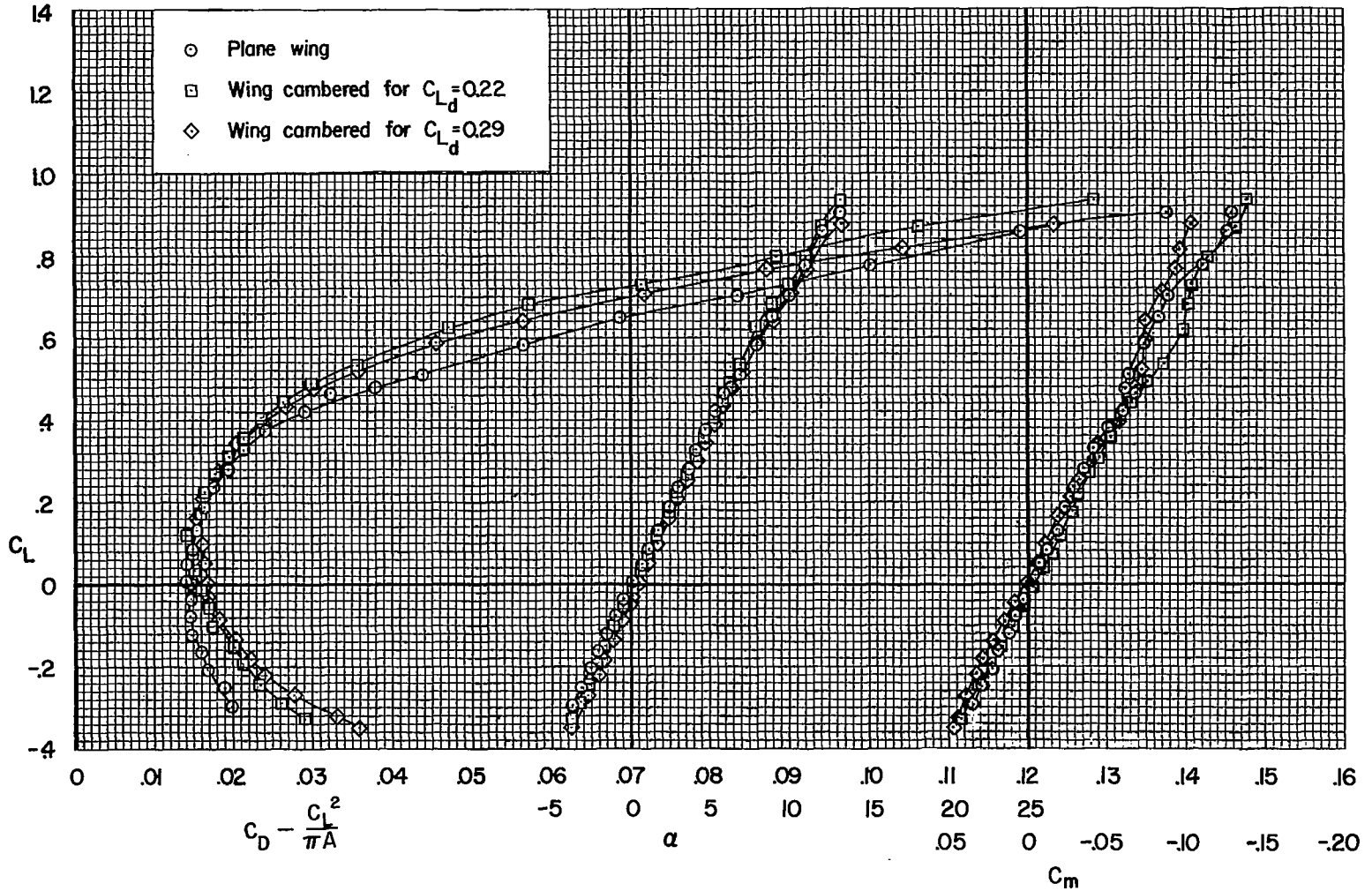

(e) M = 0.94

Figure 9.- Continued.

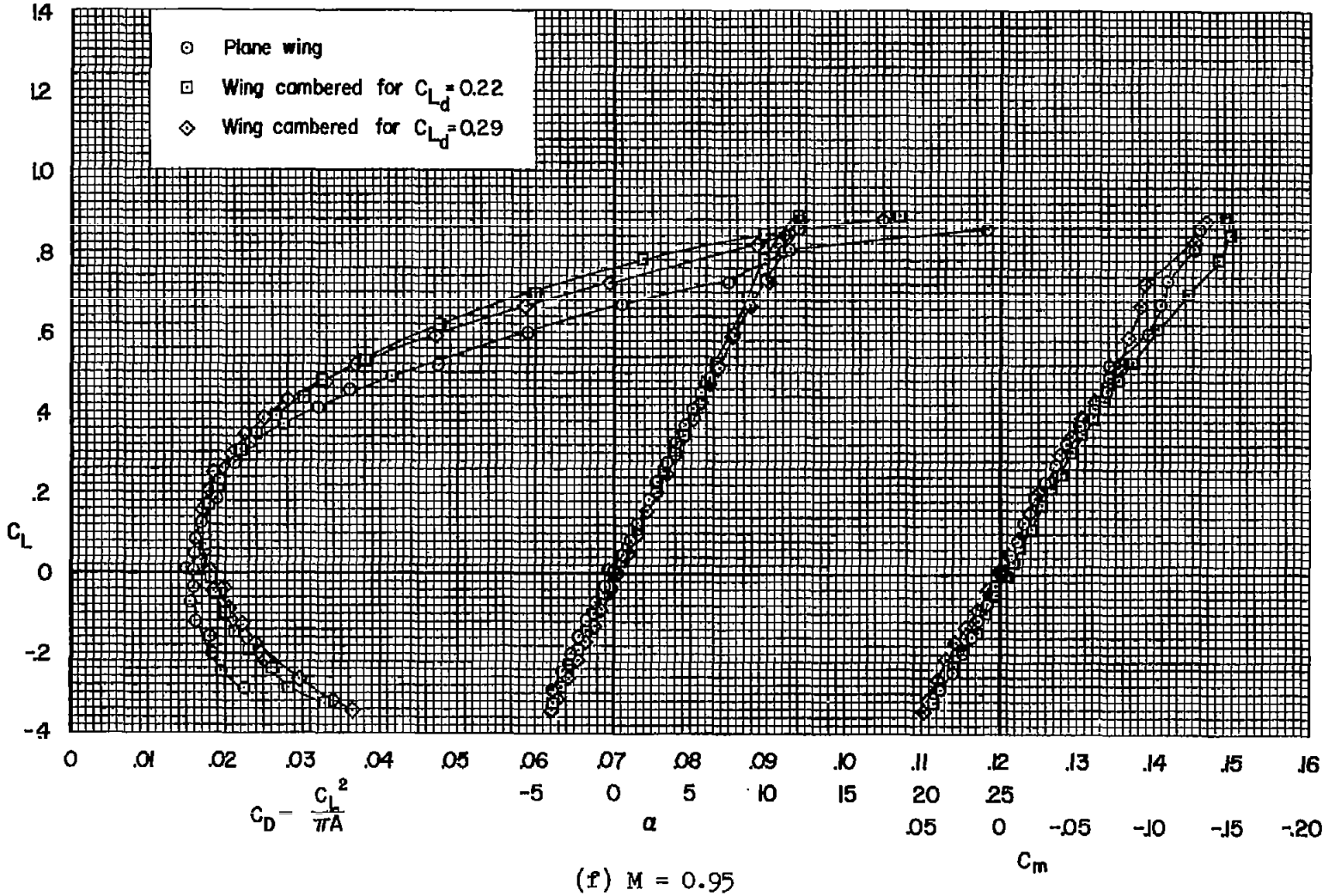

(f) M = 0.95

Figure 9.- Continued.

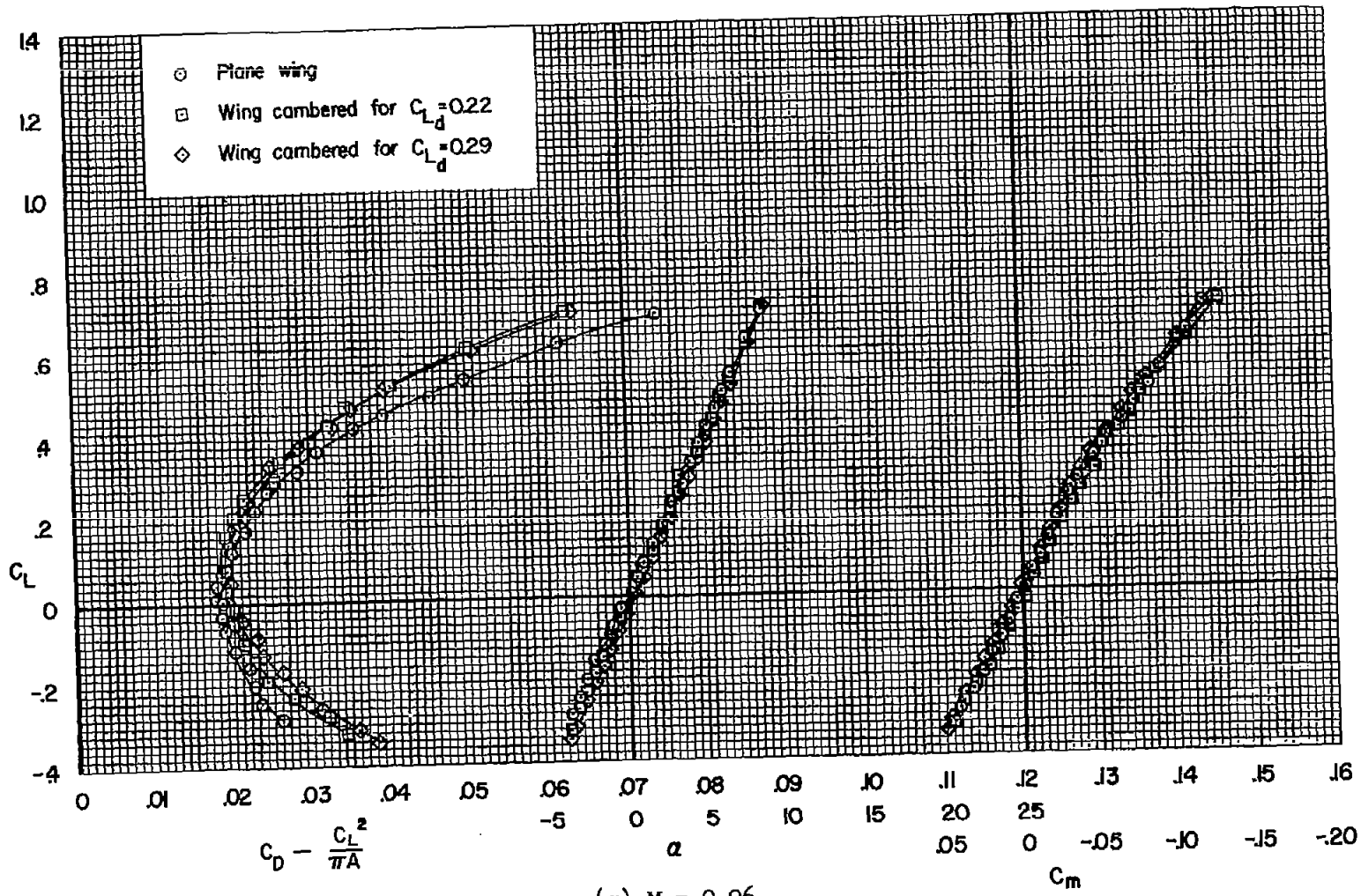

(g) M = 0.96

Figure 9.- Concluded.

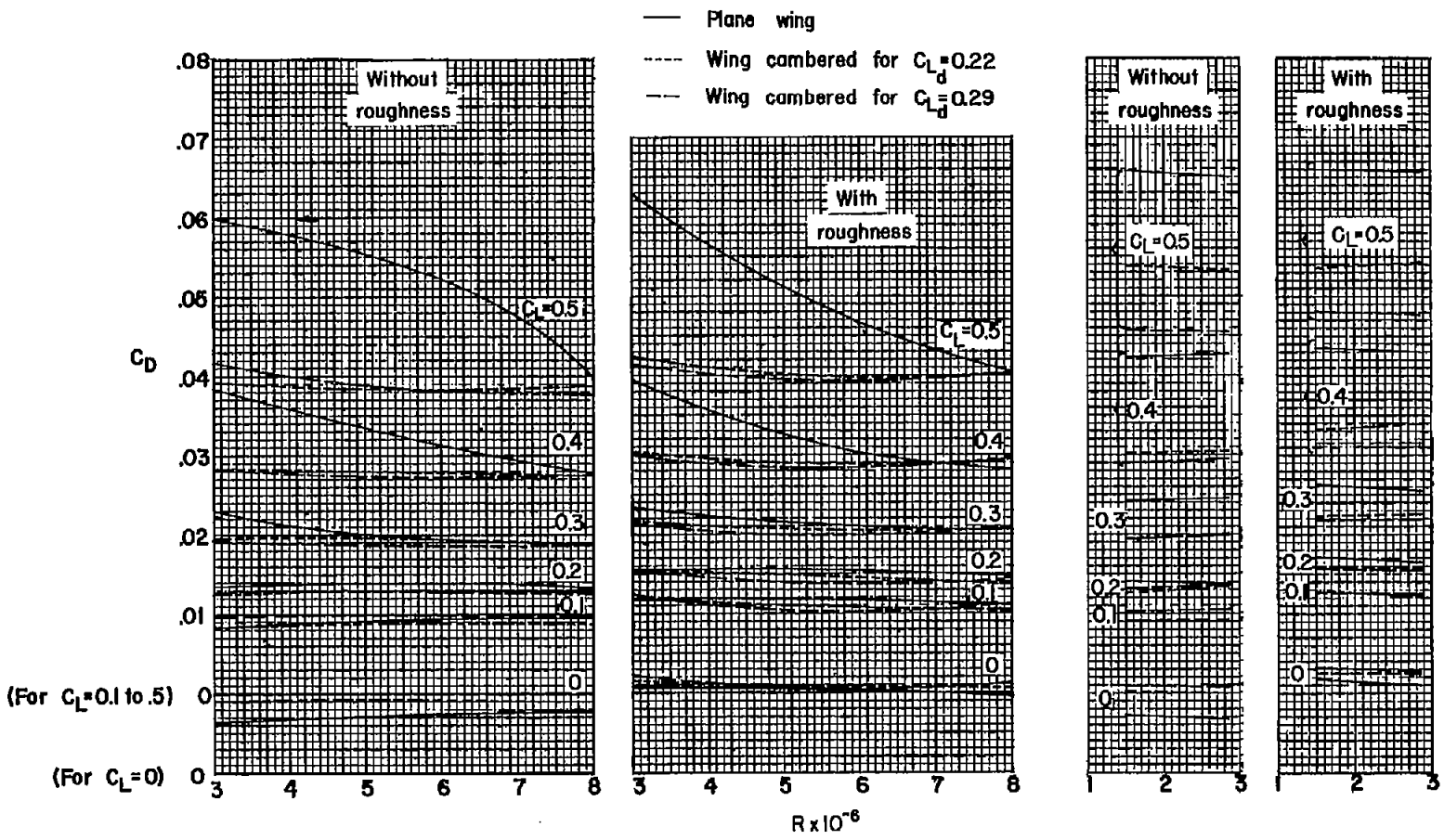

(a) M = 0.22

(b) M = 0.60

Figure 10.- The variation with Reynolds number of the drag coefficient at constant lift coefficient.

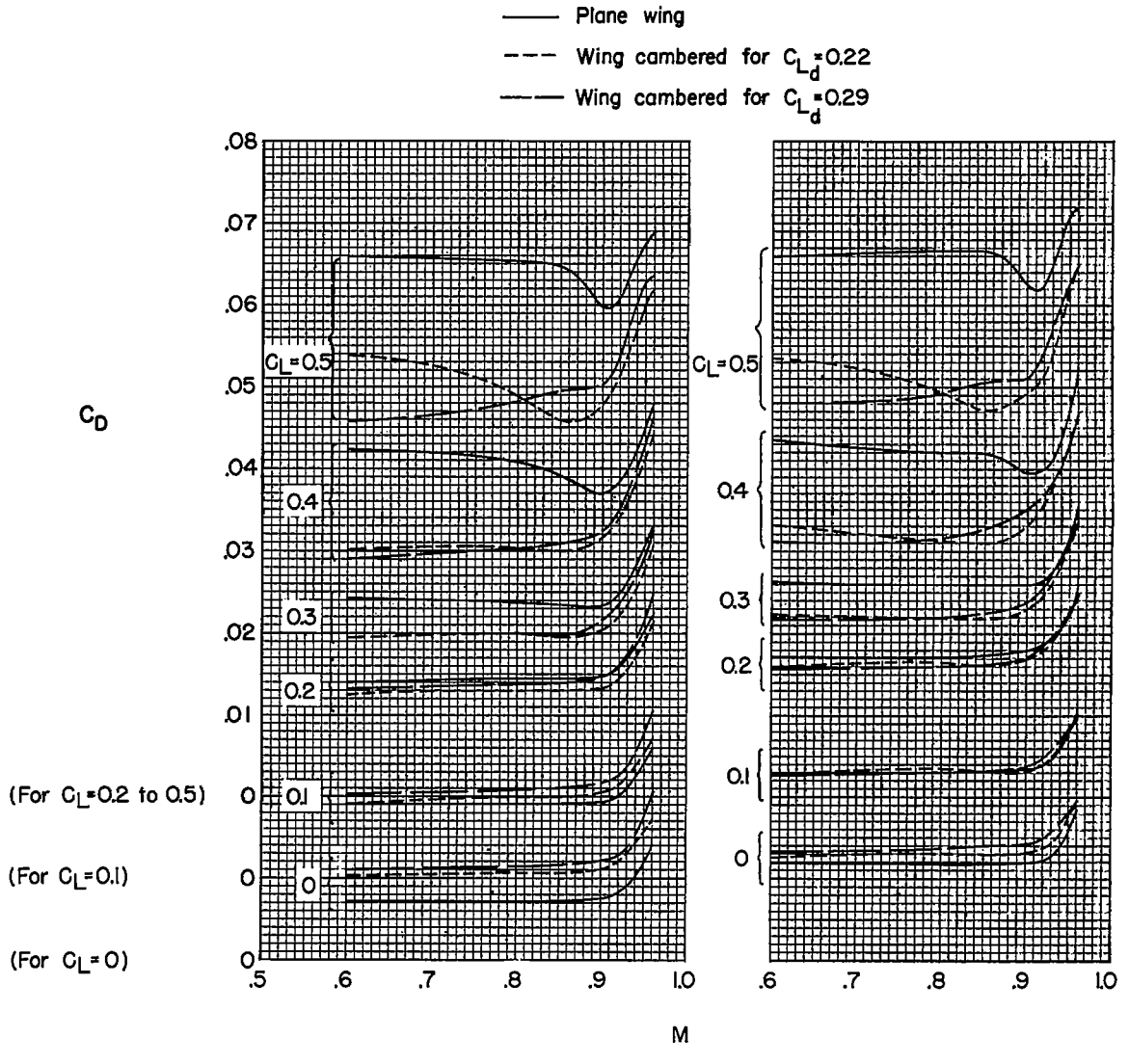

(a) Without roughness. (b) With roughness.

Figure 11.- The variation with Mach number of the drag coefficient at constant lift coefficient; R = 1.5×10^6.

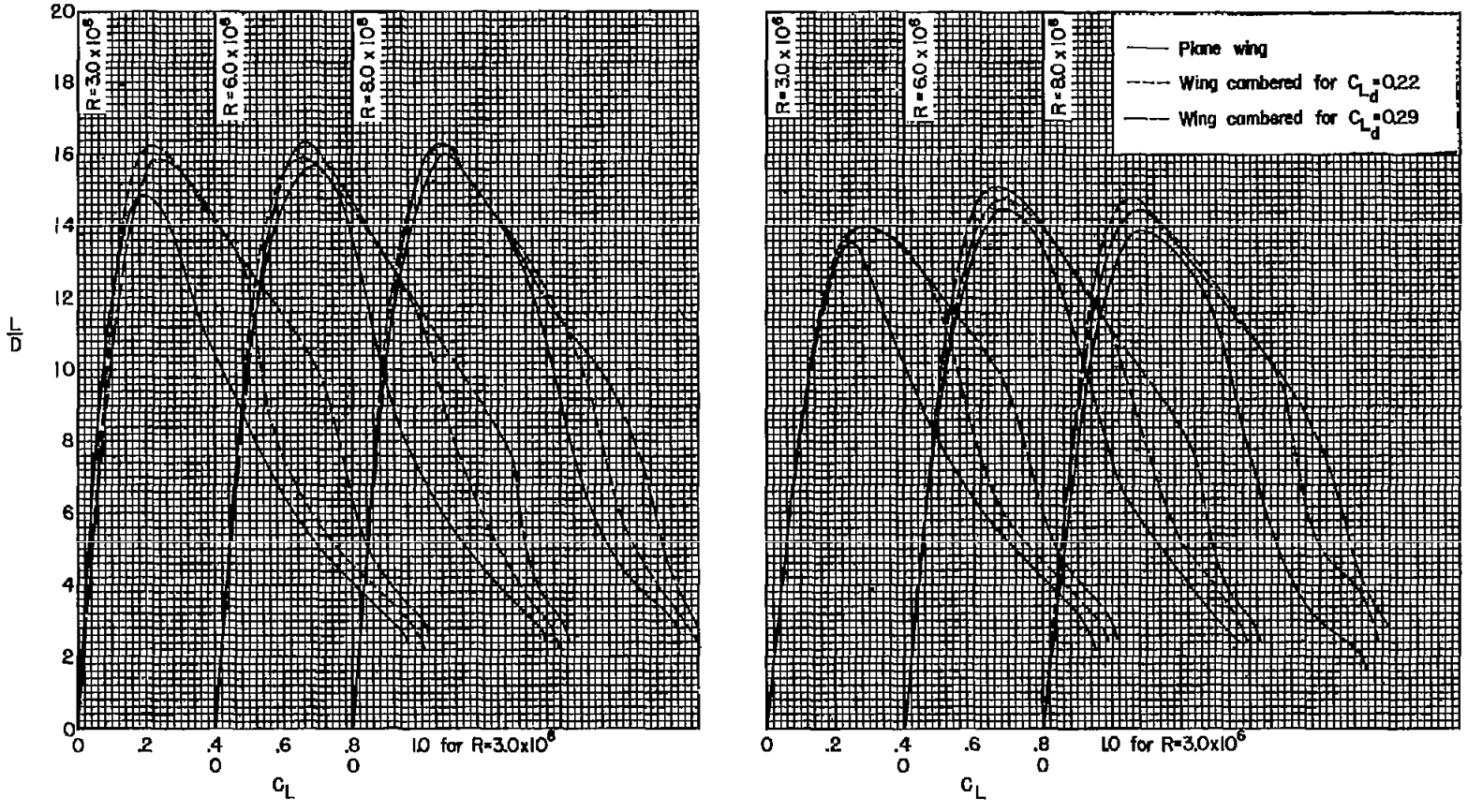

(a) Without roughness.

(b) With roughness.

Figure 12.- Effect of conical camber on the lift-drag ratios at various Reynolds numbers; M = 0.22.

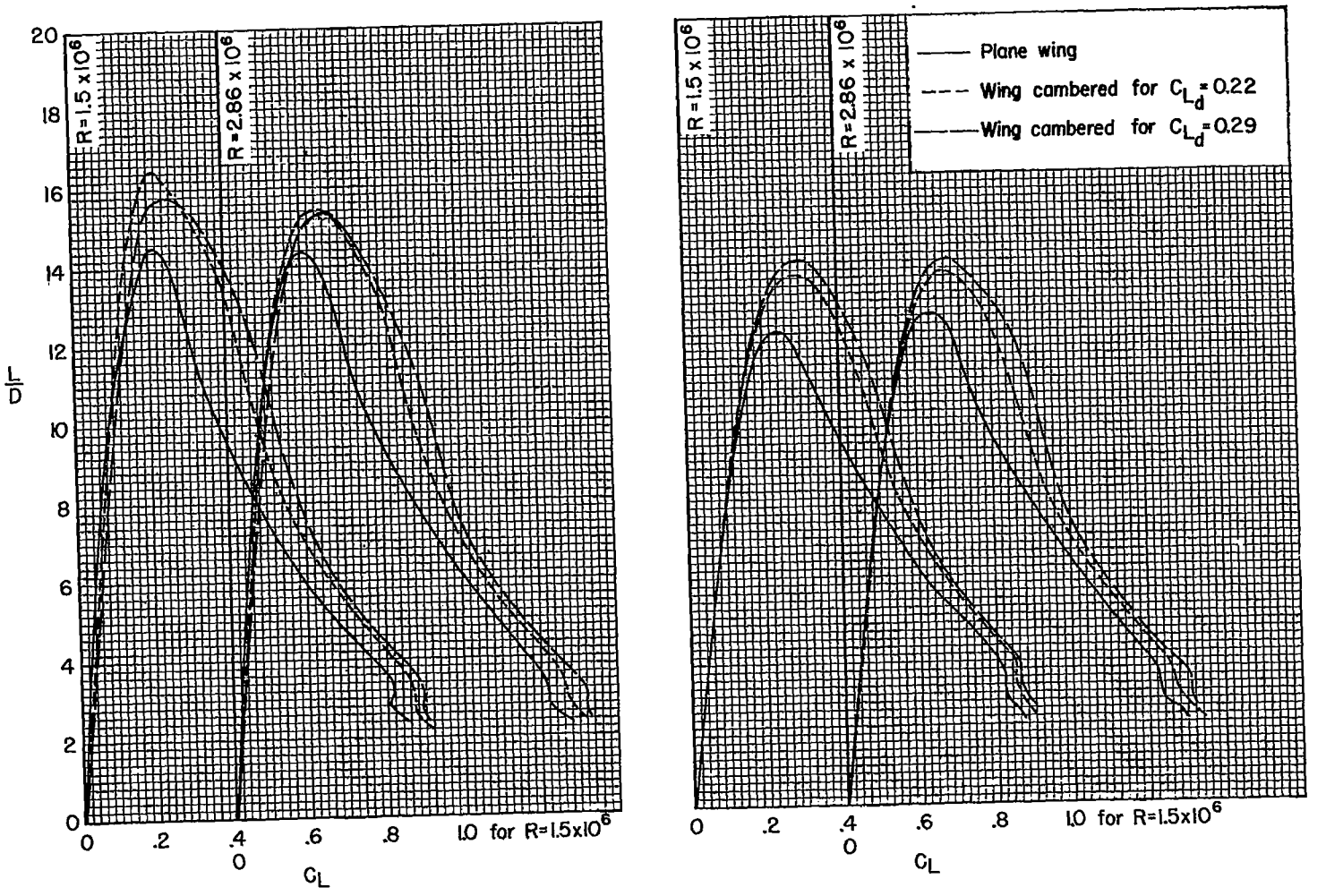

(a) Without roughness.

(b) With roughness.

Figure 13.- Effect of conical camber on the lift-drag ratios at two Reynolds numbers; M = 0.60.

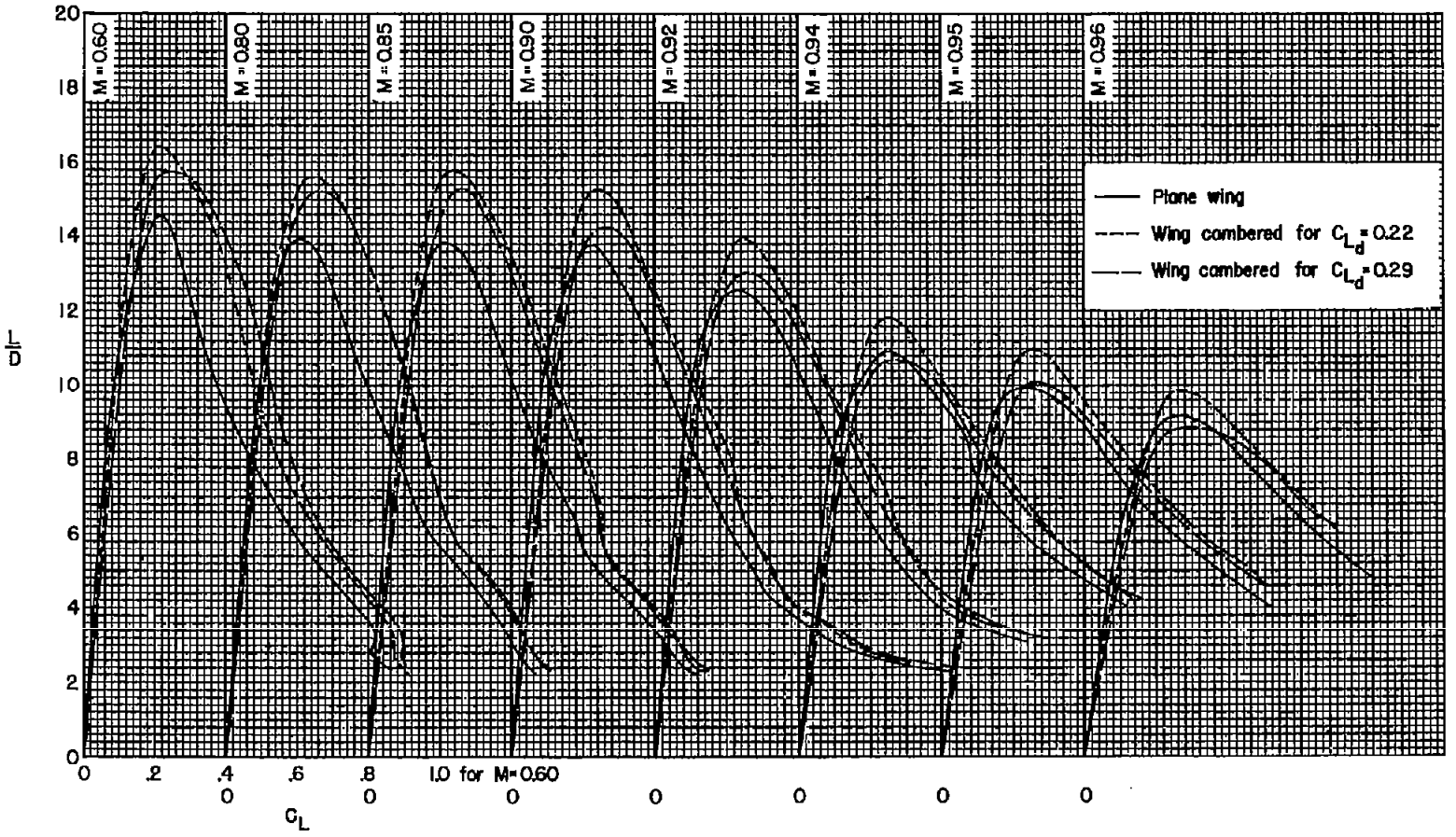

(a) Without roughness.

Figure 14.- Effect of conical camber on the lift-drag ratios at various Mach numbers; R = 1.5×10^6.

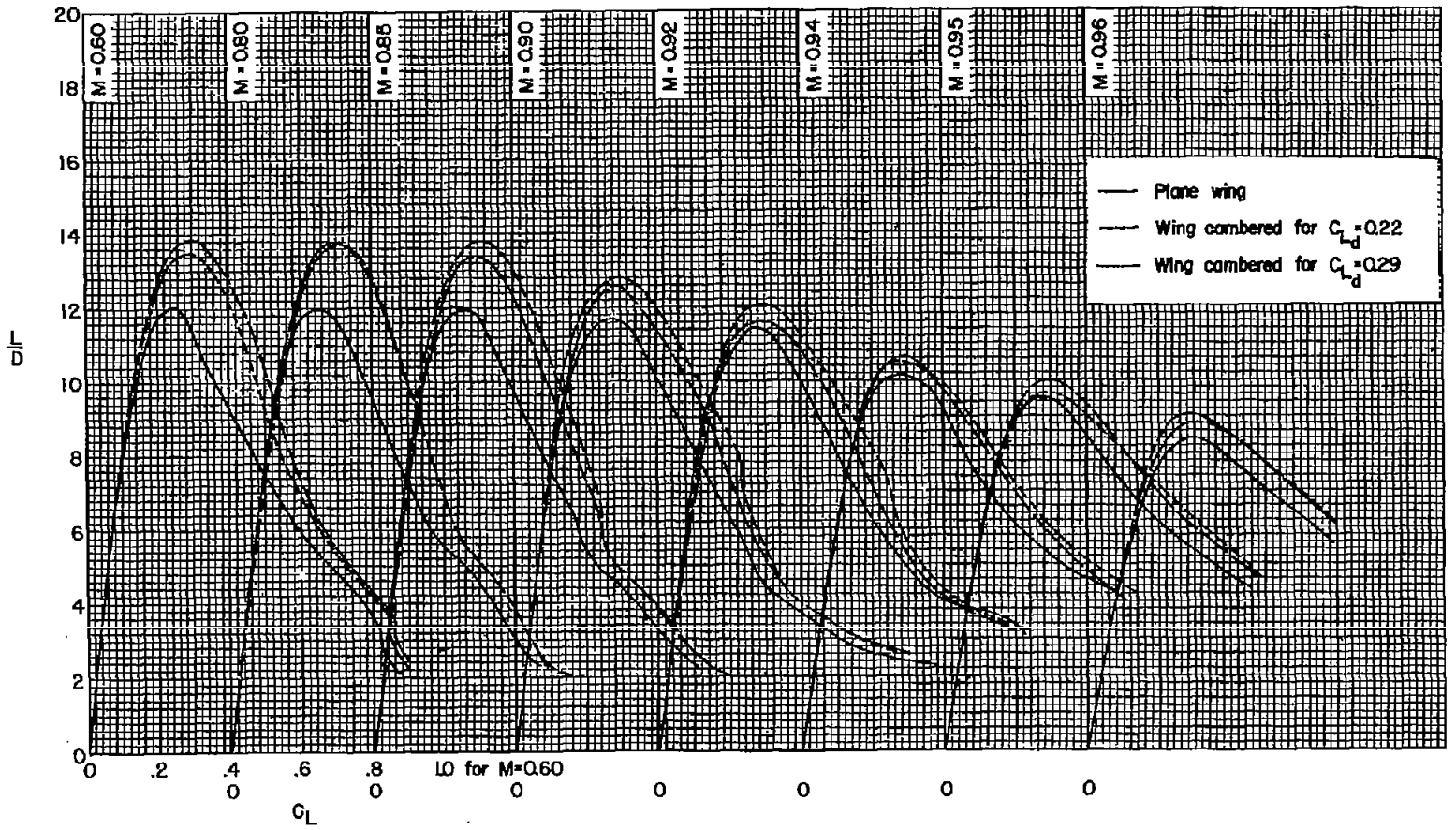

(b) With roughness.

Figure 14.- Concluded.

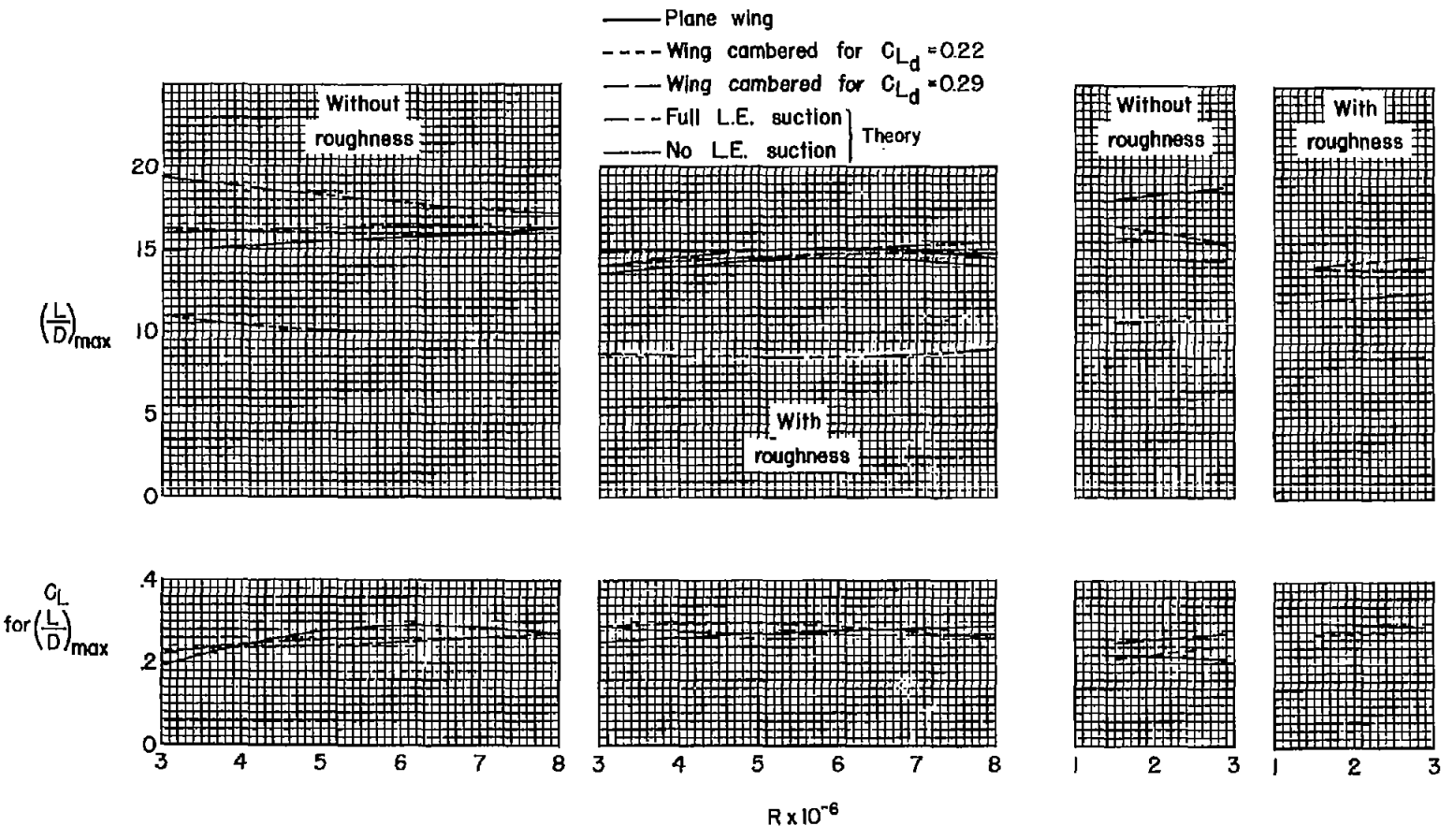

(a) M = 0.22 (b) M = 0.60

Figure 15.- The variation with Reynolds number of the maximum lift-drag ratios and the lift coefficients for maximum lift-drag ratios.

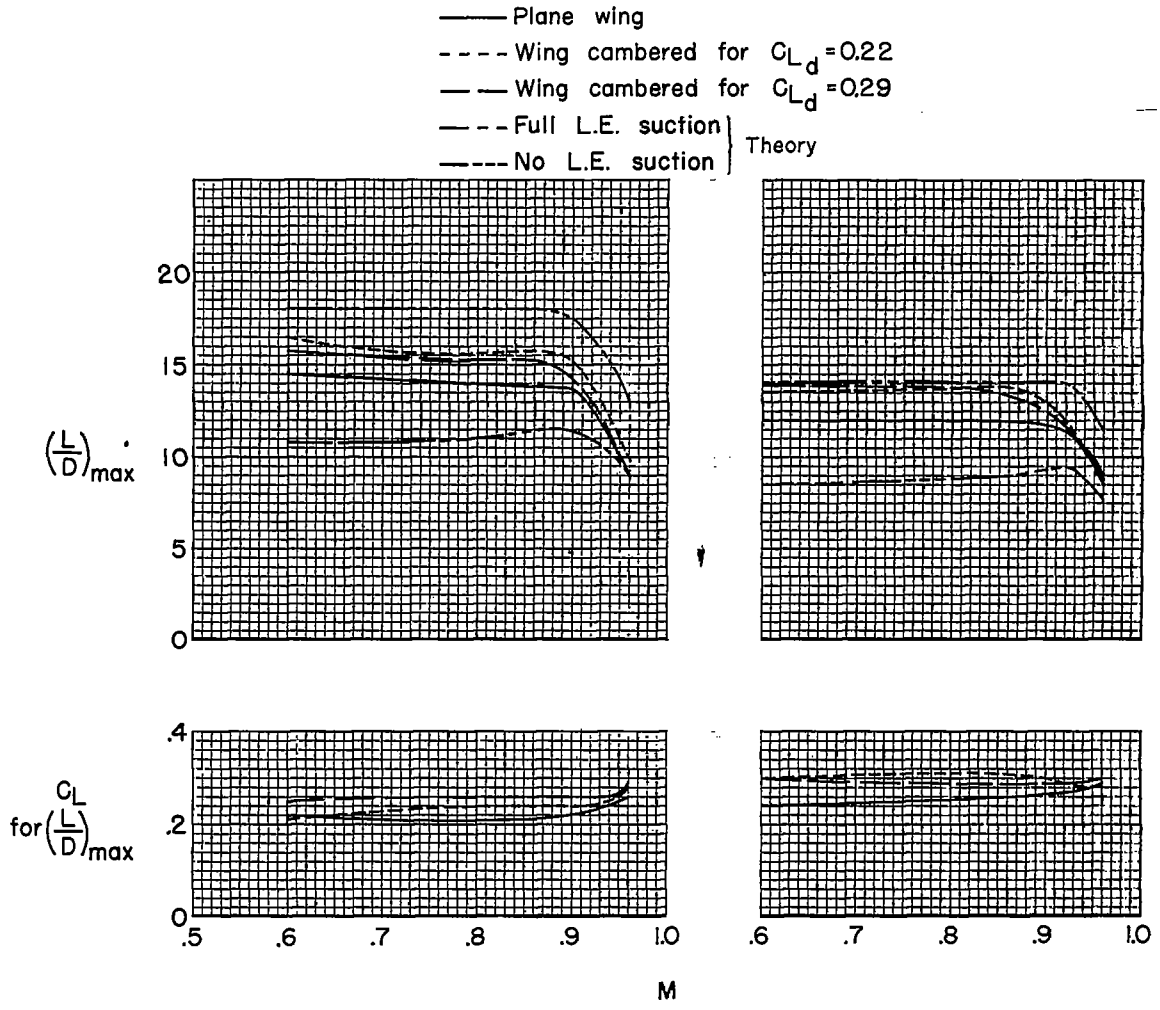

(a) Without roughness. (b) With roughness.

Figure 16.- The variation with Mach number of the maximum lift-drag ratios and the lift coefficients for maximum lift-drag ratios; R = 1.5×10^6.

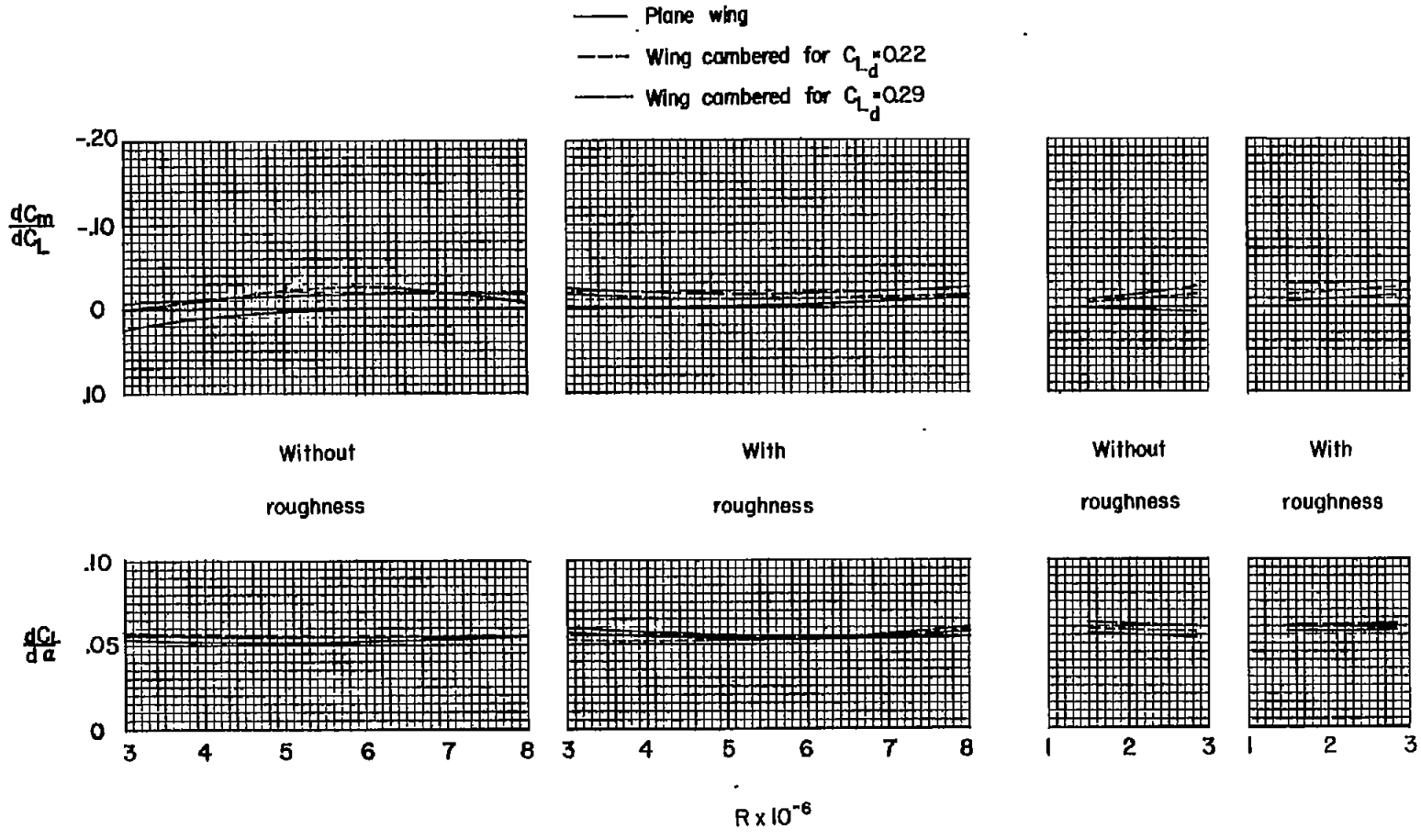

(a) M = 0.22 (b) M = 0.60

Figure 17.- The variation with Reynolds number of the lift and pitching-moment curve slopes; $C_L = 0$.

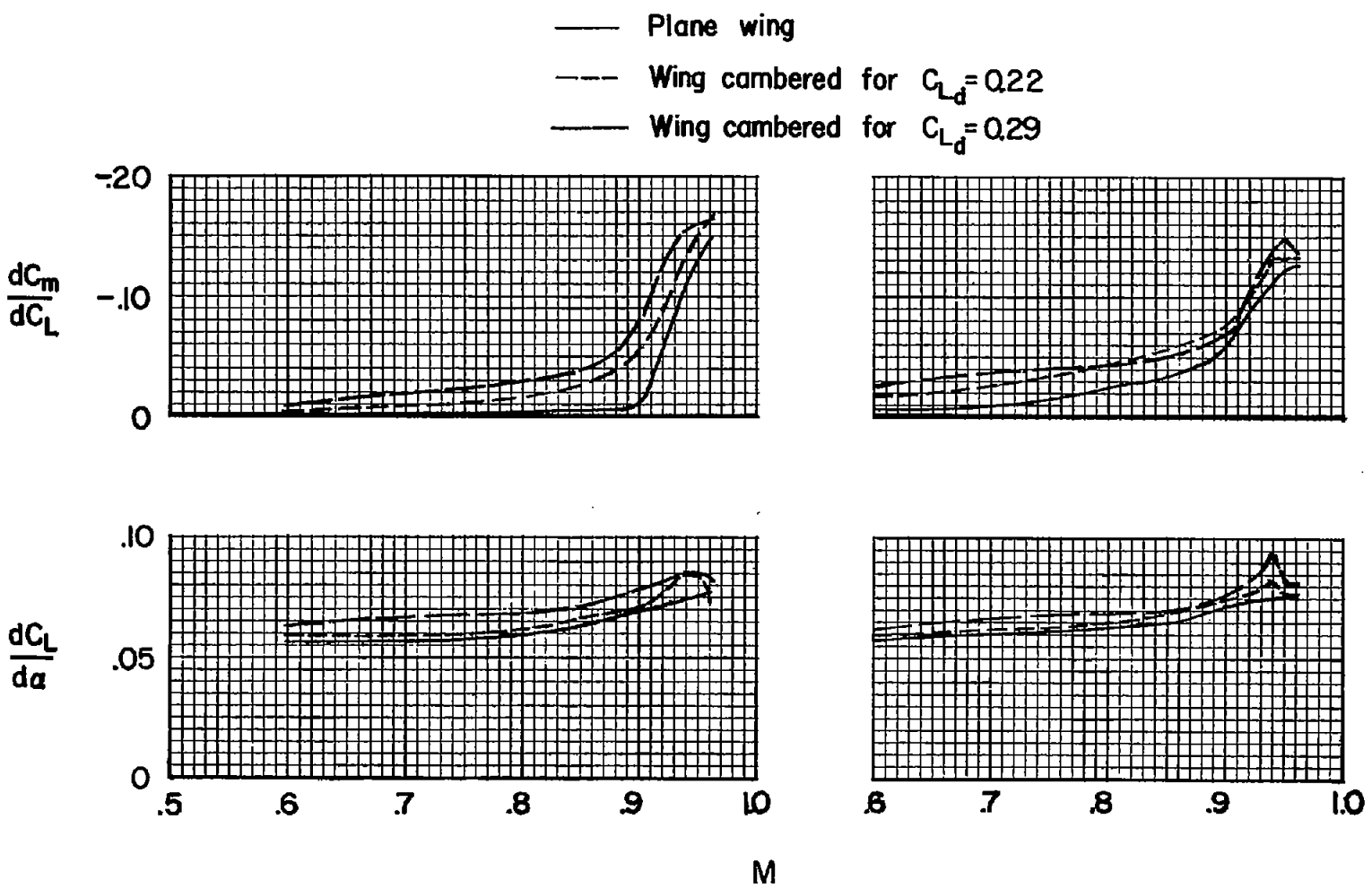

(a) Without roughness.

(b) With roughness.

Figure 18.- The variation with Mach number of the lift and pitching-moment curve slopes; $R = 1.5 \times 10^6$, $C_L = 0$.

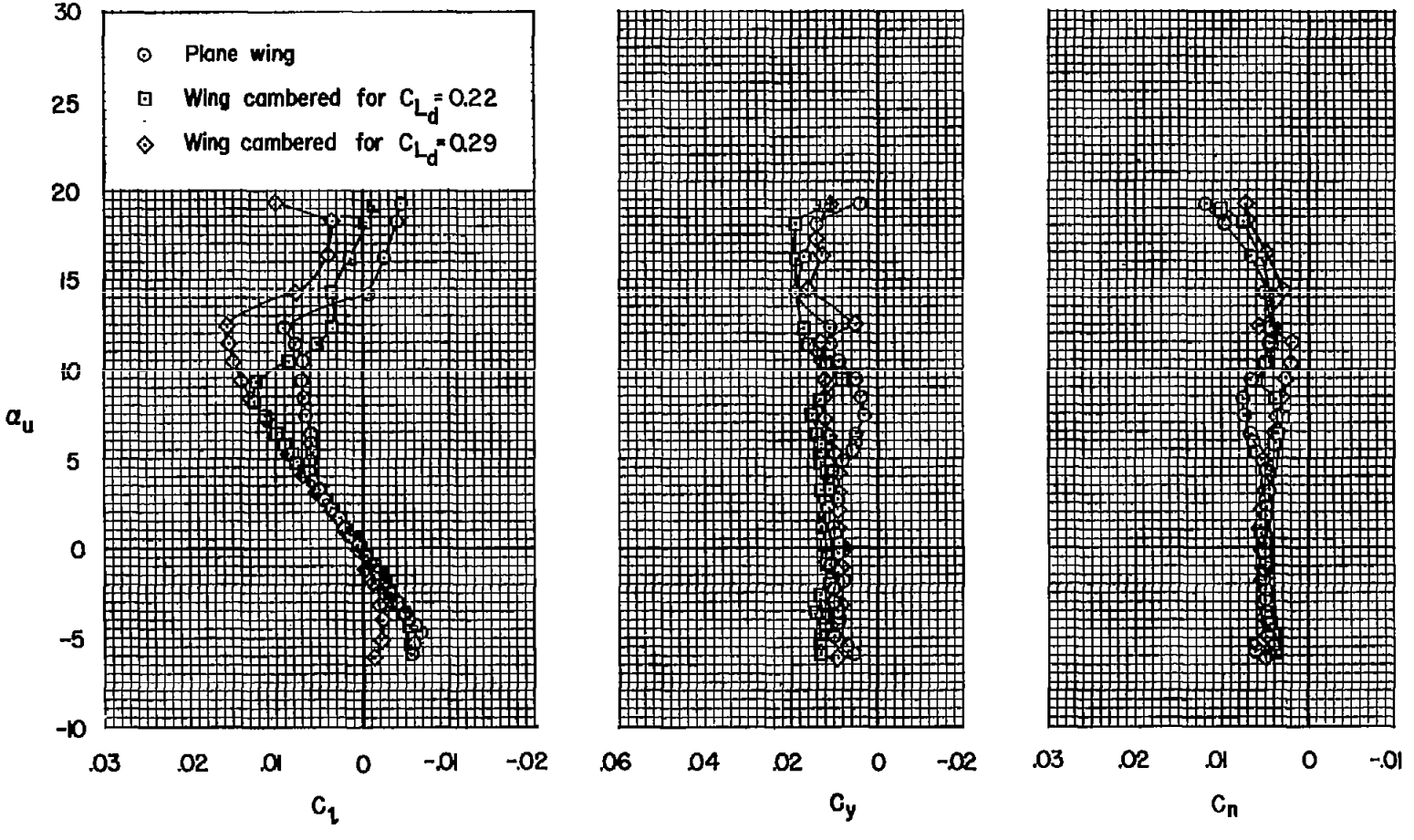

(a) R = 3×10^6

Figure 19.- Effect of conical camber on the rolling-moment, side-force, and yawing-moment coefficients; with roughness, M = 0.22, $\beta = -6^\circ$.

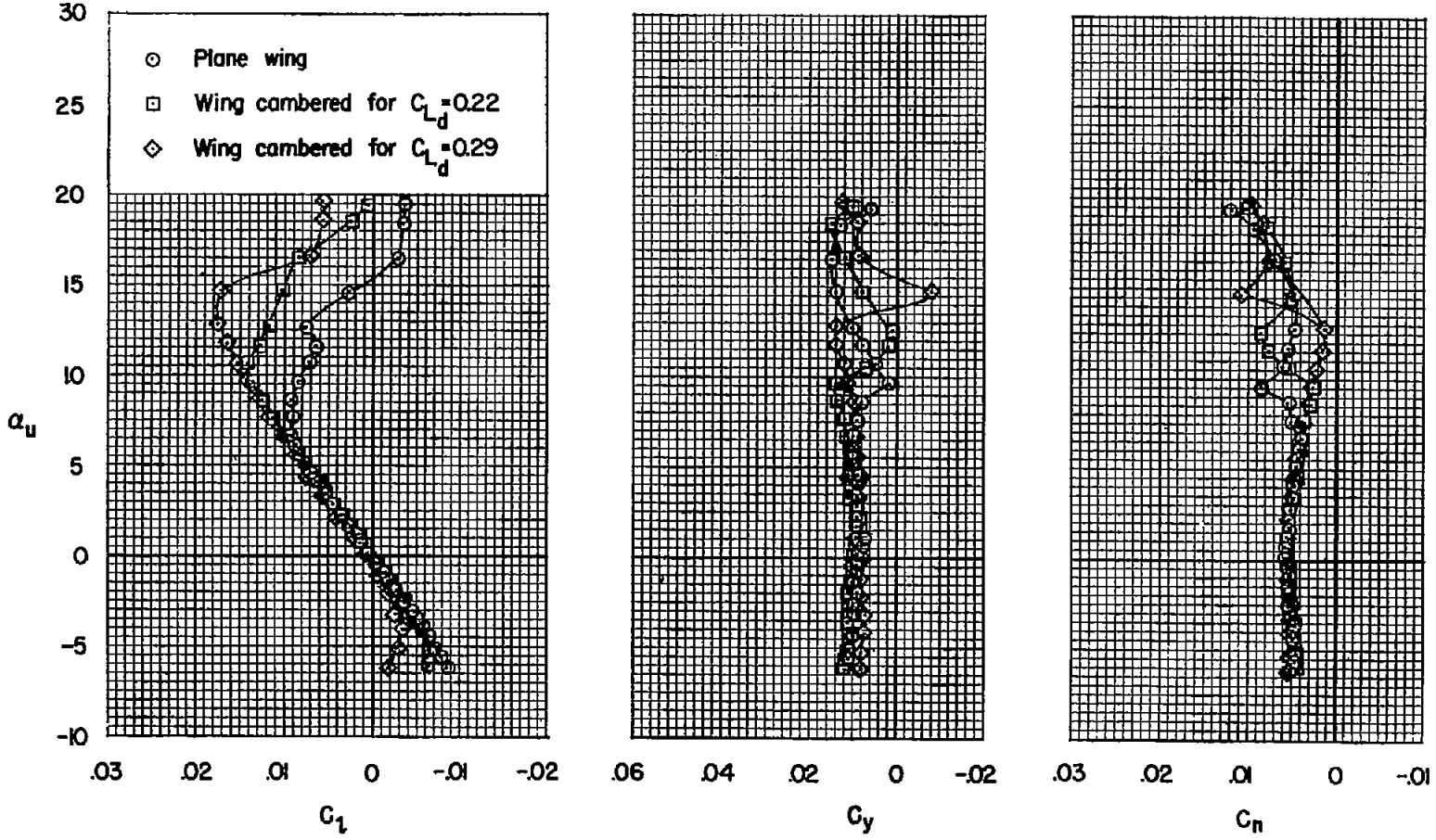

(b) R = 6×10^6

Figure 19.- Continued.

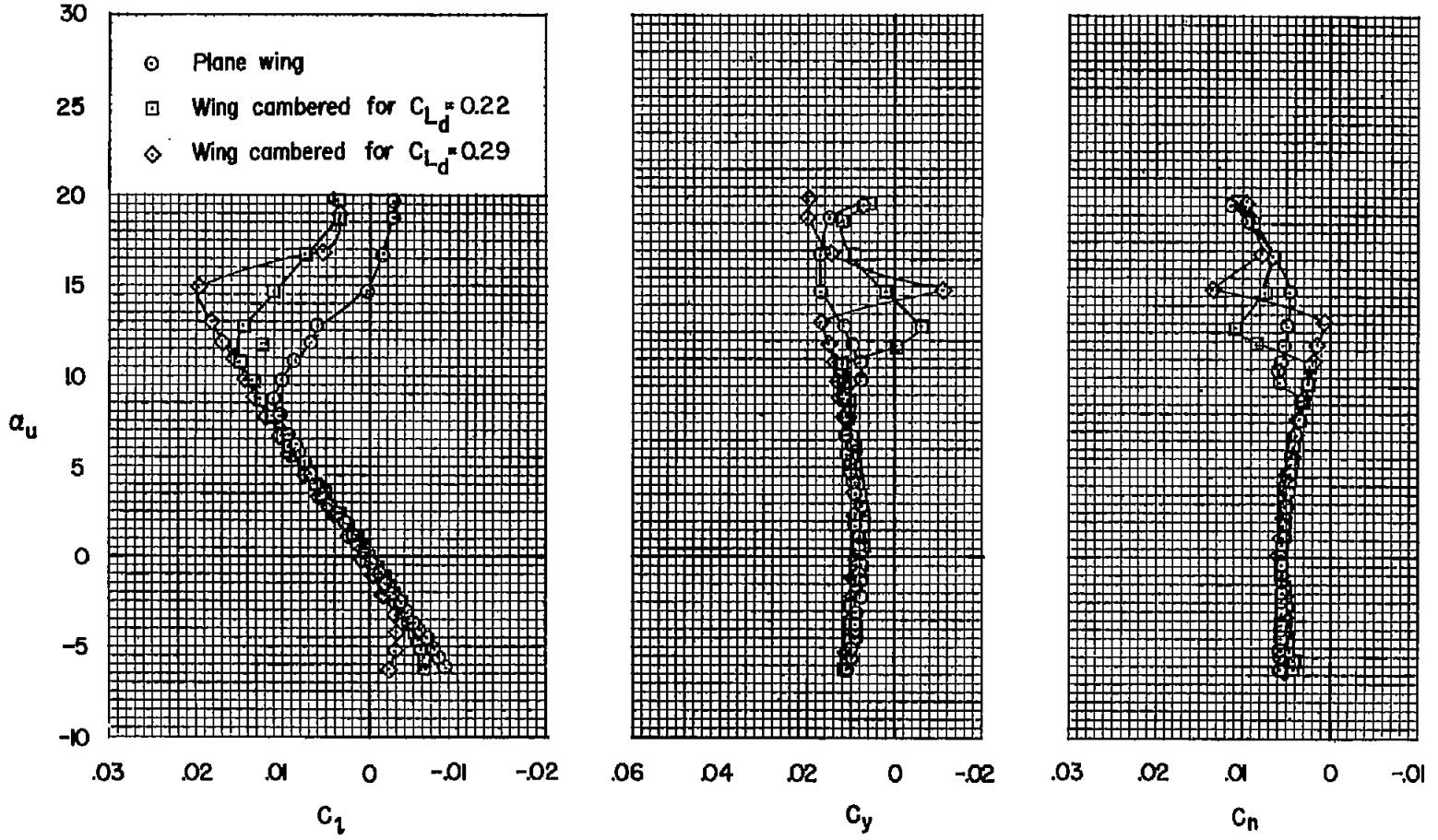

(c) R = 8×10^6

Figure 19.- Concluded.

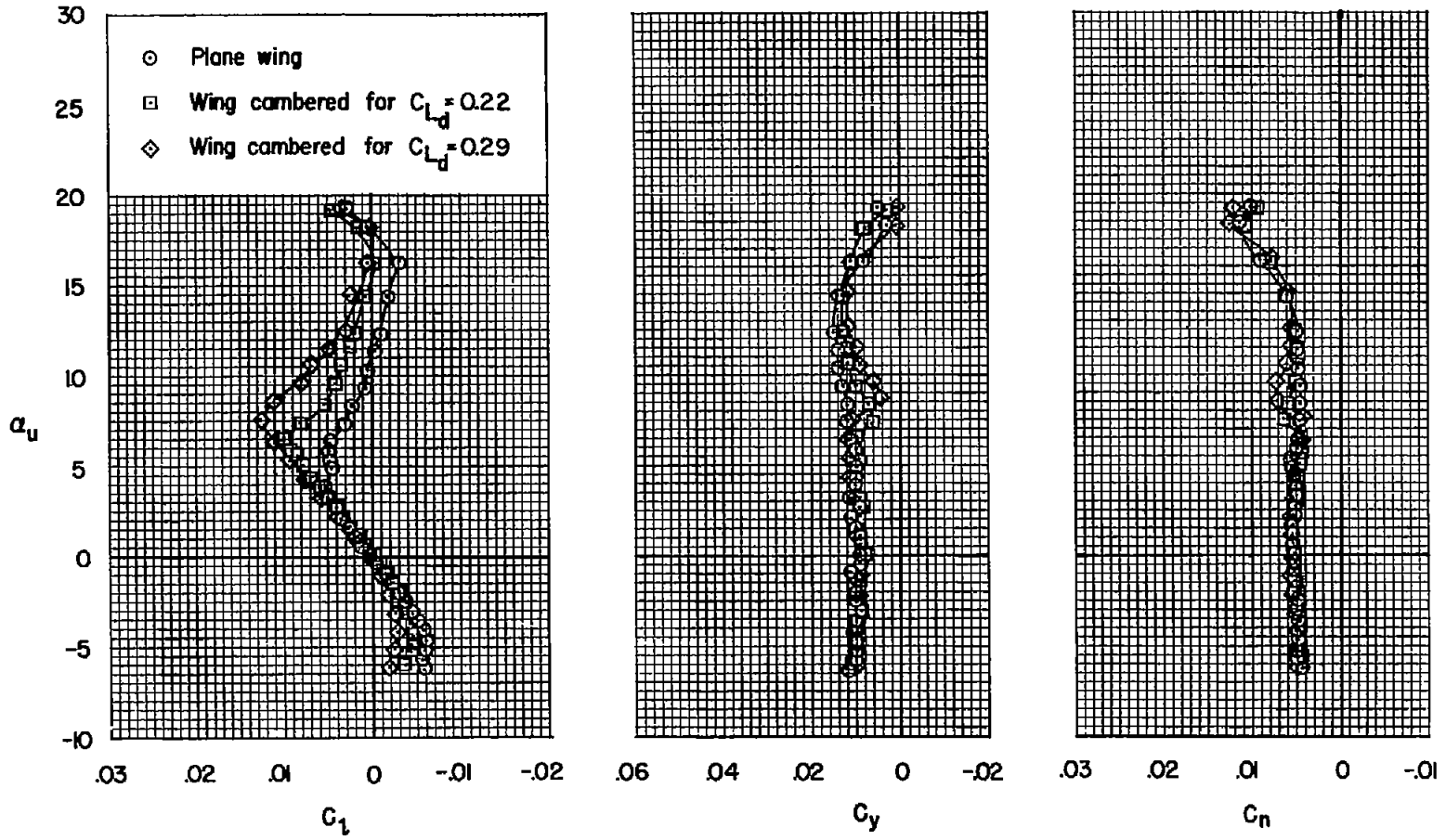

(a) R = 1.5×10^6

Figure 20.- Effect of conical camber on the rolling-moment, side-force, and yawing-moment coefficients; with roughness, M = 0.60, $\beta = -6^\circ$.

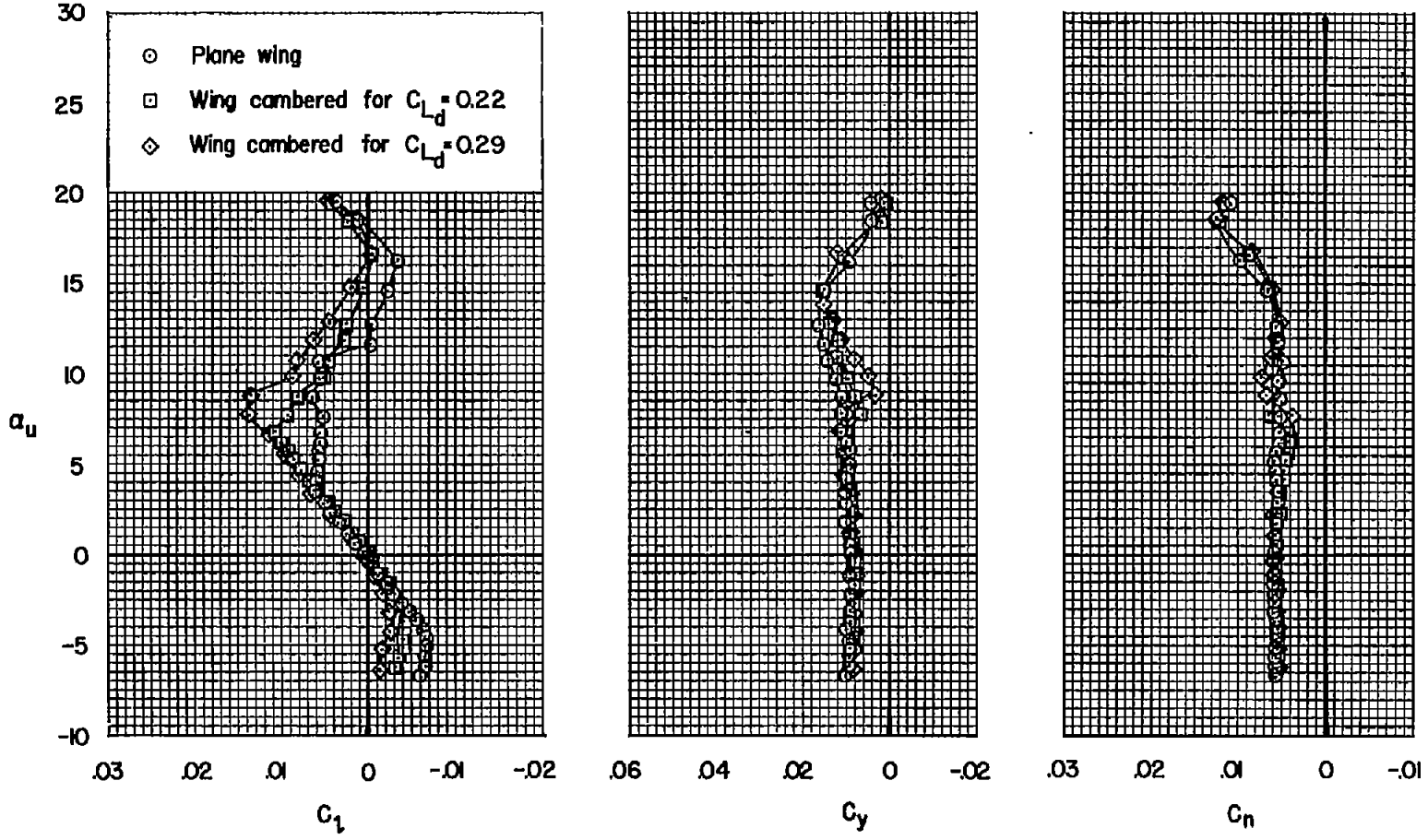

(b) R = 2.86×10^6

Figure 20.- Concluded.

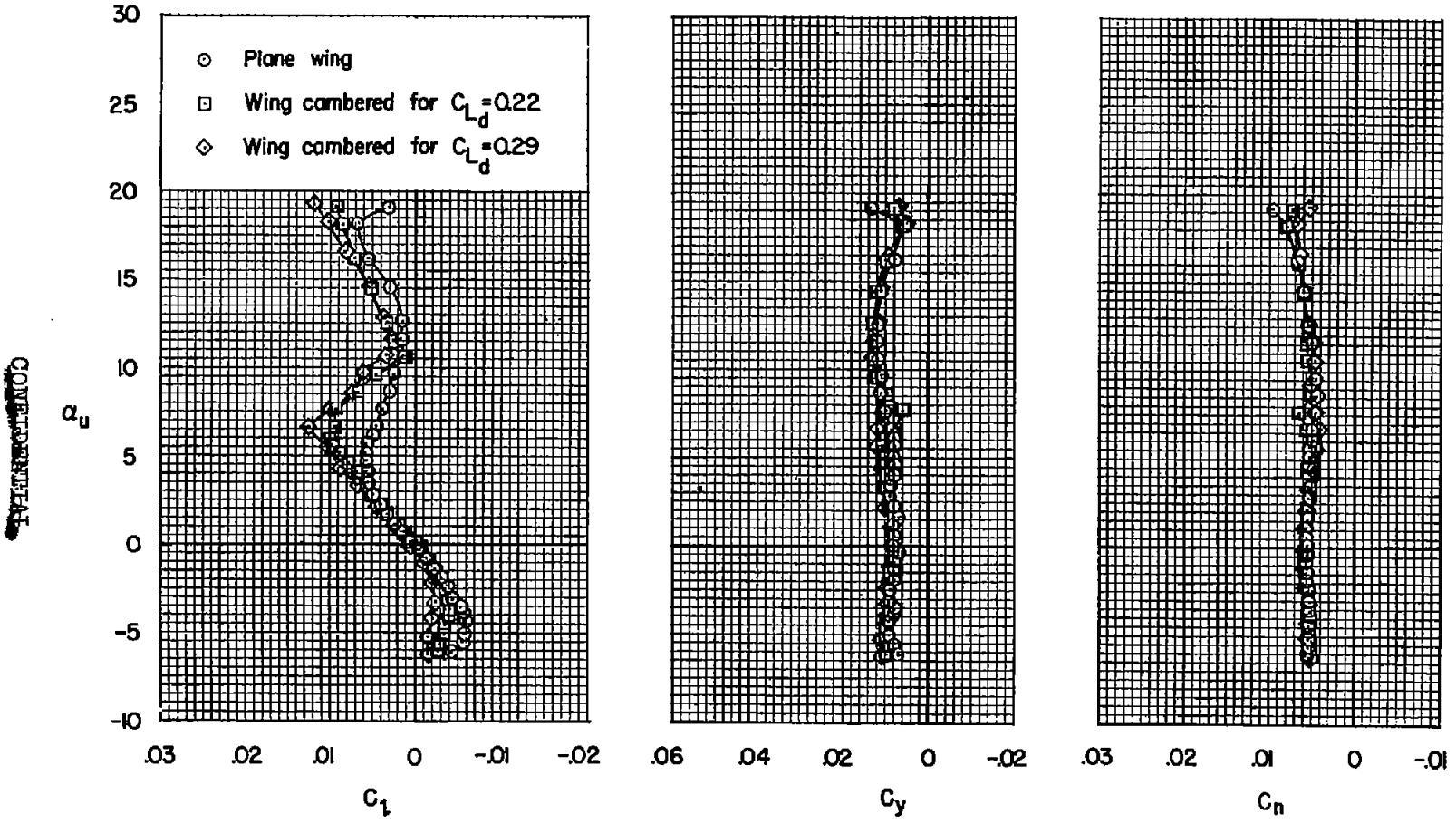

(a) M = 0.80

Figure 21.- Effect of conical camber on the rolling-moment, side-force, and yawing-moment coefficients; with roughness, $R = 1.5 \times 10^6$, $\beta = -6^\circ$.

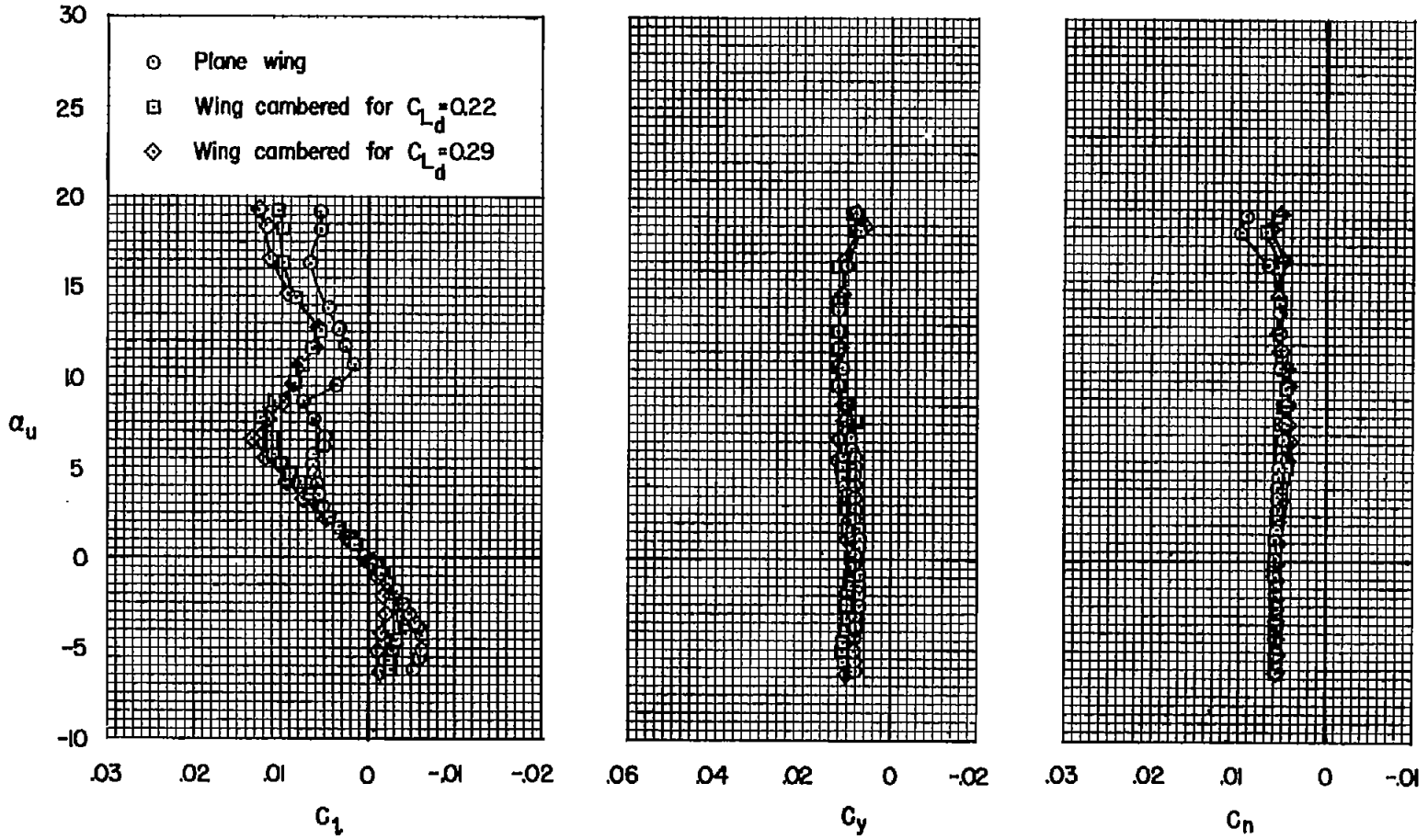

(b) M = 0.85

Figure 21.- Continued.

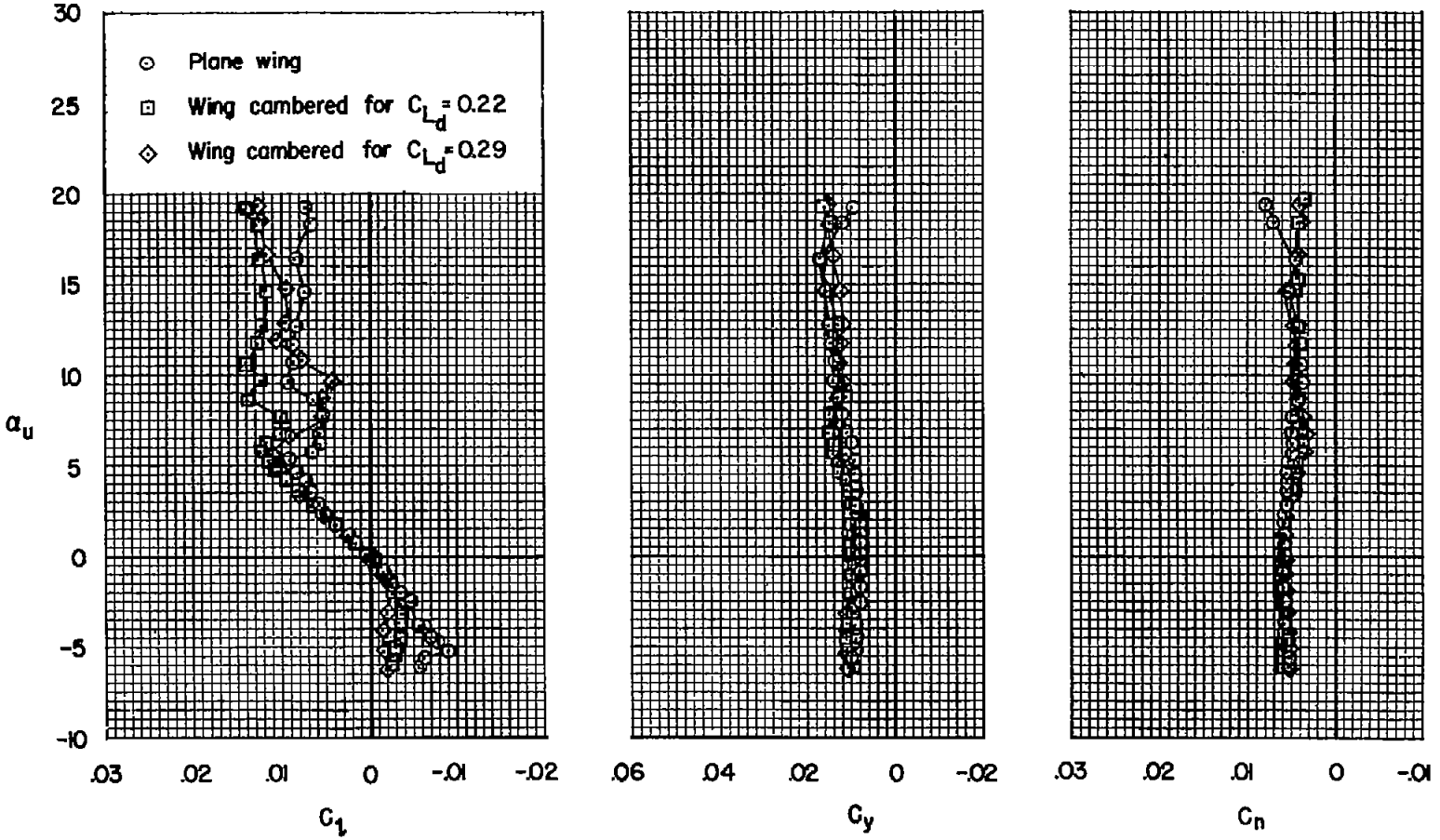

(c) M = 0.90

Figure 21.- Continued.

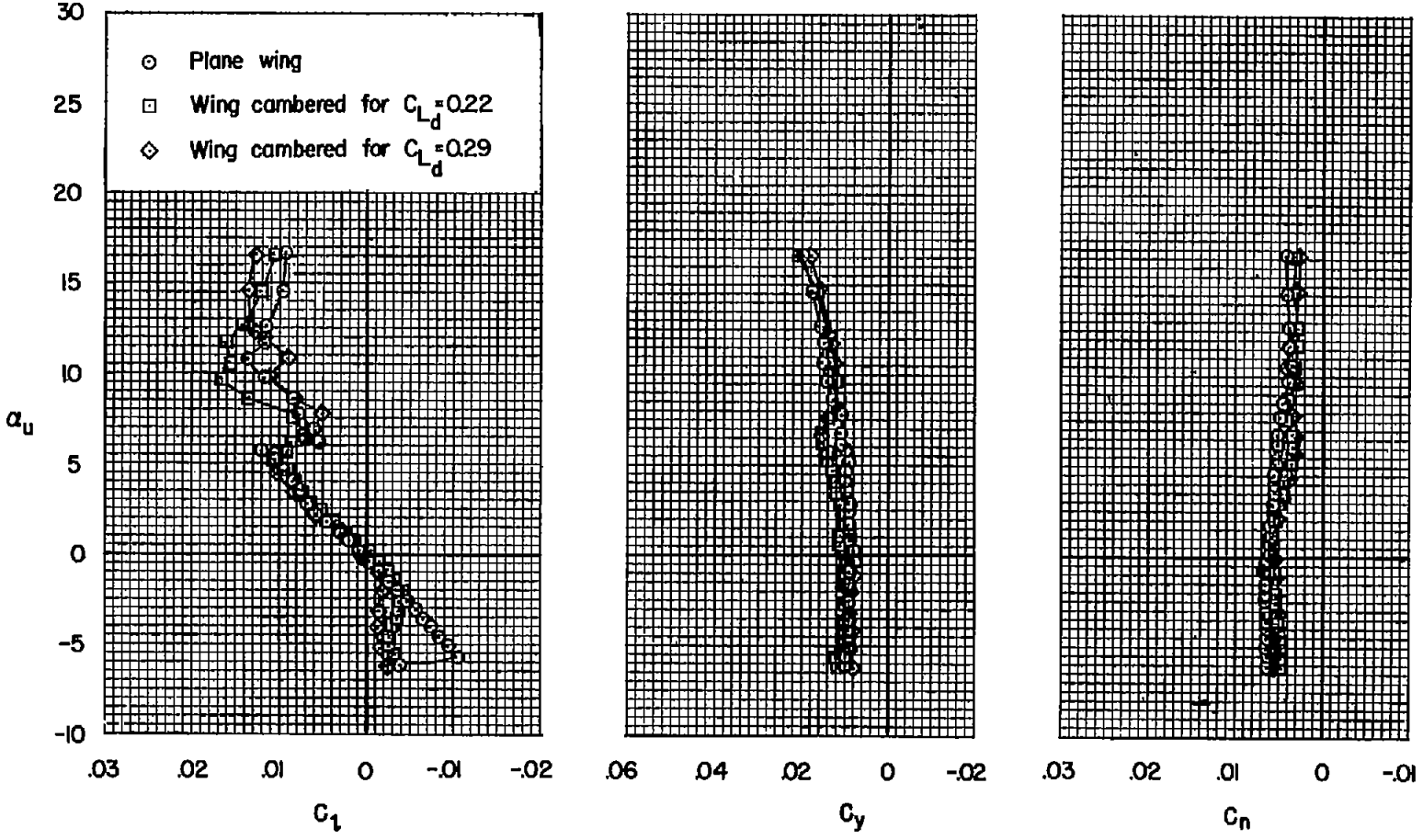

(d) M = 0.92

Figure 21.- Continued.

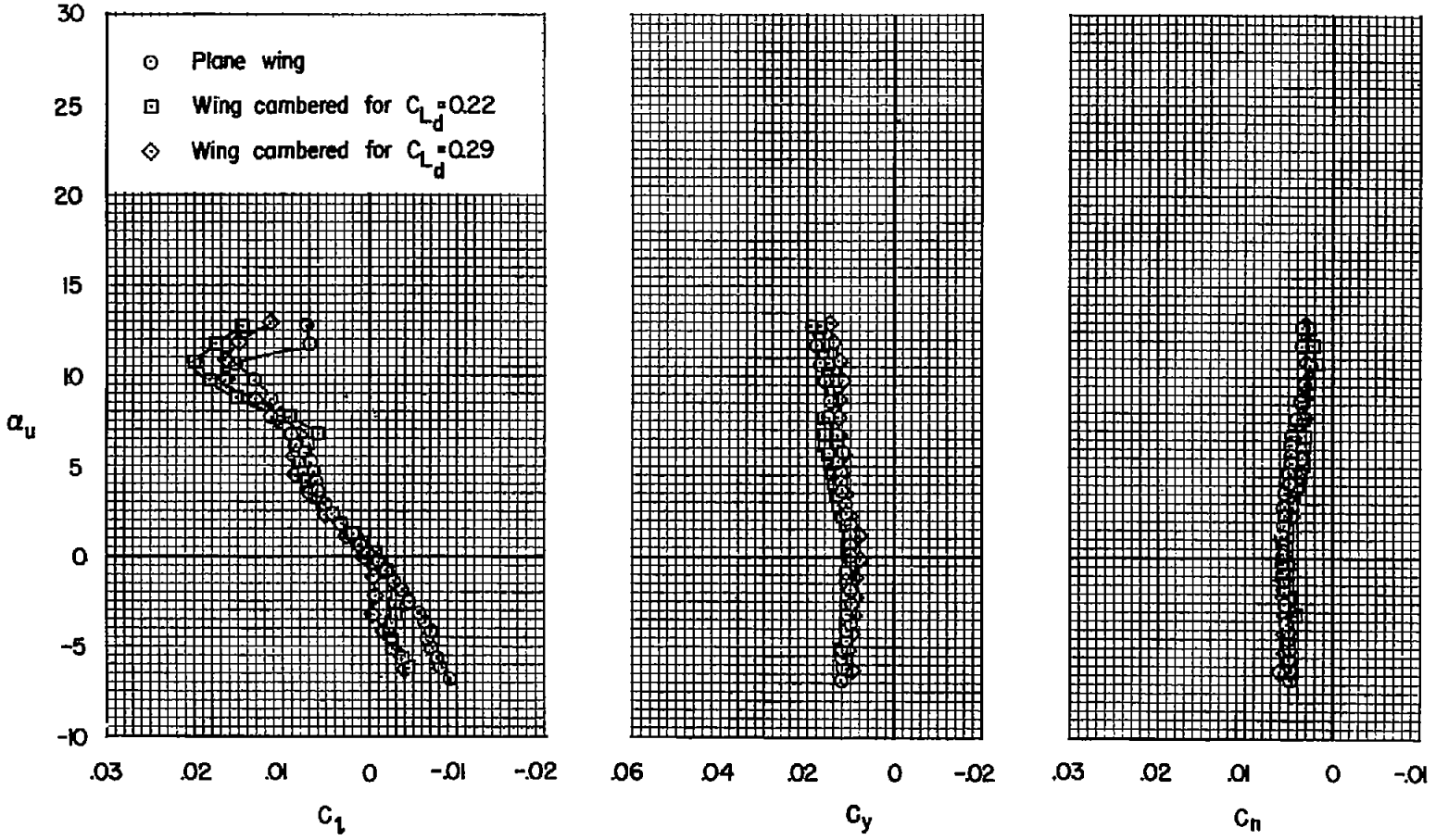

(e) M = 0.94

Figure 21.- Continued.

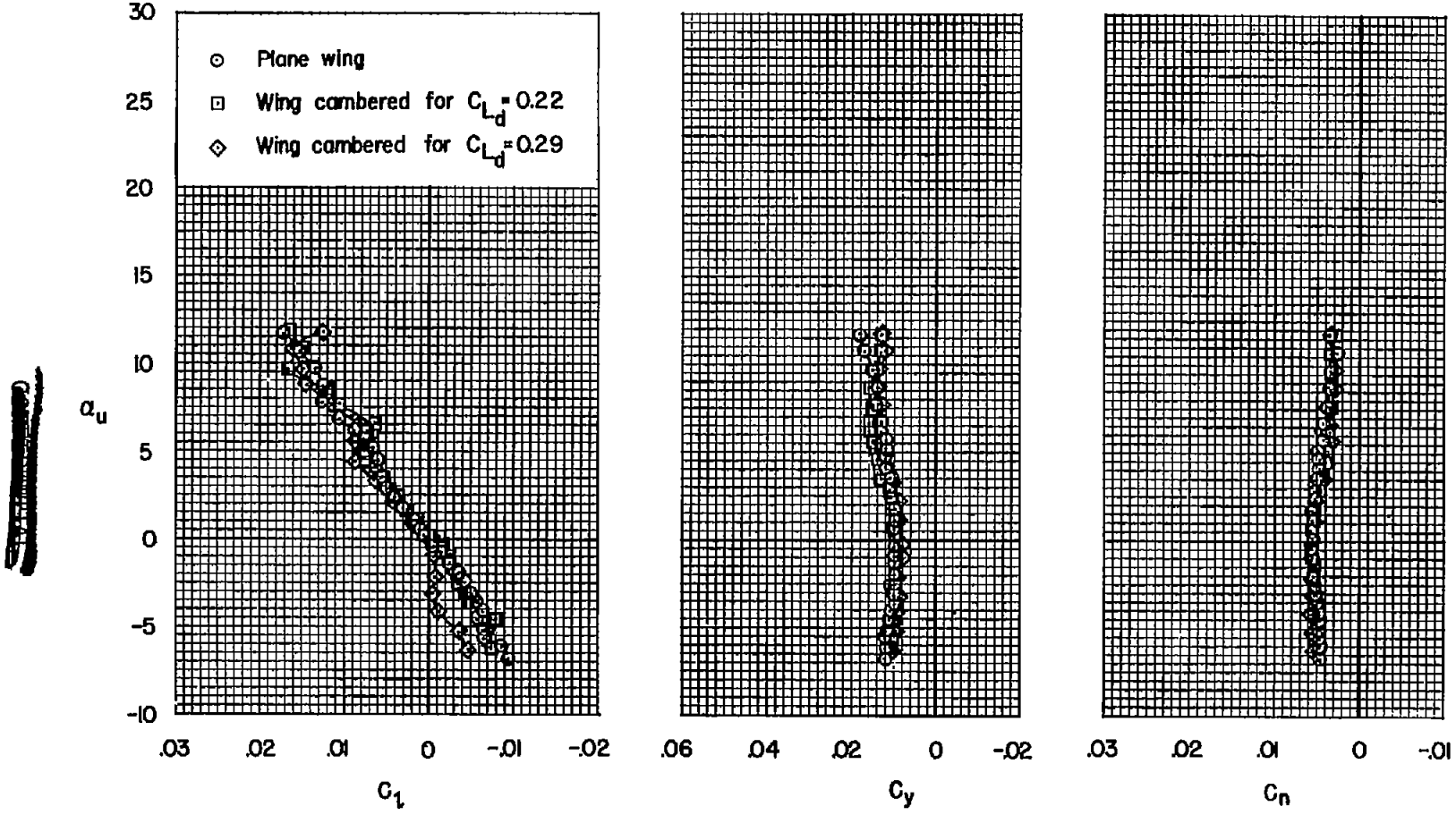

(f) M = 0.95

Figure 21.- Continued.

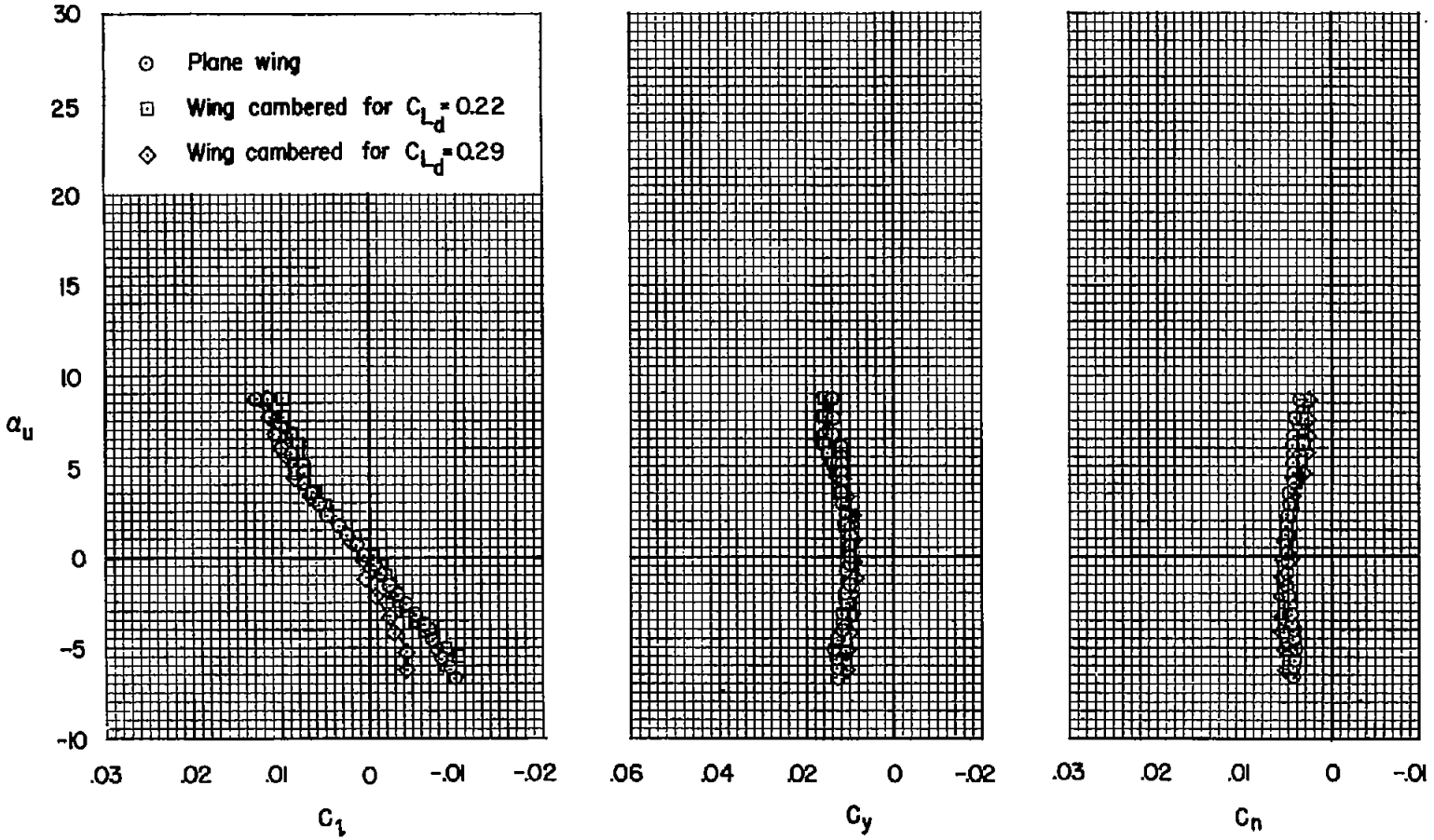

(g) M = 0.96

Figure 21.- Concluded.

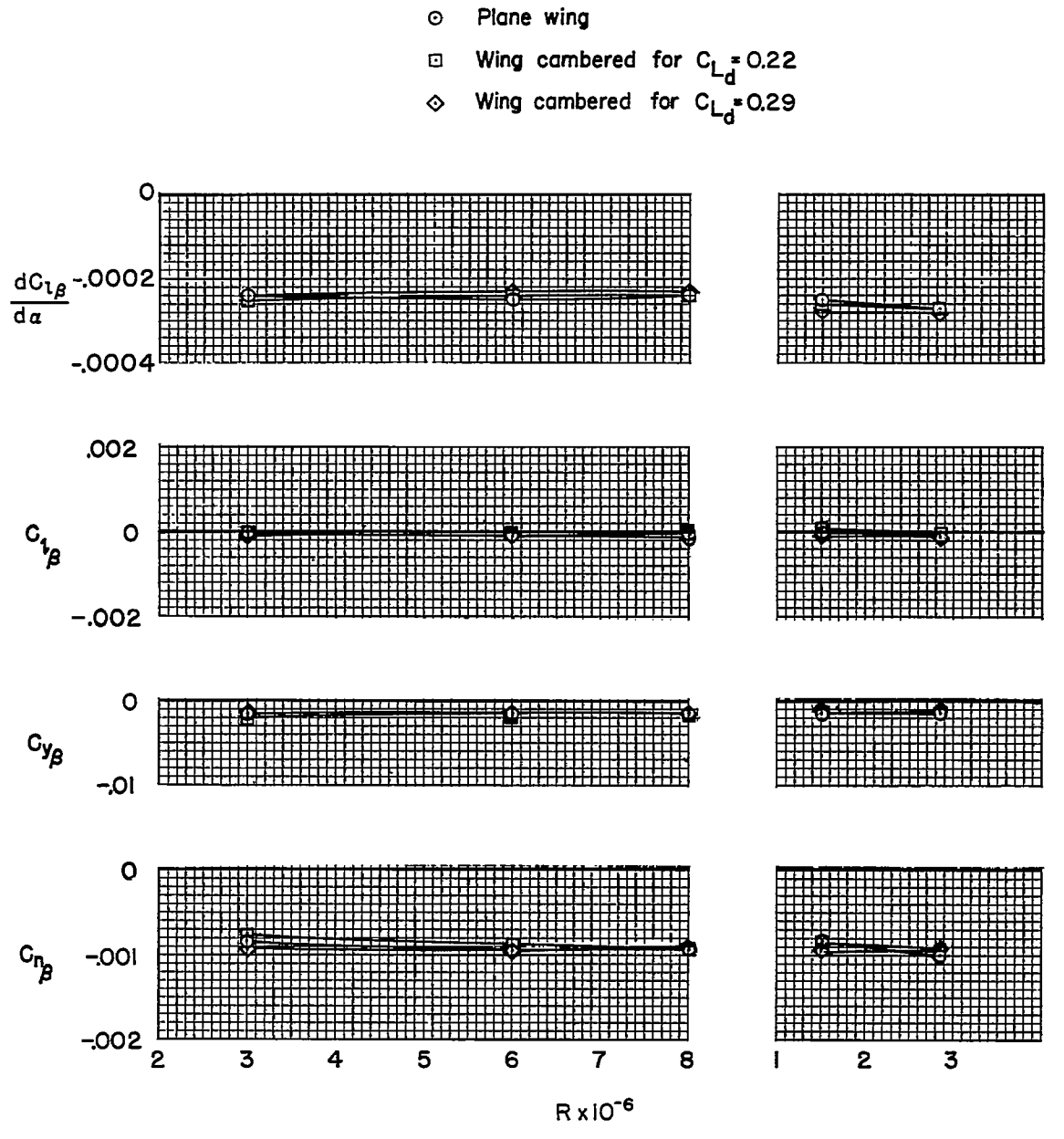

(a) M = 0.22 (b) M = 0.60

Figure 22.- The variation with Reynolds number of the lateral and directional stability characteristics; with roughness, $\alpha_u \cong 0$.

[redacted]

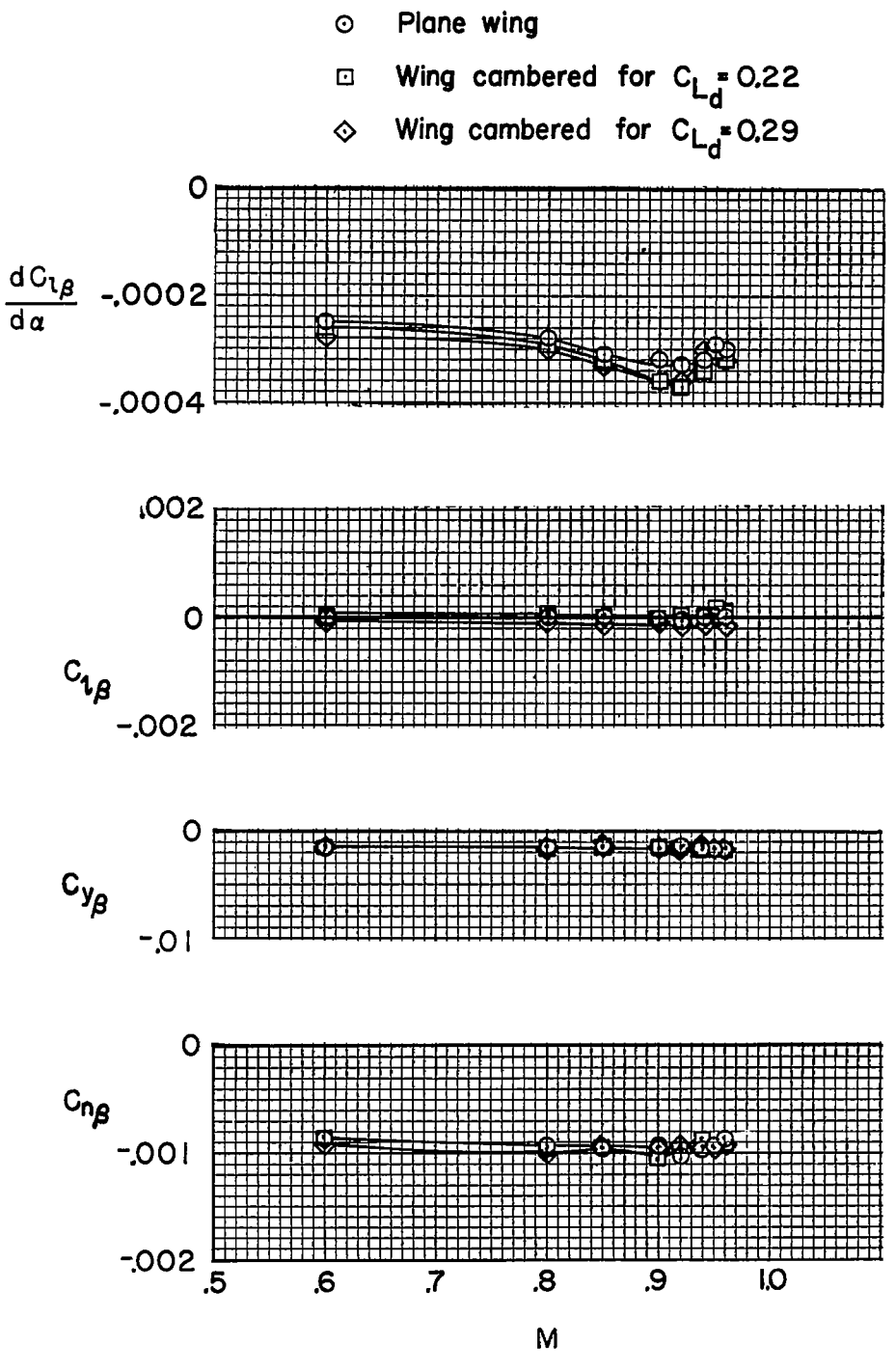

Figure 23.- The variation with Mach number of the lateral and directional stability characteristics; with roughness, R = 1.5×10^6, $\alpha_u \cong 0$.

NACA - Langley Field, Va.